Karlsruher Institut für Technologie

Entwicklung und Durchführung experimenteller Methoden zur verbesserten Modellierbarkeit uranhaltiger salinarer Lösungen (EDUKEM)

Abschlussbericht Teilprojekt C, KIT–INE

Marcus Altmaier, Nese Cevirim-Papaioannou, Kathy Dardenne, David Fellhauer, Xavier Gaona, Jun-Yeop Lee, Ezgi Yalcintas

KIT SCIENTIFIC WORKING PAPERS 145

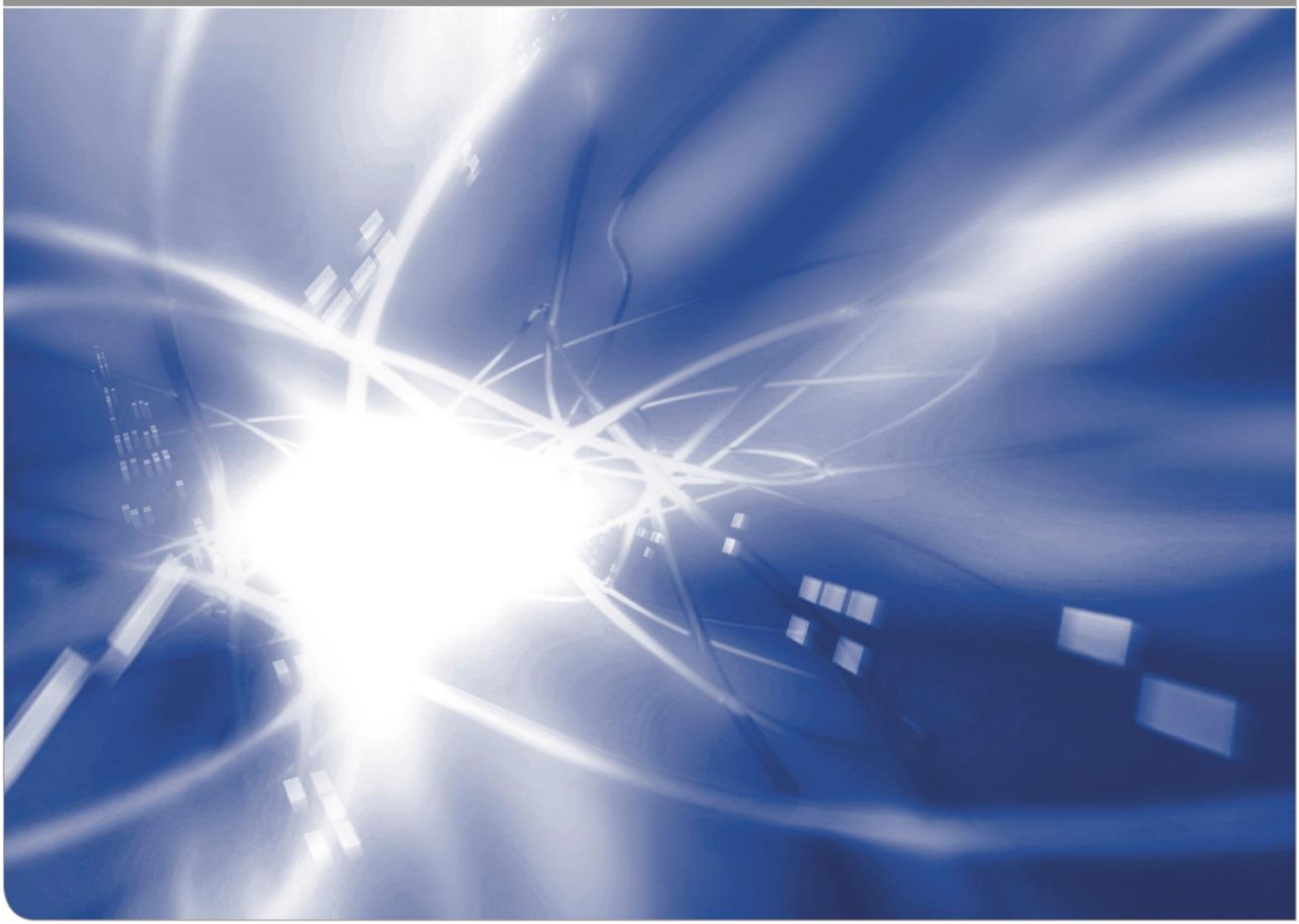

Institut für Nuklear Entsorgung (INE)

Das diesem Bericht zugrundeliegende Vorhaben wurde mit Mitteln des Bundesministeriums für Wirtschaft und Energie (BMWi) unter dem Förderkennzeichen 02E11334C gefördert. Die Verantwortung für den Inhalt dieser Veröffentlichung liegt bei den Autoren.

Gefördert durch:

Bundesministerium für Wirtschaft und Energie

aufgrund eines Beschlusses des Deutschen Bundestages

Institut für Nukleare Entsorgung (INE)

Hermann-von-Helmholtz-Platz 1
76344 Eggenstein-Leopoldshafen
www.ine.kit.edu

Impressum

Karlsruher Institut für Technologie (KIT)
www.kit.edu

2020

ISSN: 2194-1629
DOI: 10.5445/IR/1000119086

Inhaltsverzeichnis

A. Deutschsprachige Zusammenfassung

Die von KIT-INE innerhalb des Verbundprojekts EDUKEM durchgeführten Arbeiten liefern ein verbessertes wissenschaftliches Verständnis der Chemie von Uran in wässrigen Lösungen. Die Arbeiten fokussieren auf vier Unterthemen, (i) Redoxchemie von Uran, (ii) Löslichkeitsbegrenzung von Uran(VI) und Uran(IV), (iii) Hydrolysereaktionen und (iv) Carbonatkomplexierung. Die Studien tragen zu einer verbesserten Beschreibung der Uranchemie im Kontext des Safety Case bei, und liefern zudem grundlegende Informationen zu anderen Forschungsfeldern, in denen eine quantitative Beschreibung der wässrigen Uranchemie notwendig ist. Die gewählten experimentellen (geo)chemischen Randbedingungen in den Arbeiten von KIT-INE umfassen stark saure bis hyperalkalische pH_m-Bedingungen, decken den gesamten Bereich von oxidierenden bis stark reduzierenden Redoxbedingungen ab, und behandeln verdünnte bis hochkonzentrierte wässrige Salzlösungen. Es werden Studien mit hexavalentem U(VI) durchgeführt, stellvertretend für oxidierende oder redox-neutrale geochemische Bedingungen, sowie mit tetravalentem U(IV), welches unter den im Endlager zu erwartenden stark reduzierenden Bedingungen vorliegt. Der Fokus liegt auf Systemen und Bedingungen, für die relevante Lücken in der thermodynamischen Beschreibung identifiziert wurden, oder auf Themen der Uranchemie, die in der Fachöffentlichkeit aufgrund von vorhandenen Kenntnisdefiziten ungeklärt sind und kontrovers diskutiert werden. Einige der gewählten experimentellen Randbedingungen können als repräsentativ für bestimmte Wirtsgesteine (z.B. Kristallin, Ton, Salz) oder Abfallformen (z.B. zementierte Abfälle) angesehen werden, und liefern potentiell direkte Informationen für einen spezifisch anwendungsorientierten Bezug im Kontext der Endlagerung langlebiger radioaktiver Stoffe. Die Arbeiten wurden im Kontrollbereich des KIT-INE durchgeführt, und nutzen die dort vorhandenen vielfältigen modernen analytischen bzw. spektroskopischen Möglichkeiten.

Das <u>Redoxverhalten von Uran</u> wurde in verdünnten bis konzentrierten NaCl-Lösungen unter reduzierenden Bedingungen über den gesamten pH_m-Bereich, von sauren bis hyperalkalischen Bedingungen, untersucht. Die Arbeiten liefern neue Erkenntnisse zu relevanten Redoxtransformationsprozessen, insbesondere hinsichtlich der Reduktion von U(VI) zu U(IV) in wässrigen Systemen. Zudem konnten zuverlässige Methoden zur chemischen Stabilisierung von reduziertem U(IV) in Lösung etabliert werden, was einen entscheidenden Einfluss auf die Planung und Durchführung weiterführender experimenteller Studien im U(IV)-System hat. Die Experimente decken einen breiten pH_m-Bereich ab, und untersuchen grundlegende Prozesse, auch durch systematische Variation von Redoxbedingungen und redoxaktiven Chemikalien.
Die im Rahmen von EDUKEM von KIT-INE neu gewonnenen Löslichkeitsdaten, in Kombination mit Flüssig-Flüssig-Extraktion und XANES, bestätigen, dass U(VI) in reduzierenden aquatischen

Systemen mit ($pe + pH_m$) ≤ 4) zu U(IV) reduziert wird, wobei die Transformationsprozesse stark von Kinetik überprägt sind. Die Reduktion von U(VI) erfolgt in zwei Schritten, wobei in einem ersten Schritt die schnelle Ausfällung einer U(VI)-Festphase erfolgt, die in einem zweiten, langsameren Schritt, in die UO_2(am,hyd) Festphase reduziert wird. Die geochemischen Hauptparameter, die diesen Prozess kontrollieren, sind die initiale U(VI)-Konzentration $[U(VI)]_0$, pH_m, das Redoxpotential E_h, die Konzentration an redox-aktiven Chemikalien, die Verfügbarkeit von redox-aktiven Oberflächen sowie die Gesamtkonzentration an NaCl (in alkalischen Systemen). Unter den ungünstigsten untersuchten experimentellen Bedingungen wurde die vollständige Reduktion erst nach 635 Tagen beobachtet. Die pH_m-unabhängige Uranlöslichkeit, die nach Erreichen der Gleichgewichtsbedingungen im schwach sauren bis hyperalkalischen Bereich (bis $pH_m \approx 14.5$) beobachtet wurde, bestätigt das Vorliegen der wässrigen $U(OH)_4$(aq)-Spezies im Gleichgewicht mit der löslichkeitsbestimmenden Festphase UO_2(am,hyd). Dieser Befund zeigt eindeutig, dass die in früheren kontrovers diskutierten Arbeiten postulierten anionischen Hydrolysespezies ($U(OH)_5^-$ und $U(OH)_6^{2-}$) keine relevante Rolle in der Lösungschemie von U(IV) in stark alkalischen Systemen besitzen, wie sie z.B. in der Umgebung von zement-basierten Materialien auftreten können. Die exzellente Übereinstimmung von experimentellen Arbeiten und thermodynamischen Modellrechnungen bestätigen die Verwendung der Größe ($pe + pH_m$) als Parameter einer belastbaren Vorhersage der Uran-Redoxchemie unter verdünnten bis hochsalinaren endlagerrelevanten Bedingungen. Die systematische Untersuchung des Einflusses von redox-aktiven Chemikalien zur Stabilisierung stark reduzierender Bedingungen in den Experimenten, z.B. Sn(II), $Na_2S_2O_4$ oder gemischte (Sn(II) + TiO_2, Sn(II) + Fe(0) und Sn(II) + Fe_3O_4(cr)) Systeme, erlaubt die Etablierung von zuverlässigen chemischen Methoden für die Redoxstabilisierung der tetravalenten U(IV)-Oxidationsstufe. Dieses hat eine wichtige Bedeutung für die Planung und Durchführung belastbarer experimenteller Arbeiten in diesem System, und kann perspektivisch in der Zukunft für verschiedene weiterführende Arbeiten zur U(IV)-Chemie verwendet werden.

Die <u>Löslichkeit von U(VI)</u> wurde in verdünnten bis konzentrierten NaCl-, KCl- und $MgCl_2$-Lösungen über den gesamten sauren bis hyperalkalischen pH_m–Bereich untersucht. Die löslichkeitsbestimmenden U(VI)-Festphasen wurden durch XRD, SEM-EDS, TG-DTA, quantitative chemische Analyse und XAFS detailliert analysiert und charakterisiert. In sauren NaCl-Lösungen und in allen untersuchten $MgCl_2$-Systemen, konnte $UO_3 \cdot 2H_2O$(cr) (Metaschöpit) als einzige relevante U(VI)-Festphase im untersuchten System identifiziert werden. Die Festphasen $Na_2U_2O_7 \cdot H_2O$(cr) und $K_2U_2O_7 \cdot 1.5H_2O$(cr) sind die löslichkeitsbestimmenden U(VI)-Festkörper in alkalischen NaCl- und KCl-Systemen. Auf Basis von U(VI)-Löslichkeitsdaten, spektroskopischen Analysen, detaillierter Festphasencharakterisierung und der Auswertung von potentiometrischen Befunden aus der Literatur, konnte ein konsistenter und umfassender Satz an

thermodynamischen Konstanten und (SIT, Pitzer) Aktivitätskoeffizienten für das System UO_2^{VI}–H^+–K^+–Na^+–Mg^{2+}–Cl^-–OH^-–H_2O(l) abgeleitet werden. Die neu entwickelten thermodynamischen Modelle sind ein belastbares Werkzeug für die Berechnung von U(VI)-Löslichkeitsbegrenzungen und der U(VI)-Speziation in verschiedenen endlagerrelevanten Systemen. Die innerhalb von EDUKEM gewonnenen Daten und Modellparameter können für Datenbasisprojekte wie THEREDA oder die NEA-TDB zu Verfügung gestellt werden.

Die Löslichkeit von U(VI) wurde zusätzlich bei Anwesenheit von Carbonat und Calcium im pH_m-neutralem Bereich analysiert. Obwohl die Bildung und thermodynamische Stabilität der wässrigen Ca–U(VI)–CO_3 Komplexe seit längerem in der Literatur dokumentiert ist, sind zuverlässige Löslichkeitsstudien der analogen ternären Festphasen nur unzureichend vorhanden. Die im Rahmen von EDUKEM von KIT-INE durchgeführten Arbeiten bestätigen, dass Liebigit $Ca_2UO_2(CO_3)_3 \cdot 9H_2O$(cr) die U(VI)-Löslichkeit im ternären System Ca–U(VI)–CO_3 in verdünnten (≤ 0.5 M) NaCl Lösungen bestimmt. In pH_m-neutraler 5.0 M NaCl-Lösung transformiert Liebigit in Andersonit $Na_2CaUO_2(CO_3)_3 \cdot xH_2O$(cr). Andersonit besitzt, relativ zur Löslichkeit von Liebigit in verdünnten wässrigen Systemen (log [U] ≈ –2), eine signifikant geringere Löslichkeit in NaCl-reichen carbonathaltigen Lösungen (log [U] ≈ –4).

Arbeiten von KIT-INE zum Einfluss von Nitrat auf die U(VI)-Löslichkeit wurde in konzentrierten NaCl-, $CaCl_2$- und $MgCl_2$-Lösungen bei hohen Nitratkonzentrationen (>1 M) durchgeführt, und zeigen keinerlei löslichkeitserhöhende Effekte verglichen mit der U(VI)-Löslichkeit in analogen nitratfreien Systemen. Angesichts dieses Befundes erscheint eine spezifische thermodynamische Beschreibung dieser Systeme als nicht notwendig.

Die <u>Uran(IV)-Löslichkeit</u> wurde über den gesamten sauren bis hyperalkalischen pH_m-Bereich in verdünnten bis konzentrierten NaCl-, $MgCl_2$- und $CaCl_2$-Lösungen untersucht, wobei die im Rahmen der Redoxstudien von KIT-INE innerhalb von EDUKEM neu etablierten chemischen Verfahren zur Stabilisierung von U(IV) zum Einsatz kamen. Eine größere Menge einer U(IV)-Oxyhydroxid-Festphase wurde zur späteren Verwendung in U(IV)-Löslichkeitsexperimenten in einer Ar-Box unter alkalischen und reduzierenden Bedingungen synthetisiert, und über drei Monate hinweg equilibriert. Die detaillierte Analyse dieser Festphase mittels XRD, EXAFS, SEM-EDS, TG-DTA und quantitativer chemischer Analyse bestätigt die erwartete Bildung einer (nano-)kristallinen $UO_2 \cdot H_2O$(ncr) Festphase.

In reduzierenden sauren NaCl- und $MgCl_2$-Lösungen zeigt die Löslichkeit von $UO_2 \cdot H_2O$(ncr) einen starken Anstieg mit zunehmendem pH_m. Obwohl diese Daten einen sehr ähnlichem Trend hinsichtlich der Abhängigkeit von log [U] *vs.* pH_m zeigen, sind die im Rahmen dieser Arbeit gewonnenen U(IV)-Löslichkeitsdaten um etwa zwei Größenordnungen niedriger als die meisten bisher mit der UO_2(am,hyd) Festphase durchgeführten Löslichkeitsstudien. Dieses Verhalten ist eindeutig mit der höheren Kristallinität (und somit höheren thermodynamischen Stabilität) der

im Rahmen von EDUKEM präparierten U(IV)-Festphase korreliert. Abhängig von der Ionenstärke zeigen die Löslichkeitsdaten oberhalb von $pH_m \approx 4 / 5$ ein pH_m-unabhängiges Verhalten, bei deutlich niedrigeren Konzentrationen als in früheren Arbeiten mit stärker amorphem UO_2(am,hyd) Bodenkörper gefunden wurden. In Bestätigung der von KIT-INE durchgeführten Uran-Redoxexperimente zeigen die Löslichkeitsstudien eindeutig die Prädominanz der gelösten $U(OH)_4$(aq)-Spezies in dem hyperalkalinen pH_m-Bereich. Hierdurch kann das Vorliegen von anionischen U(IV)-Hydrolysespezies in hyperalkalischen Systemen eindeutig ausgeschlossen werden. Sämtliche U(IV)-Löslichkeitsexperimente in $CaCl_2$–Lösungen liegen unterhalb der Nachweisgrenze von ICP–MS. Obwohl die anhand der Analogie mit anderen tetravalenten Actiniden (Th(IV), Np(IV), Pu(IV)) erwartete Bildung des ternären Komplexes $Ca_4[U(OH)_8]^{4+}$ unter den gegebenen experimentellen Randbedingungen nicht explizit nachgewiesen werden konnte, sind die im Rahmen dieser Arbeit abgeleiteten Obergrenzen für log $*\square^\circ_{(4,1,8)}$ konsistent mit den Abschätzungen in Fellhauer *et al.* (2010). Die im Rahmen von EDUKEM von KIT-INE durchgeführten Arbeiten zur U(IV)-Löslichkeit stellen einen wichtigen Beitrag zu Berechnung von Löslichkeitsbegrenzungen dar, und stellen darüber hinaus, eine belastbare experimentelle Basis zu Verfügung, um im Rahmen von U(IV)-Löslichkeitsexperimenten den Einfluss von zusätzlichen potentiell komplexierenden Liganden auf die U(IV)-Löslichkeit untersuchen zu können. Ein löslichkeitserhöhender Einfluss von Liganden kann direkt gegen die vorhandenen bekannten Löslichkeitsdaten im reinen System verglichen und ggf. quantifiziert werden.

Die Kombination der neuen U(IV)-Löslichkeitsstudien von KIT-INE im Rahmen von EDUKEM, mit detaillierter Festphasencharakterisierung und thermodynamischen Daten für U(IV)-Hydrolysespezies aus NEA–TDB und Neck und Kim (2001), erlaubt die Ableitung konsistenter thermodynamischer Daten und Aktivitätskoeffizienten für das umfangreiche System U^{IV}–Na^+–Mg^{2+}–Ca^{2+}–H^+–Cl^-–OH^-–H_2O(l). Die durchgeführten Arbeiten stellen die bisher umfassendste experimentelle Basis im Kontext thermodynamischer Studien im U(IV)-System dar, wobei explizit die ausgesprochen detaillierten Analysen der löslichkeitsbestimmenden U(IV)-Oxyhydroxid-Festphasen hervorgehoben werden muss. Die thermodynamischen Daten und Modellparameter können in Datenbasisprojekte wie THEREDA oder NEA-TDB implementiert werden.

Die Löslichkeit von U(IV) ist in alkalischen NaCl-Lösungen bei Anwesenheit von Carbonat relativ zum carbonat-freien System signifikant um ca. 3 log_{10}-Einheiten erhöht. Auf Basis von Analysen der Steigung von Löslichkeitskurven (log [U(IV)] vs. pH_m), und der thermodynamischen Analyse von U(IV)-Löslichkeitsdaten bei unterschiedlichen Carbonatkonzentrationen und Ionenstärken, konnte ein konsistentes chemisches Modell abgeleitet werden, in welchem der beobachtete Löslichkeitsanstieg eindeutig mit dem dominant vorliegenden ternären Komplex $U(OH)_2(CO_3)_3^{4-}$ korreliert werden kann. Der analoge ternäre Komplex gleicher Stöchiometrie konnte in separaten Studies von KIT-INE (innerhalb des ENTRIA-Projekts) für Np(IV)- und Pu(IV)-Systeme

identifiziert werden. Diese Befunde unterscheiden sich deutlich von früheren Studien von Altmaier et al. im Th(IV)-System (2005, 2006), in denen bei Anwesenheit von Carbonat, unter vergleichbaren (geo)chemischen Bedingungen, die prädominant vorliegenden Th(IV)-Komplexe $Th(OH)(CO_3)_4^{5-}$ und $Th(OH))_2(CO_3)_2^{2-}$ identifiziert wurden. Der Unterschied zwischen Th(IV) und anderen tetravalenten Actiniden (An(IV), mit An = U, Np und Pu) ist höchstwahrscheinlich mit Unterschieden in den Ionenradien der jeweiligen An^{4+}-Kationen begründet, die sich auch in einer deutlich geringeren Hydrolysetendenz von Th(IV) verglichen mit U(IV), Np(IV) und Pu(IV) wiederspiegelt. Diese Differenzen im chemischen Verhalten sind relevant hinsichtlich der Verwendung von Th(IV) als direktes chemisches Analog für andere tetravalente Actiniden, und beeinträchtigt die Entwicklung von thermodynamischen Modellen auf Basis des Analogieprinzips. Die neu abgeleiteten chemischen und thermodynamischen Daten und Modellparameter für das U(IV)-OH-CO_3 System können in nationalen (THEREDA) und internationalen (NEA-TDB) Datenbasisprojekte berücksichtigt werden.

B. Beschreibung der durchgeführten Arbeiten von KIT-INE innerhalb EDUKEM

1. Introduction and scope of work

Uranium is the main element present in spent nuclear fuel and accordingly contributes with the largest inventory to the nuclear waste. Although with a relatively minor contribution to the overall dose of the waste, "UO_2" is the matrix embedding all other radionuclides in spent fuel, which requires an accurate knowledge on the solution chemistry and solubility phenomena. Uranium is also a redox-sensitive actinide, and accordingly, its chemical behavior is strongly dependent on the redox boundary conditions of the system. Disposal of spent fuel in deep geological formations such as crystalline/granite, clay and rock salt is the option favored by international consensus. Water intrusion is a possible scenario that needs to be accounted for in the context of the long-term Safety Assessment of these repositories. The composition of the pore water contacting the waste will largely vary depending upon host-rock, backfill and other technical barriers, as well as the waste itself. Although a vast number of studies have previously investigated the solution chemistry of uranium, a number of key fundamental uncertainties remain. These affect to redox behavior, solid phases controlling solubility, hydrolysis and carbonate complexation, especially in the alkaline to hyperalkaline pH conditions of relevance in the context of nuclear waste disposal. Source term estimations (*i.e.* robust limiting values of the aqueous radionuclide concentration in the vicinity of the waste) are determined from the solubility limits using reliable experimental data and quality assured thermodynamic constants and parameters. Although thermodynamic data available for aqueous actinide systems is very extensive for acidic pH conditions, dedicated thermodynamic studies targeting alkaline conditions of relevance in nuclear waste disposal are instead very limited.

In this context, this work aims at a comprehensive description of four main aspects of the solution chemistry of uranium, namely redox processes, solubility phenomena, hydrolysis and complexation with carbonate. The study covers from very acidic to hyperalkaline pH conditions, tackles oxidizing to very reducing systems and extends from dilute to very concentrated salt systems. Both the hexavalent U(VI) oxidation state, predominant under oxidizing to redox neutral conditions, and the tetravalent U(IV) oxidation state, relevant for strongly reducing conditions as expected in a nuclear waste repository, were investigated. Studies on redox transformation processes in the uranium system and improved chemical redox stabilization methods for U(IV) in experimental studies were integrated in EDUKEM as a key contribution from KIT-INE. Although the work is mostly intended for a fundamental understanding of these main aspects / processes, some of the investigated systems cover boundary conditions of high relevance in different repository concepts for nuclear waste disposal, thus providing insight on the retention and migration behaviour of uranium in such conditions. The combination of fundamental research with an applied character is highlighted throughout the discussion of the results obtained within

this project. As ultimate goals, this work aims at providing robust solubility upper limits to be considered in source term estimations, as well as at deriving comprehensive thermodynamic and (SIT, Pitzer) activity models for systems of relevance in the context of nuclear waste disposal. These thermodynamic data can be implemented in thermodynamic databases (*i.e.* NEA–TDB, THEREDA) and further used in geochemical calculations of relevance in the framework of the nuclear waste disposal Safety Case.

2. Excecutive summary

The work performed by KIT-INE within EDUKEM is providing improved fundamental scientific understanding on the solution chemistry of uranium, with focus on four main aspects, namely redox behavior, solubility, hydrolysis and complexation with carbonate. This contributes to an improved scientific description of uranium chemistry in the context of the nuclear waste disposal Safety Case, and other fields of environmental concern where a quantitative description of uranium solubility and speciation is required. The geochemical boundary conditions investigated in this project by KIT-INE systematically cover from very acidic to hyperalkaline pH_m values, from very reducing to oxidizing, and from dilute solutions to concentrated salt brine systems. Focus is given to conditions and systems for which relevant thermodynamic datagaps have been identified or controversial discussions are ongoing in the interested scientific/technical community. Some of these conditions are representative of different potential repository concepts (*e.g.* crystalline, clay, salt-rock) or wasteforms (e.g. cementitious systems), and can provide relevant direct input to specific application oriented topics in the context of nuclear waste disposal. The reported studies were performed in the controlled area of KIT-INE, making use of the excellent analytical and spectroscopic tools available for the work on radionuclides at this facility.

The **redox behaviour of uranium** was investigated in reducing, dilute to concentrated NaCl solutions from acidic to hyperalkaline pH_m conditions. The work provides new insight into relevant uranium redox transformation processes, especially regarding the reduction of U(VI) to U(IV) in aqueous solution, but also provides important information on reliable chemical U(IV) redox stabilisation methods as prerequisite for targeted experimental studies in the highly repository relevant U(IV) system. Studies are performed over a wide pH_m range and systematically investigate processes, also considering systematic variations in overall redox conditions and redox active chemicals.

Solubility data, in combination with solvent extraction and XANES confirm that U(VI) is reduced to U(IV) in reducing systems with $(pe + pH_m) \leq 4$, although the reduction process is strongly affected by kinetics. The reduction occurs in two steps, involving a first, fast precipitation of a U(VI) solid phase, and a second, slower reaction with the transformation of this solid phase into UO_2(am, hyd). The main parameters affecting the reduction kinetics are identified as $[U(VI)]_0$, pH_m, E_h, concentration of the reducing chemicals, presence of redox-active surfaces and [NaCl] (in alkaline systems). In the less favoured conditions of our study, a complete reduction is only observed after 635 days. The pH_m-independent solubility observed (after attaining equilibrium conditions) from weakly acidic to hyperalkaline conditions (up to $pH_m \approx 14.5$) confirms the predominance of $U(OH)_4$(aq) in the aqueous phase, in equilibrium with UO_2(am, hyd). These results clearly disregard a predominant role of anionic hydrolysis species ($U(OH)_5^-$ and $U(OH)_6^{2-}$) in the solution chemistry of U(IV), as was controversially proposed and discussed in previous literature. The excellent agreement between experimental

observations obtained in this work and thermodynamic calculations supports the use of (pe + pH_m) measurements as an accurate tool to predict the redox behaviour of uranium in dilute to concentrated saline systems under repository relevant boundary conditions. The systematic investigation of redox active chemicals in the studies of KIT-INE within EDUKEM, e.g. Sn(II), $Na_2S_2O_4$ or mixed (Sn(II) + TiO_2, Sn(II) + Fe(0) and Sn(II) + Fe_3O_4(cr)) reducing systems, allowed to establish highly reliable chemical methods for the stabilization of tetravalent uranium, the relevant uranium oxidation state expected under the strongly reducing conditions of an operative nuclear waste repository. This has significant impact on designing reliable experimental studies in the U(IV) system and can be used in future studies related to aquatic U(IV) chemistry.

The **solubility of U(VI)** was investigated in dilute to concentrated NaCl, KCl and $MgCl_2$ systems from acidic to hyperalkaline pH_m conditions. Solid phases were thoroughly characterized using XRD, SEM-EDS, TG-DTA, quantitative chemical analysis and XAFS. In acidic NaCl solutions and in all investigated $MgCl_2$ systems, $UO_3{\cdot}2H_2O$(cr) was identified as the only solid phase controlling the solubility of U(VI). On the other hand, $Na_2U_2O_7{\cdot}H_2O$(cr) and $K_2U_2O_7{\cdot}1.5H_2O$(cr) are the solid phases controlling the solubility in alkaline NaCl and KCl systems, respectively. Based on the combination of the solubility measurements, spectroscopic data, solid phase characterization, as well as potentiometric data available in the literature, chemical, thermodynamic and (SIT, Pitzer) activity models for the system UO_2^{VI}–H^+–K^+–Na^+–Mg^{2+}–Cl^-–OH^-–H_2O(l) were derived. These models represent an accurate and robust tool for the calculation of U(VI) solubility and aqueous speciation in a variety of geochemical conditions relevant in the context of nuclear waste disposal and will be contributing to database projects like THEREDA or NEA-TDB.

The solubility of U(VI) was also investigated in the presence of carbonate and calcium under near-neutral pH_m conditions. Although the formation and stability of ternary aqueous complexes Ca–U(VI)–CO_3 have been reported in the literature, solubility studies of the analogous ternary solid phases are very sparse. Solubility studies conducted within this work confirm that liebigite, $Ca_2UO_2(CO_3)_3{\cdot}9H_2O$(cr), controls the solubility of uranium for the ternary system Ca–U(VI)–CO_3 in dilute ($\leq$ 0.5 M) NaCl solutions. On the other hand, liebigite transforms into andersonite, $Na_2CaUO_2(CO_3)_3{\cdot}xH_2O$(cr), in near-neutral 5.0 M NaCl solutions. The latter phase defines a significantly lower solubility of U(VI) in concentrated NaCl systems containing carbonate (log [U] $\approx$ –4), compared to the solubility of liebigite in dilute systems (log [U] $\approx$ –2).

Studies on the impact of dissolved nitrate on U(VI) solubility were performed in concentrated NaCl, $CaCl_2$ and $MgCl_2$ solution and indicate no significant increase in U(VI) concentrations relative to the U(VI)-concentration level defined by hydrolysis processes under the absence of nitrate. In view of these findings, no chemical or thermodynamic models were developed for these systems.

U(IV) solubility was investigated in reducing, dilute to concentrated NaCl, $MgCl_2$ and $CaCl_2$ solutions under acidic to hyperalkaline pH_m conditions. A U(IV) solid phase was precipitated in alkaline, reducing conditions and aged for three months before further use in solubility experiments. A thorough characterization of this solid using XRD, EXAFS, SEM-EDS, TG-DTA and quantitative chemical analysis confirmed the formation of a (nano-)crystalline $UO_2 \cdot H_2O$(ncr) phase.

In acidic NaCl and $MgCl_2$ solutions, the solubility of $UO_2 \cdot H_2O$(ncr) shows a steep decrease with increasing pH_m. Although following a very similar trend in terms of log [U] *vs.* pH_m, solubility data determined in this work is approximately two orders of magnitude lower than most of the previous solubility studies with UO_2(am, hyd). This observation highlights the more crystalline character of the solid phase compared to previous solubility studies. Solubility data measured above $pH_m \approx 4 / 5$ (depending upon ionic strength) show a pH_m-independent behaviour and are significantly lower than previous studies with UO_2(am, hyd). As in the case of redox experiments, these results support the predominance of $U(OH)_4$(aq) in solution for this pH_m-range, thus ruling out a predominant role of anionic hydrolysis species of U(IV) in hyperalkaline systems. All solubility measurements in $CaCl_2$ solutions resulted below the detection limit of standard ICP–MS. Although unable to confirm the formation of the ternary complex $Ca_4[U(OH)_8]^{4+}$ expected in analogy to the previously reported species for Th(IV), Np(IV) and Pu(IV), upper limits derived in this work for log $*\beta^\circ_{(4,1,8)}$ are consistent with the estimates provided in Fellhauer *et al.* (2010) based upon linear free energy relationships. The reported studies by KIT-INE on U(IV) solubility offer highly robust experimental "baseline information" for the study of U(IV) complexation reactions using a solubility approach (see studies on carbonte below), as the impact of additional ligands can be evaluated directly against the corresponding systems under absence of complexing ligands.

The combination of solubility data determined in the present work, solid phase characterization and thermodynamic data reported in the NEA–TDB and Neck and Kim (2001) for U(IV) hydrolysis species allowed deriving accurate thermodynamic and activity models for the system U^{IV}–Na^+–Mg^{2+}–Ca^{2+}–H^+–Cl^-–OH^-–H_2O(l). This is the most comprehensive thermodynamic study undertaken so far for U(IV) and especially is involving the most accurate solid phase characterization of the solubility-controlling U(IV)-oxohydroxide phase. The generated thermodynamic data feed into thermodynamic database projects, e.g. THEREDA or NEA-TDB.

The solubility of U(IV) is significantly enhanced in alkaline NaCl solutions containing carbonate (up to 3 log_{10}-units), compared to carbonate-free systems. Slope analyses and fit of solubility data at different carbonate concentrations and ionic strengths result in a consistent chemical model, where the enhanced solubility can be properly explained by the definition of the complex $U(OH)_2(CO_3)_3^{4-}$. The same ternary complex has been reported in analogous solubility studies with Np(IV) and Pu(IV). These observations differ from previous solubility studies with Th(IV) in the presence of carbonate, which identified the predominance of the ternary complexes $Th(OH)(CO_3)_4^{5-}$ and $Th(OH)_2(CO_3)_2^{2-}$ under analogous

conditions. The discrepancies between Th(IV) and other An(IV) (with An = U, Np and Pu) probably reflect differences in size between the corresponding An^{4+} cations, which are also responsible for the significantly weaker hydrolysis of Th(IV), compared to U(IV), Np(IV) and Pu(IV). Such differences pose questions on the use of Th(IV) as analogue of other tetravalent actinides and affect the development of thermodynamic model using the analogy concept. The chemical and thermodynamic data derived for the U(IV)-OH-CO_3 systems will contribute to national (THEREDA) and international (NEA-TDB) database projects, amongs others.

3. Experimental

3.1 Chemicals. pH and E_h measurements

All solutions were prepared with ultrapure water purified with Milli-Q-academic apparatus (Millipore Milli-Q Advantage A10 with Millipore Millipak® 40 0.22 μm; 18.2 MΩ·cm at 25°C, 4 ppb TOC) and purged with Ar during 1 hour before use. All sample/solid preparation steps were carried out in an Ar-glove box (< 1 ppm O_2) at T = (22 ± 2) ºC. All chemicals used were of reagent grade or above. A nitrate-free 0.42 M $^{238}UO_2Cl_2$ stock solution and uranyl nitrate ($UO_2(NO_3)_2 \cdot 6H_2O$, Merck) were used to prepare samples in all experiments.

A combination glass pH electrode (type ROSS, Orion), freshly calibrated against dilute standard pH buffers (pH 1–13, Merck), was used to determine the molal H^+ concentration, $[H^+]$ (with $pH_m = -\log [H^+]$). In salt solutions of ionic strength $I \geq 0.1$ m, the measured pH value (pH_{exp}) is an operational value related to $[H^+]$ by $pH_m = pH_{exp} + A_m$, where A_m is given as a function of the NaCl, KCl, $MgCl_2$ and $CaCl_2$ concentration [2003ALT/MET, 2008ALT/NEC, 2017BAU/YAL]. This approach is equivalent to calibrating the electrode vs. standard samples with fixed proton concentration at constant background electrolyte concentrations and relates the potential In those systems with $[H^+] > 0.01$ M or $[OH^-] > 0.01$ M, pH_m values were calculated from the initial $[H^+]$ and from the known hydroxide concentration and the conditional ion product (K'_w) of water, respectively. In $MgCl_2$ and $CaCl_2$ solutions, the maximum pH_m values (pH_{max}) are fixed at ~9 and ~12, respectively, by the precipitation of $Mg(OH)_2$(s) and $Ca(OH)_2$(s) (or corresponding hydroxochlorides at Ca/Mg concentrations above ~2 m) [2003ALT/MET].

Redox potentials were measured with a Pt combination electrode with Ag/AgCl reference system (Metrohm) and converted into E_h *vs.* standard hydrogen electrode (SHE) by correcting for the potential of the Ag/AgCl reference electrode at 3 M KCl and 22 °C.

3.2 Redox experiments

The redox behaviour of uranium was investigated in dilute to concentrated NaCl solutions in the presence of individual and mixed reducing chemical systems (Sn(II), $Na_2S_2O_4$, Sn(II) + TiO_2, Sn(II) + Fe(0), Sn(II) + Fe_3O_4). Experiments were performed covering a wide pH range, $2 \leq pH_m \leq 14.5$. In a first step, the inactive background solutions were equilibrated until attaining the targeted, stable pH_m and E_h readings. A nitrate-free U(VI) stock solution was added to the equilibrated background solutions

to obtain initial uranium concentrations of $3.0 \cdot 10^{-5}$ and $4.2 \cdot 10^{-4}$ M, resulting in 40 independent batch samples. The values of E_h, pH_m and uranium concentration (ICP–MS) were monitored at periodic time intervals for up to 635 days. After attaining equilibrium conditions (assumed after constant E_h, pH_m and $[U]_{aq}$ measurements), aqueous and solid phases of selected samples were characterized by solvent extraction and XANES.

3.3 Solubility experiments

3.3.1 Preparation of U(IV) and U(VI) solid phases

UO_2(s, hyd) was obtained from the precipitation in alkaline conditions of an acidic U(IV) stock solution. In a first step, a 0.1 M U(VI) stock solution was prepared in 1.0 M HCl and transferred to a glass vessel with a magnetic stirrer, a Pt-working electrode and two galvanic cells (filled with 1.0 M HCl) containing the Pt-counter electrode (Metrohm) and the Ag/AgCl reference electrode (Metrohm, filled with 3.0 M KCl). The redox potential was adjusted to –280 mV (with respect to the Ag/AgCl reference electrode) by using a potentiostat (Princenton Applied Research, Model 362). In the first four hours of the electrolysis, the color of the solution converted slowly from yellow to pale green, which evolved to a dark green solution after t = 4 hours. The electrolysis process was terminated at $t \approx 10$ hours after ensuring by UV-vis the redox purity of the resulting solution. The pH of the resulting U(IV) solution was shifted to pH ≈ 3 with NaOH. Afterwards, this solution was added drop by drop to a $Na_2S_2O_4$ solution at pH ≈ 12.5 in a Kautex bottle under gentle agitation. The resulting solid was aged during 3 months and characterized (XRD, SEM-EDS, quantitative chemical analysis, TG-DTA, XAFS) before its use in the solubility experiments.

Metaschoepite, $UO_3 \cdot 2H_2O$(cr), was prepared by very slow titration of a 0.01 M U(VI) solution with 0.05 M carbonate-free NaOH. An automatic titroprocessor 686 (Metrohm) was used to add minute amounts of the NaOH solution into the strongly agitated uranium containing solution up to the quantitative precipitation of metaschoepite in the pH range 4 – 5. The resulting solid phase was aged for one week, washed several times with water and dried under Ar-atmosphere at room temperature. Sodium uranate, $Na_2U_2O_7 \cdot xH_2O$(cr), was prepared by solid phase transformation of metaschoepite under alkaline pH conditions. A uranyl nitrate solution was first quantitatively precipitated to pale yellow metaschoepite in a NaCl solution at pH = 4–5 following the approach described above. The metaschoepite was then quickly titrated to pH = 11. The solid phase transformation was completed within one week, resulting in an intense yellow-orange compound. Sodium diuranate was aged for several months at pH = 11 in frequently stirred 1.0 M NaCl. Potassium uranate, $K_2U_2O_7 \cdot xH_2O$(cr), was prepared by the slow addition

of a nitrate-free U(VI) stock solution to a 2.43 M KCl + 0.07 M KOH solution under continuous agitation and pH monitoring. The precipitation and storage of the resulting solid was performed under Ar atmosphere. Approximately 300 mg of solid phase were obtained in this process. The resulting solid phase was aged for 2 months and then characterized using XRD, quantitative chemical analysis using ICP-MS, SEM-EDS and TG-DTA. Liebigite, $Ca_2UO_2(CO_3)_3 \cdot 10H_2O$(cr), was kindly provided by HZDR and thoroughly characterized before its use in solubility experiments.

3.3.2 Preparation of solubility samples

The solubility of U(IV) was investigated from undersaturation conditions in dilute to concentrated NaCl, $MgCl_2$ and $CaCl_2$ solutions at $1.0 \leq pH_m \leq 14.5$. Sn(II) solutions or suspensions as $Sn(OH)_2$(s) (depending on the pH_m) were prepared in the corresponding background electrolyte solutions. The very reducing conditions set by Sn(II) stabilize uranium in the +IV redox state within the complete pH-range investigated. Before the addition of the U(IV) solid phase, the background electrolyte solutions containing Sn(II) were equilibrated during two weeks until attaining stable pH and E_h readings. Finally, 3-5 mg of U(IV) precipitate were added to each sample after washing 3 times with the corresponding pre-equilibrated background electrolyte and added to 2-30 ml of matrix solution. Uranium concentrations, pH_m and E_h values were measured at regular time intervals from 6 to 605 days.

Solubility experiments on the U(IV)-carbonate system were performed from undersaturation conditions in the presence of Sn(II) as reducing chemical. A first series of experiments was conducted in solutions with total carbonate concentrations of $C_{tot} = [HCO_3^-] + [CO_3^{2-}] = 0.1$, 0.04 and 0.015 M at constant ionic strength $I = 0.5$ M $NaHCO_3$–Na_2CO_3–NaCl. A second series of experiments was prepared with $C_{tot} = 0.02$ M at different ionic strengths, $I = 0.1$, 0.5, 2.0 and 4.0 M $NaHCO_3$–Na_2CO_3–NaCl. The pH values in the working solutions were set in the range $8.5 \leq pH_m \leq 12$. A last set of experiments was performed in 0.1 M Na_2CO_3 solutions as a function of [NaOH] = 0.01–0.6 M.

The solubility of $UO_3 \cdot 2H_2O$(cr), $Na_2U_2O_7 \cdot xH_2O$(cr) and $K_2U_2O_7 \cdot xH_2O$(cr) solid phases was studied from undersaturation conditions at $T = (22 \pm 2)$ °C. $UO_3 \cdot 2H_2O$(cr) was equilibrated in independent batch samples with 0.03, 0.5, 2.5 and 5.0 M NaCl at $pH_m \leq 7$. A second series of batch samples with $Na_2U_2O_7 \cdot xH_2O$(cr) was prepared in 0.5, 2.5 and 5.0 M NaCl–NaOH solutions at $8 \leq pH_m \leq 14.5$. A third series of samples in 0.5, 2.5 and 5.0 M NaCl systems was prepared in the presence of both $UO_3 \cdot 2H_2O$(cr) and $Na_2U_2O_7 \cdot xH_2O$(cr), aiming at the characterization of the equilibrium between both solid phases. The solubility of $K_2U_2O_7 \cdot xH_2O$(cr) was investigated in 0.1, 0.5, 1.0, 3.0 and 4.0 M KCl solutions at $7.5 \leq pH_m \leq 14.6$. The pH_m and uranium concentration were measured at regular time intervals from 6 to 250

days. The concentration of U-238 was measured by ICP–MS after phase separation by ultrafiltration (10 kD ≈ 2 nm, Pall Life Science).

The solubility of liebigite, $Ca_2UO_2(CO_3)_3 \cdot 10H_2O$(cr), was investigated from undersaturation conditions. Independent batch experiment containing $Ca_2UO_2(CO_3)_3 \cdot 10H_2O$(cr) were prepared in water, 0.5 and 5.0 M NaCl solutions at $pH_m \approx 8$ to minimize degassing of CO_2(g) and precipitation of calcite. pH_m, [U] and [Ca] were monitored at regular time intervals up to 130 days. Aqueous concentrations of U and Ca were determined by ICP-MS/OES after filtration with 0.1 μm pore size siringes).

Solid phases of selected solubility experiments were characterized by XRD, SEM–EDS, quantitative chemical analysis and TG–DTA, and compared with the „Starting material" and available reference data.

3.4 XANES/EXAFS measurements and data evaluation

Uranium L_{III}-edge (17166 eV) XANES/EXAFS spectra (5–8 replicates per sample) were collected at room temperature under a continuous flow of Ar. The INE-Beamline [2012ROT/BUT] is equipped with a Ge(422) double crystal monochromator (DCM) coupled with a collimating and a focusing Rh coated mirrors before and after the DCM, respectively. The beam spot size on the sample is below 1mm diameter. The DCM-crystals were detuned at 70% and the incident beam intensity was held constant by means of a piezo driven feedback system to the second crystal. The incident and transmitted beam intensities were measured by argon-filled ionization chambers. U L_{III} EXAFS signal was recorded in fluorescence mode using simultaneously 4-elements and 1-element Silicon drift Vortex detectors. The ACT-Beamline [2017ZIM/DAR] is equipped with a pair of Si(311) crystals in the double crystal monochromator (DCM, FMB Oxford, Oxford, United Kingdom). The monochromatic radiation delivered by the DCM is focused by an Rh-coated toroidal mirror into a spot-size below 1 mm diameter at the sample position. A five pixel LEGe solid state detector (Canberra, Olen, Belgium) is used for collecting U L_{III} fluorescence radiation. In both beamlines, the energy calibration was performed by assigning the energy of 17038 eV to the first inflection point of the K-edge absorption spectrum of the Y metal foil, recorded simultaneously in transmission geometry.

XANES/EXAFS data reduction and analysis were performed with the ATHENA/ARTEMIS programs of the Demeter 0.9.26 package following standard procedures [2005RAB/NEW].

4. Results and discussion

4.1. Redox chemistry of uranium

The redox chemistry of uranium was investigated in 0.1 and 5.0 M NaCl solutions with $2 \leq pH_m \leq 14.5$. Individual (Sn(II), $Na_2S_2O_4$) and mixed (Sn(II) + TiO_2, Sn(II) + Fe(0) and Sn(II) + Fe_3O_4(cr)) reducing systems were used in order to follow the reduction kinetics and to evaluate the effect of surfaces on the reduction process. Data were evaluated by systematizing the experimentally measured E_h and pH_m in *Pourbaix* diagrams and comparing the measured uranium concentration of each sample with the calculated U(IV) and U(VI) solubility for the investigated pH_m and [NaCl] conditions. The expected difference in solubility between U(IV) and U(VI) within the complete pH_m-range investigated is taken as main criteria for the evaluation of U(VI) reduction. For selected samples, the oxidation state of uranium in the aqueous and solid phases was additionally investigated by solvent extraction and XANES techniques.

4.1.1 Sn(II) systems in 0.1 and 5.0 M NaCl

The redox behavior of U(VI/IV) was investigated at three Sn(II) concentrations (2, 10 and 20 mM) starting with two different initial uranium concentrations ($4.2 \cdot 10^{-4}$ M and $3.0 \cdot 10^{-5}$ M). Figure 1a shows the monitored E_h-pH_m values in this system during the equilibration time (238 days). All experimental values are below the calculated U(VI/IV) borderline and confirm the strong reducing capacity of Sn(II) regardless of its concentration.

Figure 1b shows the measured uranium concentration in this system together with the solubility of U(VI) ($UO_3 \cdot 2H_2O$(cr) and $Na_2U_2O_7 \cdot H_2O$(cr)) and U(IV) (UO_2(am, hyd)) solid phases calculated for 0.1 M NaCl systems. Measured uranium concentration in the samples with $[U(VI)]_0 = 3.0 \cdot 10^{-5}$ M and [Sn(II)] = 20 mM showed the decrease of uranium concentration to 10^{-8} - 10^{-9} M within 59 days of contact time. This concentration range is in excellent agreement with the solubility expected for UO_2(am, hyd), and clearly below (1 to 3 orders of magnitude, depending upon pH_m) the solubility of $Na_2U_2O_7 \cdot H_2O$(cr). These observations strongly support the complete reduction of the initial U(VI) to U(IV). For the samples with $[U(VI)]_0 = 4.2 \cdot 10^{-4}$ M and [Sn(II)] = 10 mM, reduction started to occur after 59 days, and it is only complete after 238 days. Very slow reduction was observed in the sample containing $[U(VI)]_0 = 4.2 \cdot 10^{-4}$ M, [Sn(II)] = 2 mM and $pH_m = 12.8$. In this case, the solubility control by $Na_2U_2O_7 \cdot H_2O$(cr) was clearly observed with the first drop in uranium concentration to $[U] \approx 10^{-5}$ M within 19 days. This concentration of uranium was retained even at t = 238 days, and only after 635 days uranium

concentration decreased down to 10^{-8} – 10^{-9} M, corresponding to the complete reduction of U(VI) to U(IV). These results most probably indicate that $Na_2U_2O_7{\cdot}H_2O$(cr) and UO_2(am, hyd) solid phases co-exist for a long time until the solid phase transformation is completed. However, the solubility was controlled by the more soluble solid phase in such cases.

Solubility data support that the complete reduction of U(VI) to U(IV) was achieved in all investigated systems, in good agreement with thermodynamic calculations and E_h-pH_m measurements. It must be noted that reduction kinetics are strongly affected by $[U(VI)]_0$, [Sn(II)] and pH_m. The slowest reduction (t = 635 days) was observed in the sample containing the lowest [Sn(II)] (2 mM) and highest $[U(VI)]_0$ ($4.2{\cdot}10^{-4}$ M) at pH_m = 12.8, whereas the fastest reduction ($t \approx 59$ days) was obtained for those samples with highest [Sn(II)] (20 mM) and lowest $[U(VI)]_0$ ($3.0{\cdot}10^{-5}$ M) at $10 \leq pH_m \leq 12$. The slower kinetics especially under alkaline conditions can be explained with the decreasing stability field of U(IV), accordingly resulting in smaller Δpe (as $|pe_{exp} - pe_{borderline}|$) with increasing pH_m (see Figure 1b).

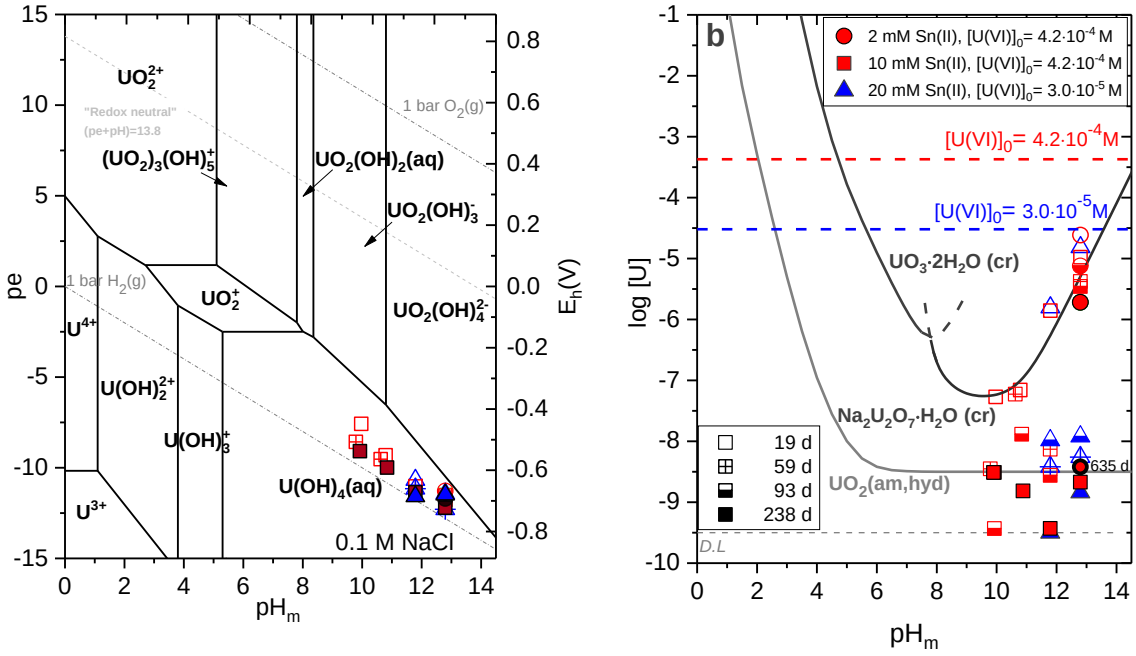

Figure 1. *(a) Pourbaix diagram of uranium calculated for [U] = $3.0{\cdot}10^{-5}$ M and 0.1 M NaCl. (b) concentrations of uranium measured after 10 kD ultrafiltration for 0.1 M NaCl systems with [Sn(II)] = 2, 10 and 20 mM, and $[U(VI)]_0$ = $4.2{\cdot}10^{-4}$ and $3.0{\cdot}10^{-5}$ M. Solid lines correspond to solubility curves of $UO_3{\cdot}2H_2O$(cr), $Na_2U_2O_7{\cdot}H_2O$(cr) and UO_2(am, hyd). Dashed horizontal lines show the initial U(VI) concentrations in the experiments.*

Considering the results above, a set of samples were prepared in the presence of 20 mM Sn(II) with $3 \cdot 10^{-5}$ M initial uranium concentration in 0.1 M NaCl solutions, but extending the pH_m range to 2–13. Sn(II) provides strong reducing conditions (pe + pH_m = 2 ± 1) within the complete pH_m range as shown in Figure 2a. In all cases, experimental (pe + pH_m) values are in the predominance area of U(IV) in the complete pH_m-range investigated.

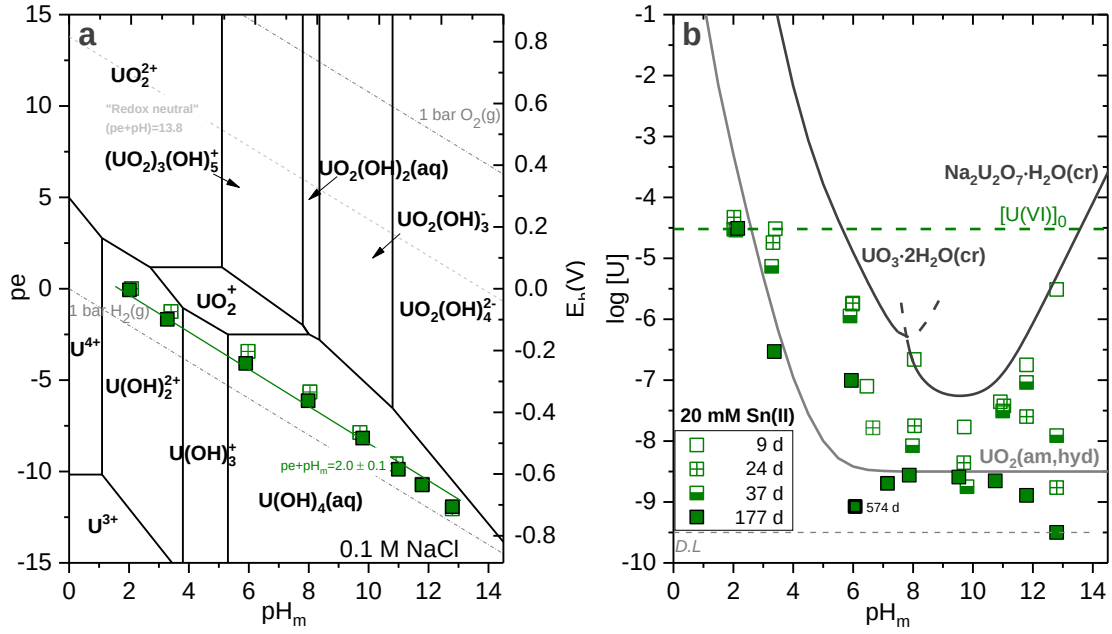

Figure 2. *(a) Pourbaix diagram of uranium calculated for [U] = $3.0 \cdot 10^{-5}$ M and 0.1 M NaCl. (b) Concentrations of uranium measured after 10 kD ultrafiltration for 0.1 M NaCl systems with [Sn(II)] = 20 mM, and $[U(VI)]_0$ = $3.0 \cdot 10^{-5}$ M. Solid lines correspond to solubility curves of $UO_3 \cdot 2H_2O$(cr), $Na_2U_2O_7 \cdot H_2O$(cr) and UO_2(am, hyd). Dashed horizontal line shows the initial U(VI) concentrations in the experiments.*

Figure 2b shows uranium concentrations measured from 9 days up to 177 days. A very significant decrease of [U] in agreement with the reduction of U(VI) to U(IV) was observed within $t \leq 177$ days for those samples at $pH_m \geq 4$. A longer contact time (t = 574 days) was required to observe complete reduction in the sample at pH_m = 5.9, possibly due to the closeness of its (pe + pH_m) to the stability field of U(V) at this pH_m. The reduction behaviour of the sample at pH_m = 2.2 could not be interpreted by the solubility difference of U(VI) and U(IV) solid phases since both solids are completely dissolved at this pH and [U]. Therefore, solvent extraction and XANES analysis are performed for this sample (see Section 3.4). The solubility behaviour of the data obtained within $2 \leq pH_m \leq 12.8$ is in excellent agreement with thermodynamic calculations performed for U(IV). This observation is not only a strong evidence of the complete reduction of U(VI) to U(IV), but also hints towards the expected role of

UO_2(am, hyd) as solubility controlling solid phase in equilibrium with the hydrolysis species proposed in [2001NEC/KIM].

The redox behavior of U(VI/IV) was also investigated in 5.0 M NaCl in the presence of 20 mM Sn(II) with $3 \cdot 10^{-5}$ M initial uranium concentration. Figures 3a and 3b show the *Pourbaix* and solubility diagrams calculated for I = 5.0 M NaCl. The Sn(II/IV) redox couple was impacted by ionic strength, showing slightly less reducing conditions (pe + $pH_m = 4 \pm 1$) in this system. A similar behaviour was reported for Sn(II) solutions in 5.0 M NaCl by Yalcintas *et al.* [2015YAL/GAO]. In all samples, measured E_h values after 178 days were well within the predominance area of U(IV) species. Measured uranium concentrations after 178 days of contact time showed that all the samples in neutral to hyper-alkaline pH region are at the detection limit of ICP-MS (for this NaCl concentration). The slight decrease in uranium concentration observed at $pH_m \approx 4$ is consistent with the reduction of U(VI) to U(IV) and a solubility-control by UO_2(am, hyd). Solvent extraction performed to determine the oxidation state of U in this sample confirmed the predominance of U(IV). The redox behaviour of uranium could not be conclusively evaluated in the samples at pH_m = 7.6 and 11.9. The higher detection limit imposed by the concentrated salt system is indeed consistent (for this pH_m-region) with a solubility control of either $Na_2U_2O_7 \cdot H_2O$(cr) or UO_2(am, hyd). Although the reduction of U(VI) is expected considering that E_h values of both samples are within the stability field of U(IV), it cannot be concluded without further experimental evidences that 178 days are sufficient for the complete reduction to U(IV). Note for instance that up to 574 and 635 days were required in specific systems (see discussion above) to attain the complete reduction of U(VI) into U(IV). Additional insights on the sample at pH_m = 11.9 are gained by XANES analysis as discussed in Section 4.1.3. The clear decrease of [U] observed at pH_m = 13.2 and 14.5 is well below the solubility of $Na_2U_2O_7 \cdot H_2O$(cr), thus strongly supporting the complete reduction to U(IV). No evidence was found indicating the formation of anionic hydrolysis species ($U(OH)_5^-$ and $U(OH)_6^{2-}$) reported previously, even at pH_m = 14.5.

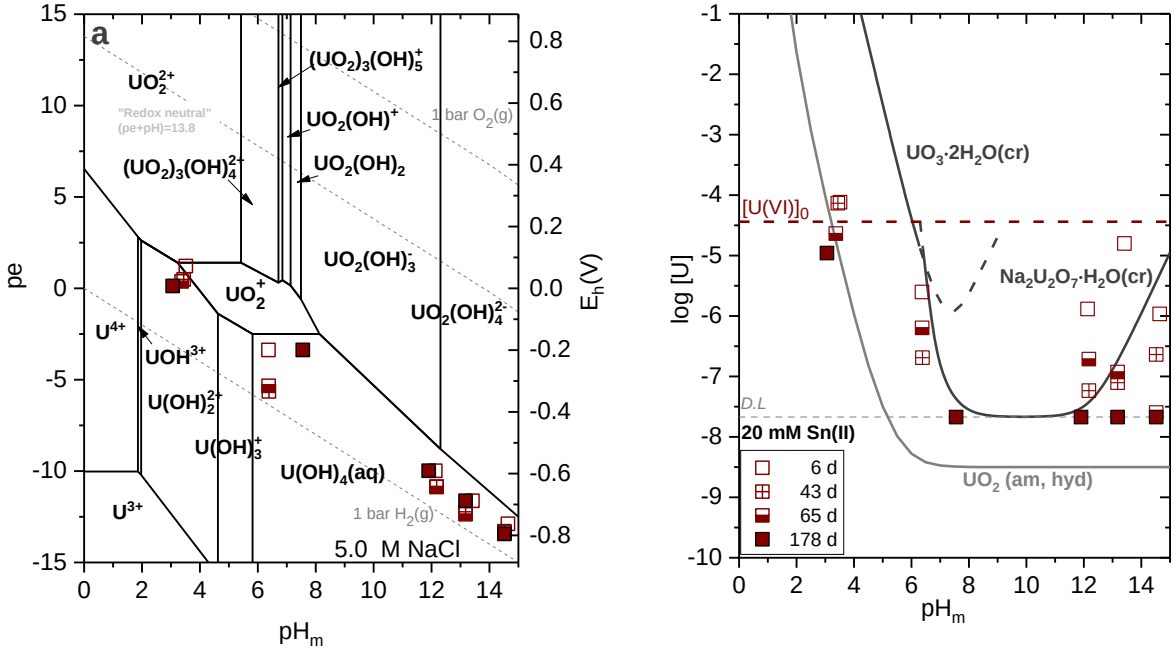

Figure 3. *(a) Pourbaix diagram of uranium calculated for [U] = 3.0·10^{-5} M and 5.0 M NaCl. (b) Concentrations of uranium measured after 10 kD ultrafiltration for 5.0 M NaCl systems with [Sn(II)] = 20 mM, and [U(VI)]$_0$ = 3.0·10^{-5} M. Solid lines correspond to solubility curves of $UO_3{\cdot}2H_2O$(cr), $Na_2U_2O_7{\cdot}H_2O$(cr) and UO_2(am, hyd). Dashed horizontal line shows the initial U(VI) concentrations in the experiments.*

4.1.2 $Na_2S_2O_4$ systems in 0.1 M NaCl

The redox behavior of U(VI/IV) was investigated in the presence of 20 mM $Na_2S_2O_4$ in 0.1 M NaCl solutions at $pH_m \geq 12$. Figure 4a shows that $Na_2S_2O_4$ is a strong reducing system with pe values at the border of water reduction (pe + $pH_m \approx 0$), thus in the stability field of U(IV). A fast decrease of uranium concentration to the solubility limit of U(IV) ($\approx 10^{-9}$ M) was observed within 9 days, indicating the complete reduction of U(VI). Fujiwara *et al.* [2005FUJ/YAM] conducted similar U redox experiments in the presence of $Na_2S_2O_4$, but using higher initial uranium concentration than the present work ($[U(VI)]_0 = 1\cdot10^{-3}$ M). The authors observed relatively higher uranium concentration after 56 days of equilibration time (see Figure 4b), with an increasing trend of the solubility with increasing pH. This observation was explained by the authors with the formation of $U(OH)_5^-$ and $U(OH)_6^{2-}$ species. Note that a very similar increase in uranium concentration under similar reducing conditions was interpreted in [1983RYA/RAI] as the partial oxidation of U(IV) to U(VI). The concentrations of uranium measured

in the present study under hyperalkaline conditions (≈ 10^{-9} M) agree very well with thermodynamic calculations for the solubility of UO_2(am, hyd) in equilibrium with $U(OH)_4$(aq) species, thus disregarding the formation of anionic U(IV) species within the investigated pH_m-range.

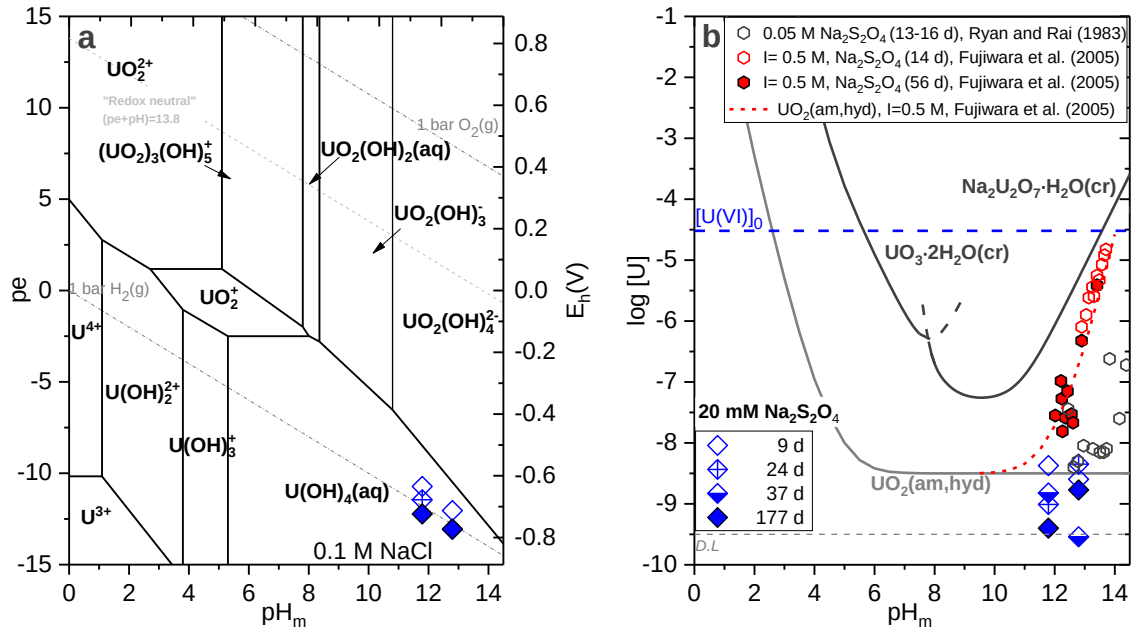

Figure 4. *(a) Pourbaix diagram of uranium calculated for [U] = 3.0·10^{-5} M and 0.1 M NaCl. (b) Red diamonds: concentrations of uranium measured in this work after 10 kD ultrafiltration for 0.1 M NaCl systems with [$Na_2S_2O_4$] = 20 mM and [U(VI)]$_0$ = 3.0·10^{-5} M; red/ black hexagon: solubility data reported in [2005FUJ/YAM] and [1983RYA/RAI], respectively. Solid lines correspond to solubility curves of $UO_3{\cdot}2H_2O$(cr), $Na_2U_2O_7{\cdot}H_2O$(cr) and UO_2(am, hyd). Dashed red line corresponds to the solubility of UO_2(am, hyd) at I = 0.5 M calculated including the formation of $U^{IV}(OH)_5^-$ and $U^{IV}(OH)_6^{2-}$ as reported in [2005FUJ/YAM]. Dashed horizontal line shows the initial U(VI) concentration in the experiments.*

4.1.3 Redox speciation of uranium in the aqueous and solid phases. XANES analysis.

U-L_{III}-edge XANES spectra of selected aqueous (measured at CAT-ACT beamline) and solid samples (measured at INE-beamline) are shown in Figure 5a and Figure 5b. Table 1 summarizes the edge positions of spectra together with the experimental conditions. Some significant differences were observed in the edge position (white line, WL) of solid and aqueous references for U(IV) and U(VI), arising from the use of different beamlines and impact of the difference between aqueous and solid

moieties. Accordingly, spectra collected of unknown aqueous / solid samples were compared with reference spectra of aqueous species/ solid compounds obtained at the same beamline.

XANES spectrum of the aqueous sample containing 20 mM Sn(II) in 0.1 M NaCl at $pH_m \approx 2$ agrees very well with the reference spectrum of U(IV). The combination of this observation with E_h measurements, solubility behaviour and solvent extraction unequivocally confirms the complete reduction of U(VI) to U(IV) in this sample, in agreement with thermodynamic calculations.

Solid phases of two solubility samples were investigated by XANES: (i) 0.1 M NaCl at $pH_m = 10.9$, with 20 mM Sn(II) + 15mg Fe(0), and (ii) 5.0 M NaCl at $pH_m = 11.9$, with 20 mM Sn(II). Figure 5b shows that the edge position of the solid phase equilibrated in 0.1 M NaCl matches very well with the edge position of UO_2(am, hyd) reference. However, a shift to higher energies (≈ +1.5 eV) compared to the U(IV) solid reference was observed in the solid phase equilibrated in 5.0 M NaCl. Although the predominance of U(IV) can be safely proposed based on the absence of the typical shoulder of uranyl/uranate moieties, the shift in energy with respect to U(IV) reference supports that a mixture of U(IV) and U(VI) solid phases is present in the investigated sample. This observation is consistent with the expected slow solid phase transformation of a rapidly precipitated $Na_2U_2O_7 \cdot H_2O$(cr) to UO_2(am, hyd). XANES data under discussion were collected after 330 days of equilibration time, thus indicating that longer equilibration times are needed to achieve a complete reduction at this pH_m in 5.0 M NaCl. Note however that the same equilibration time was sufficient to achieve a complete reduction of U(VI) to U(IV) in a 0.1 M NaCl solution at $pH_m = 10.9$. This observation can be rationalized by considering the equilibrium reaction defining the transformation of $Na_2U_2O_7 \cdot H_2O$(cr) (first, fast precipitated U(VI) solid phase) to UO_2(am, hyd) (end-member, U(IV) solid phase thermodynamically expected):

$$0.5\ Na_2U_2O_7 \cdot H_2O(cr) + 2e^- + 3H^+ \Leftrightarrow UO_2(am, hyd) + Na^+ + 2H_2O(l) \quad (1)$$

Reaction (1) shows that the transformation of $Na_2U_2O_7 \cdot H_2O$(cr) into UO_2(am, hyd) is favoured at lower pH_m, pe and [NaCl], thus providing a consistent picture with XANES data collected for samples in 0.1 M NaCl at $pH_m = 10.9$ (complete reduction after $t = 330$ days) and 5.0 M NaCl at $pH_m = 11.9$ (incomplete reduction after $t = 330$ days). This observation supports again that redox transformations of U(VI) to U(IV) are strongly affected by kinetics.

Table 1. *XANES results of selected aqueous and solid samples. Solid and aqueous, U(IV) and U(VI) references measured at INE- and ACT- Beamline, respectively.*

Sample	pH_m[a]	E_h[b] [mV]	Contact time [days]	Edge position (eV)	Beamline
Solid phase					
Reference $Na_2U_2O_7 \cdot H_2O$(cr)	≈ 12	n. m.		17180.0	INE
Reference UO_2(am, hyd)	≈ 12	n. m.		17177.0	INE
0.1 M NaCl, 20mM Sn(II) + Fe(0)	10.9	–798	330	17177.0	INE
5.0 M NaCl, 20mM Sn(II)	11.9	–799	330	17178.5	INE
Aqueous phase					
Reference U(VI), 1.0 M HCl	≈ 0	n. m.		17176.5	ACT
Reference U(IV), 1.0 M HCl,	≈ 0	n. m.		17175.2	ACT
20 mM Sn(II)	2.2	–284	330	17175.2	ACT
0.1 M NaCl, 20 mM Sn(II)					

a. ± 0.05; b. ± 20 mV; n.m: not measured.

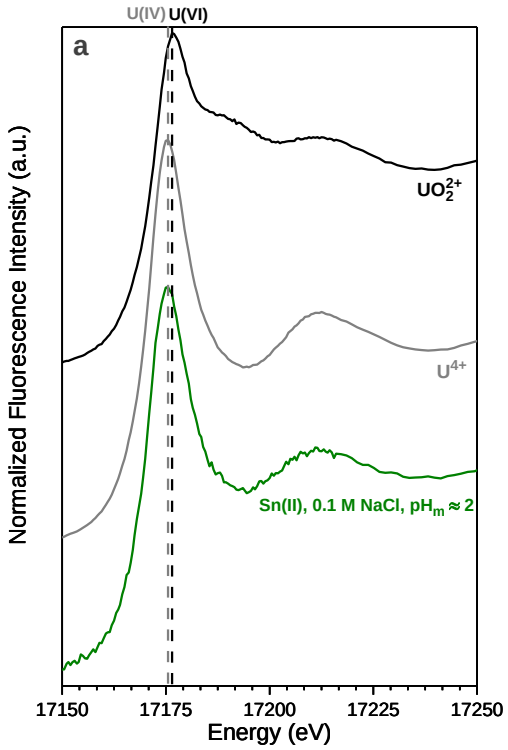

Figure 5. *U L_{III} XANES spectra collected for (a) aqueous sample in 0.1 M NaCl, 20 mM Sn(II) at pH_m ≈ 2; (b) uranium solid phases collected from solubility experiments in 0.1 M NaCl, 20 mM Sn(II) + 15 mg Fe(0) at pH_m ≈ 11 (green line), and in 5.0 M NaCl, 20 mM Sn(II) at pH_m ≈ 12 (red line). Black and grey spectra in (a) and (b) correspond to U(VI) and U(IV) references, respectively.*

4.2. Solubility, hydrolysis and complexation of U(VI). Thermodynamic description

4.2.1. Solubility and hydrolysis of U(VI) in NaCl systems

4.2.1.1 Solid phase characterization and solubility measurements

XRD diffraction patterns of the U(VI) solid phase prepared under acidic conditions perfectly match those of $UO_3 \cdot 2H_2O$(cr) (JCPDS file Nr. 43-0364). DTA analysis confirms the presence of two water molecules per uranium atom. XRD patterns of solid phases collected from selected solubility samples in acidic NaCl solutions indicate that the original $UO_3 \cdot 2H_2O$(cr) solid phase remained unaltered in the course of the experiments.

U(VI) solid phases equilibrated in alkaline NaCl solutions show XRD patterns with close similarities to clarkeite ($NaUO_2O(OH)$(cr), JCPDS file Nr. 87-1714) and $NaUO_2O(OH) \cdot H_2O$(cr) (JCPDS file Nr. 50-1586). Solid phases collected after terminating the solubility experiments in alkaline 0.51, 2.64 and 5.61 m NaCl systems retain the same XRD patterns of the original material, thus indicating that no transformation of the solid phase took place during the solubility experiments. XRD characterization of $UO_3 \cdot 2H_2O$(cr) equilibrated in 0.03 m NaCl at $pH_m = 11$ showed the incomplete transformation into the sodium uranate phase stable in more concentrated NaCl systems. DTA analysis of the dried solid phase indicates a content of 0.5 water molecules per uranium atom, whereas quantitative chemical analysis resulted in a Na : U ratio of 0.9 ± 0.1. Based on these results, the chemical formula of the solid controlling the solubility in alkaline dilute to concentrated NaCl systems can be defined as $Na_2U_2O_7 \cdot H_2O$(cr) or $NaUO_2O(OH)$(cr). The former formula is been preferred throughout this work.

Figure 6 shows the experimental solubility data of $UO_3 \cdot 2H_2O$(cr) and $Na_2U_2O_7 \cdot H_2O$(cr) determined in 0.03, 0.51, 2.64 and 5.61 m NaCl systems at pH_m = 4–14.5. $UO_3 \cdot 2H_2O$(cr) is the only solid phase controlling the solubility of U(VI) at pH_m below 6.5–8 (depending upon [NaCl]) in all investigated NaCl systems. Concentration of uranium in this pH region increases up to one order of magnitude with increasing ionic strength, expectedly due to ion interaction processes and complexation of U(VI) with chloride in concentrated NaCl systems. Changes in the slope of the solubility curve (log [U(VI)] *vs.* pH_m) with increasing ionic strength are related to changes in the aqueous speciation (*i. e.* ratio OH:U in the prevailing hydrolysis species) in equilibrium with $UO_3 \cdot 2H_2O$(cr). Solubility data of metaschoepite determined in the present work are in good agreement with previous solubility studies available in literature.

Solubility measurements in 0.03 m NaCl at pH_m = 9.5–11.5 with $UO_3 \cdot 2H_2O$(cr) as initial solid phase show a significant decrease in [U] with time. The concentration of uranium measured at short contact time ($\approx 10^{-5}$ m at $pH_m \approx 10$) agrees well with the high solubility expected for $UO_3 \cdot 2H_2O$(cr) under alkaline pH conditions. The significantly lower solubility measured after 140 days (10^{-6}–$10^{-6.5}$ m) is

indicative of a transformation process into $Na_2U_2O_7 \cdot H_2O$(cr), as confirmed by XRD. Experimental $Na_2U_2O_7 \cdot H_2O$(cr) solubility data gathered in 0.51, 2.64 and 5.61 m NaCl systems at pH_m = 8–14.5 are also shown in Figure 6. Under weakly alkaline pH conditions, the solubility follows a pH-independent behavior regardless of ionic strength. This agrees well with the equilibrium reaction 0.5 $Na_2U_2O_7 \cdot H_2O$(cr) + H_2O(l) ⇔ $UO_2(OH)_3^-$ + Na^+, which is consistent with the solid phase characterization performed in this work and aqueous speciation predicted with thermodynamic data selected in [2003GUI/FAN]. A slight decrease in [U(VI)] is observed in this pH region with increasing ionic strength, although experimental data points are scattered almost 1.5 orders of magnitude due to very low concentration of uranium, close to the detection limit of the measurement technique. At pH_m above ≈ 11 (depending upon [NaCl]), the solubility of $Na_2U_2O_7 \cdot H_2O$(cr) increases with a well-defined slope of +1 (log [U] *vs.* pH_m). This observation is consistent with a solubility control by the chemical equilibrium 0.5 $Na_2U_2O_7 \cdot H_2O$(cr) + 2H_2O(l) ⇔ $UO_2(OH)_4^{2-}$ + Na^+ + H^+. In this pH region, the solubility of U(VI) decreases about one order of magnitude with increasing ionic strength. A similar trend was reported in [2013GAO/FEL] for the solubility of $Na_2Np_2O_7$(cr) in dilute to concentrated NaCl–NaOH solutions.

Solubility samples equilibrated in the presence of both solid phases (green symbols in Figure 6) buffer the pH_m at (7.22 ± 0.15), (6.43 ± 0.15) and (6.50 ± 0.15) in 0.51, 2.64 and 5.61 m NaCl systems, respectively. Uranium concentrations measured for these systems provide a well-defined and consistent transition between solubility data collected in acidic conditions in the presence of $UO_3 \cdot 2H_2O$(cr), and [U] in equilibrium with $Na_2U_2O_7 \cdot H_2O$(cr) measured under alkaline pH conditions.

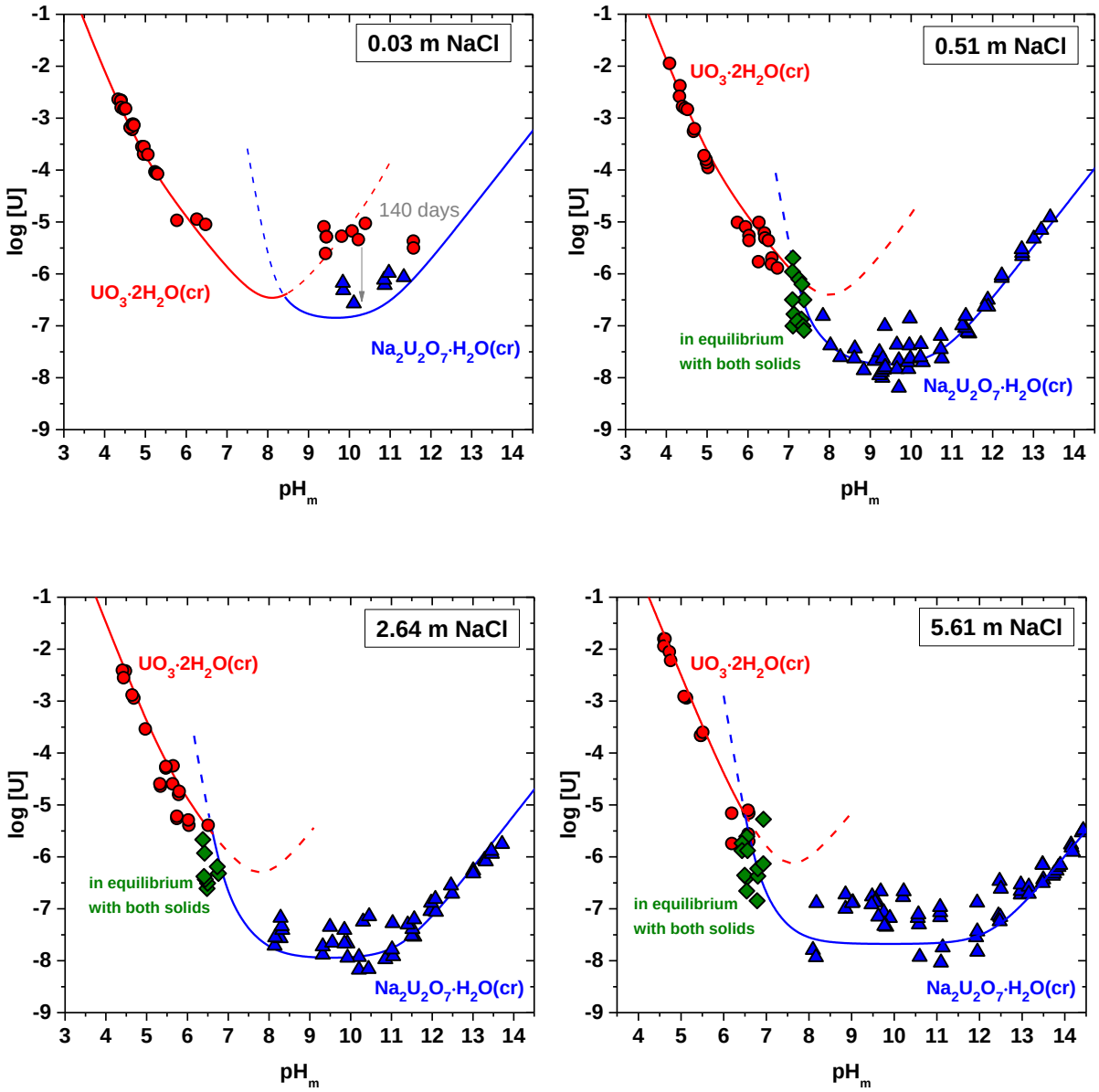

Figure 6. *Experimental solubility data of U(VI) in 0.03, 0.51, 2.64 and 5.61 m NaCl solutions. Red symbols: samples equilibrated with $UO_3{\cdot}2H_2O$(cr); blue symbols: samples equilibrated with $Na_2U_2O_7{\cdot}H_2O$(cr); green symbols: samples equilibrated with both $UO_3{\cdot}2H_2O$(cr) and $Na_2U_2O_7{\cdot}H_2O$(cr). Solid lines are the calculated solubility with the thermodynamic and SIT activity models derived in the present study.*

4.2.1.2 Chemical, thermodynamic and activity models

4.2.1.2.1 Evaluation of solubility products of $UO_3{\cdot}2H_2O$(cr) and $Na_2U_2O_7{\cdot}H_2O$(cr)

Solubility products of $UO_3{\cdot}2H_2O$(cr) and $Na_2U_2O_7{\cdot}H_2O$(cr) are evaluated in the present study based on the newly generated experimental solubility data. Conditional solubility products of $UO_3{\cdot}2H_2O$(cr) are calculated according to equation using experimental solubility data determined in 0.03, 0.51, 2.64 and 5.61 m NaCl ($4 \leq pH_m \leq 7$). Conditional hydrolysis constants at I_m required to solve equation are calculated with log ${}^*\beta^\circ_{(x,y)}$ selected in the NEA–TDB (see Table 3) and SIT ion interaction coefficients derived in this work (see Table 4). Extrapolation of log ${}^*K'_{s,0}\{UO_3{\cdot}2H_2O(cr)\}$ to $I = 0$ is conducted using the SIT linear regression shown in Figure 7, resulting in

$$\log {}^*K^\circ_{s,0}\{UO_3{\cdot}2H_2O(cr)\} = (5.35 \pm 0.13)$$

This value is considerably greater than log ${}^*K^\circ_{s,0}\{UO_3{\cdot}2H_2O(cr)\} = (4.8 \pm 0.43)$ selected in the NEA–TDB [1992GRE/FUG, 2003GUI/FAN], which resulted from the internal calculation with $\Delta_f H^\circ_m$ and S°_m determined in thermochemical studies. The later studies used a highly crystalline $UO_3{\cdot}2H_2O$(cr) material, obtained by the hydration of anhydrous UO_3(cr) synthesized at T = 500–600°C. The solubility product determined in the present work should therefore be used in thermodynamic / geochemical calculations involving $UO_3{\cdot}2H_2O$(cr) precipitated at low temperatures. The use of log ${}^*K^\circ_{s,0}\{UO_3{\cdot}2H_2O(cr)\}$ currently selected in the NEA–TDB for the evaluation of these systems can lead to the underestimation of $[U(VI)]_{tot}$.

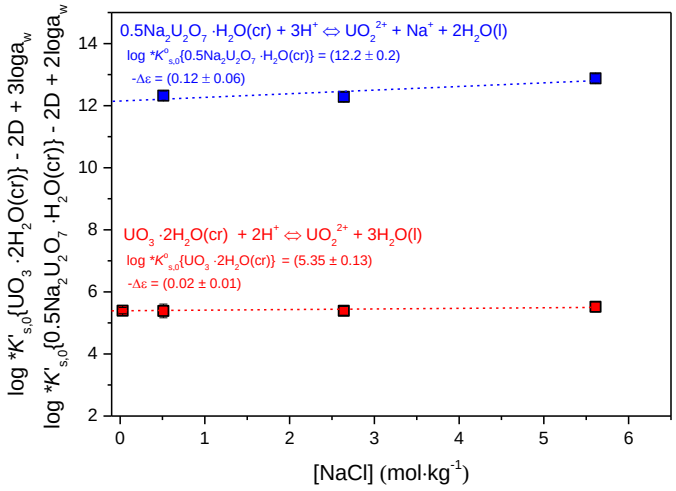

Figure 7. *SIT regression plot for the solubility product of $UO_3{\cdot}2H_2O$(cr) and $Na_2U_2O_7{\cdot}H_2O$(cr) considering experimental log ${}^*K'_{s,0}\{UO_3{\cdot}2H_2O(cr)\}$ and log ${}^*K'_{s,0}\{0.5\ Na_2U_2O_7{\cdot}H_2O(cr)\}$ obtained in NaCl systems.*

The solubility product of $Na_2U_2O_7{\cdot}H_2O(cr)$ was evaluated using the equilibrium pH_m for which the transformation of $UO_3{\cdot}2H_2O(cr)$ into $Na_2U_2O_7{\cdot}H_2O(cr)$ takes place at a given NaCl concentration. Provided that log ${}^*K'_{s,0}\{UO_3{\cdot}2H_2O(cr)\}$ is properly known, log ${}^*K'_{s,0}\{0.5\ Na_2U_2O_7{\cdot}H_2O(cr)\}$ can be determined independently of U(VI) aqueous speciation according with:

$$UO_3{\cdot}2H_2O(cr) + Na^+ \Leftrightarrow U(VI)(aq) \Leftrightarrow 0.5\ Na_2U_2O_7{\cdot}H_2O(cr) + H_2O(l) + H^+ \quad (2)$$

$$\log {}^*K'_{s,0}\{0.5\ Na_2U_2O_7{\cdot}H_2O(cr)\} = \log {}^*K'_{s,0}\{UO_3{\cdot}2H_2O(cr)\} + \log [Na^+] + pH_m \quad (3)$$

Following the Gibbs phase rule, the co-existence of both U(VI) solid phases for a given [NaCl] is attained for an invariant point with constant $[H^+]$ and $[U(VI)]_{tot}$. A large uncertainty for these quantities is experimentally measured in the solubility systems with both solid phases (green symbols in Figure 6), very likely as a result of the similar and very low values of $[H^+]$ and $[U(VI)]_{tot}$ (10^{-6}–10^{-7} m) at the transition pH_m. For this reason, we have determined the transition pH_m as the border between solubility experiments with $UO_3{\cdot}2H_2O(cr)$ (blue symbols in Figure 6), and those with co-existence of $UO_3{\cdot}2H_2O(cr)$ and $Na_2U_2O_7{\cdot}H_2O(cr)$ as confirmed by XRD. Table 2 summarizes these pH_m values, together with log ${}^*K'_{s,0}\{UO_3{\cdot}2H_2O(cr)\}$ at I_m = 0.51, 2.64 and 5.61 m NaCl calculated by SIT using $\varepsilon(UO_2^+, Cl^-) = (0.21 \pm 0.02)$ kg·mol^{-1} and $\varepsilon(H^+, Cl^-) = (0.12 \pm 0.01)$ kg·mol^{-1}. The values of log ${}^*K'_{s,0}\{0.5\ Na_2U_2O_7{\cdot}H_2O(cr)\}$ reported in the table are calculated according to equation (3).

Table 2. *Experimental pH_m values measured in solubility samples with simultaneous presence of $UO_3{\cdot}2H_2O(cr)$ and $Na_2U_2O_7{\cdot}H_2O(cr)$, and values of log ${}^*K'_{s,0}\{UO_3{\cdot}2H_2O(cr)\}$ and log ${}^*K'_{s,0}\{0.5\ Na_2U_2O_7{\cdot}H_2O(cr)\}$ calculated at I_m = 0.51, 2.64 and 5.61 mol·kg$_w^{-1}$.*

Matrix (m)	**pH_m**	**log ${}^*K'_{s,0}\{UO_3{\cdot}2H_2O(cr)\}$**	**log ${}^*K'_{s,0}\{0.5\ Na_2U_2O_7{\cdot}H_2O(cr)\}$**
0.51 m NaCl	(7.22 ± 0.15)	(5.76 ± 0.13)	(12.69 ± 0.15)
2.64 m NaCl	(6.43 ± 0.15)	(6.00 ± 0.13)	(12.85 ± 0.15)
5.61 m NaCl	(6.50 ± 0.15)	(6.5 ± 0.13)	(13.62 ± 0.15)

The values of log ${}^*K'_{s,0}\{0.5\ Na_2U_2O_7{\cdot}H_2O(cr)\}$ determined at I_m = 0.51, 2.64 and 5.61 m NaCl are extrapolated to I = 0 using the SIT linear regression in Figure 7, resulting in

$$\log {}^*K°_{s,0}\{0.5\ Na_2U_2O_7{\cdot}H_2O(cr)\} = (12.2 \pm 0.2)$$

The values of $\Delta\varepsilon\{UO_3{\cdot}2H_2O(cr), UO_2^{2+}\} = -(0.02 \pm 0.01)$ kg·mol^{-1} and $\Delta\varepsilon\{Na_2U_2O_7{\cdot}H_2O(cr), UO_2^{2+}\} = -(0.12 \pm 0.06)$ kg·mol^{-1} determined in the SIT-plots in Figure 7 are in excellent agreement with $\Delta\varepsilon\{UO_3{\cdot}2H_2O(cr), UO_2^{2+}\} = \varepsilon(UO_2^{+}, Cl^-) - 2\ \varepsilon(H^+, Cl^-) = -(0.03 \pm 0.04)$ kg·mol^{-1} and $\Delta\varepsilon\{Na_2U_2O_7{\cdot}H_2O(cr), UO_2^{2+}\} = \varepsilon(UO_2^{+}, Cl^-) + \varepsilon(Na^+, Cl^-) - 3\ \varepsilon(H^+, Cl^-) = -(0.12 \pm 0.04)$ kg·mol^{-1} calculated using $\varepsilon(UO_2^{+}, Cl^-) = (0.21 \pm 0.02)$ kg·mol^{-1}, $\varepsilon(Na^+, Cl^-) = (0.03 \pm 0.01)$ kg·mol^{-1} and $\varepsilon(H^+, Cl^-) = (0.12 \pm 0.01)$ kg·mol^{-1} as reported in [1980CIA] and [2003GUI/FAN]. This agreement provides an additional validation of the approach used for the determination of $\log {}^*K°_{s,0}\{UO_3{\cdot}2H_2O(cr)\}$ and $\log {}^*K°_{s,0}\{0.5\ Na_2U_2O_7{\cdot}H_2O(cr)\}$.

4.2.1.2.2 Thermodynamic and SIT activity models for U(VI) hydrolysis species forming in alkaline to hyperalkaline pH conditions

U(VI) solubility in dilute to concentrated NaCl solutions shows two well-defined regions in the alkaline pH-range: (i) pH-independent solubility behaviour at $8 \le pH_m \le 11$, and (ii) increase in solubility with a well-defined slope of +1 at $pH_m > 11$. Considering a solubility-control by $Na_2U_2O_7{\cdot}H_2O(cr)$, these observations are properly explained by the predominance of the species $UO_2(OH)_3^-$ and $UO_2(OH)_4^{2-}$ in the aqueous phase, respectively:

$$0.5\ Na_2U_2O_7{\cdot}H_2O(cr) + H_2O(l) \Leftrightarrow UO_2(OH)_3^- + Na^+ \quad (4)$$

$$0.5\ Na_2U_2O_7{\cdot}H_2O(cr) + 2\ H_2O(l) \Leftrightarrow UO_2(OH)_4^{2-} + Na^+ + H^+ \quad (5)$$

with

$$\log {}^*K'_{s,(1,3)} = \log\ [UO_2(OH)_3^-] + \log [Na^+] \quad (6)$$

$$\log {}^*K°_{s,(1,3)} = \log {}^*K'_{s,(1,3)} + \log\ \gamma_{UO_2(OH)_3^-} + \log \gamma_{Na^+} - \log a_w \quad (7)$$

and

$$\log {}^*K'_{s,(1,4)} = \log\ [UO_2(OH)_4^{2-}] + \log [Na^+] + \log [H^+] \quad (8)$$

$$\log {}^*K°_{s,(1,4)} = \log {}^*K'_{s,(1,4)} + \log\ \gamma_{UO_2(OH)_4^{2-}} + \log \gamma_{Na^+} + \log \gamma_{H^+} - 2 \log a_w \quad (9)$$

Conditional solubility constants $\log {}^*K'_{s,(1,3)}$ and $\log {}^*K'_{s,(1,4)}$ are determined according to equations (6) and (8) on the basis of experimental solubility data in 0.51, 2.64 and 5.61 m NaCl. These conditional constants are extrapolated to $I = 0$ in the SIT regressions shown in Figure 8, resulting in

log ${}^{*}K°_{s,(1,3)}$ = –(8.5± 0.4)

log ${}^{*}K°_{s,(1,4)}$ = –(19.7± 0.1)

Combining log ${}^{*}K°_{s,(1,3)}$ and log ${}^{*}K°_{s,(1,4)}$ with log ${}^{*}K°_{s,0}${0.5 $Na_2U_2O_7 \cdot H_2O$(cr)} determined in the previous section, we obtain

log ${}^{*}\beta°_{(1,3)}$ = –(20.7 ± 0.4)

log ${}^{*}\beta°_{(1,4)}$ = –(31.9 ± 0.2)

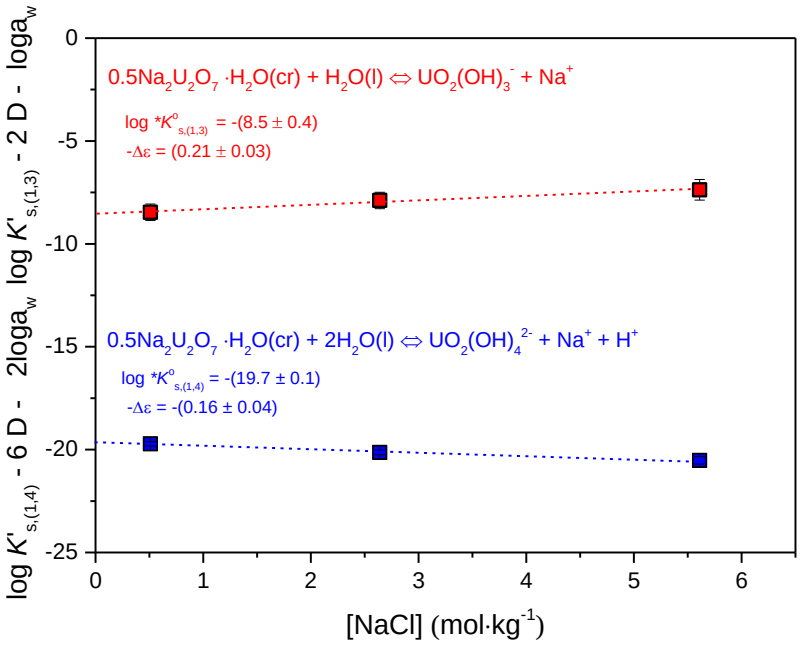

Figure 8. *Extrapolation of log ${}^{*}K'_{s,(1,3)}$ and log ${}^{*}K'_{s,(1,4)}$ determined in 0.51, 2.64 and 5.61 m NaCl to I = 0 using the SIT linear regression.*

SIT ion interaction coefficients of $UO_2(OH)_3^-$ and $UO_2(OH)_4^{2-}$ can be calculated from the slope of the corresponding SIT-plot (–$\Delta\varepsilon$ = – $\varepsilon(UO_2(OH)_3^-, Na^+)$ – $\varepsilon(Na^+, Cl^-)$, and –$\Delta\varepsilon$ = – $\varepsilon(UO_2(OH)_4^{2-}, Na^+)$ – $\varepsilon(Na^+, Cl^-)$ – $\varepsilon(H^+, Cl^-)$), using $\varepsilon(Na^+, Cl^-)$ = (0.03 ± 0.01) kg·mol^{-1} and $\varepsilon(H^+, Cl^-)$ = (0.12 ± 0.01) kg·mol^{-1} as reported in [2003GUI/FAN]:

$\varepsilon(UO_2(OH)_3^-, Na^+)$ = –(0.24 ± 0.09) kg·mol^{-1}

$\varepsilon(UO_2(OH)_4^{2-}, Na^+)$ = (0.01 ± 0.04) kg·mol^{-1}

4.2.1.2.3 Summary of chemical, thermodynamic and activity models selected in the present study for the system U^{VI}–Na^+–H^+–Cl^-–OH^-–H_2O(l)

Table 3 and Table 4 summarize the chemical, thermodynamic and SIT activity models selected in the present work. The selection is based on the evaluation of own experimental data, the use of thermodynamic data selected in the NEA–TDB and the application of empirical methods for the estimation of some ion interaction coefficients. Solubility curves calculated according to these models are compared in Figure 6 with experimental data gathered in this work in NaCl systems.

Table 3. *Solubility and hydrolysis constants at I = 0 selected in the present work for the system U^{VI}–Na^+–H^+–Cl^-–OH^-–H_2O(l).*

Solid phases		**log $^*K°_{s,0}°$**	**References**
$UO_3 \cdot 2H_2O$(cr)		(5.35 ± 0.13)	(p.w.)
$Na_2U_2O_7 \cdot H_2O$(cr)		(12.2 ± 0.2)	(p.w.)
Hydrolysis species	**(*xy*)**	**log $^*\beta°_{(x,y)}$**	
UO_2OH^+	(11)	–(5.25 ± 0.24)	[2003GUI/FAN]
$UO_2(OH)_2$(aq)	(12)	–(12.15 ± 0.17)	[2003GUI/FAN]
$UO_2(OH)_3^-$	(13)	–(20.7 ± 0.40)	(p.w.)
$UO_2(OH)_4^{2-}$	(14)	–(31.9 ± 0.2)	(p.w.)
$(UO_2)_2(OH)_2^{2+}$	(22)	–(5.62 ± 0.04)	[2003GUI/FAN]
$(UO_2)_3(OH)_4^{2+}$	(34)	–(11.9 ± 0.3)	[2003GUI/FAN]
$(UO_2)_3(OH)_5^+$	(35)	–(15.55 ± 0.12)	[2003GUI/FAN]
$(UO_2)_3(OH)_7^-$	(37)	–(32.20 ± 0.80)	[2003GUI/FAN]
$(UO_2)_4(OH)_7^+$	(47)	–(21.9 ± 1.0)	[2003GUI/FAN]

Table 4. *SIT ion interaction coefficients for UO_2^{2+} and U(VI) hydrolysis species reported in [1980CIA] and derived in the present work from experimental data and estimation methods.*

U(VI) species		**SIT coefficients**	
I	***J***	**ε(*i*,*j*)**	**References**
UO_2^{2+}	Cl^-	$(0.21 \pm 0.02)^a$	[1980CIA]
UO_2OH^+	Cl^-	$(0.10 \pm 0.10)^b$	(p.w.)
$(UO_2)_2(OH)_2^{2+}$	Cl^-	$(0.30 \pm 0.06)^c$	(p.w.)
$(UO_2)_3(OH)_4^{2+}$	Cl^-	$-(0.07 \pm 0.17)^c$	(p.w.)
$(UO_2)_3(OH)_5^+$	Cl^-	$(0.24 \pm 0.15)^c$	(p.w.)
$(UO_2)_4(OH)_7^+$	Cl^-	$(0.17 \pm 0.18)^c$	(p.w.)
$UO_2(OH)_3^-$	Na^+	$-(0.24 \pm 0.09)$	(p.w.)
$UO_2(OH)_4^{2-}$	Na^+	(0.01 ± 0.04)	(p.w.)
$(UO_2)_3(OH)_7^-$	Na^+	$-(0.24 \pm 0.09)^d$	(p.w.)
$UO_2(OH)_2(aq)$	Na^+, Cl^-	0	e.

a. This value given in [1980CIA] includes chloride complexation treated as strong ion-ion interaction; b. Estimated using the approach in [1997GRE/PUI] or from typical values for the corresponding valence type; c. Determined in the present work from potentiometric data reported elsewhere considering chloride complexation as strong ion-ion interaction; d. set equal to $\varepsilon(UO_2(OH)_3^-, Na^+)$; e. By definition in SIT.

4.2.2. Solubility and hydrolysis of U(VI) in KCl systems

4.2.2.1 U(VI) solubility in dilute to concentrated KCl–KOH solutions

Uranium(VI) solubility data determined in 0.1, 0.5, 1.0, 3.0 and 4.0 M KCl–KOH solutions are shown in Figure 9. For comparative purposes, the figure includes also U(VI) solubility data determined in Section 4.2.1 (also published as [2017ALT/YAL]) in NaCl solutions of analogous ionic strength.

An increase of the solubility following a well-defined slope of +1 was observed at pH_m above ≈ 11 in all KCl systems. This result is in excellent agreement with the solubility data determined in NaCl solutions (empty triangles in Figure 9), although the overall U(VI) solubility in KCl systems is slightly lower for the same MCl concentration. A slope of +1 in a log [U] *vs.* pH_m diagram indicates the release of one H^+ in the equilibrium reaction between the solid phase and aqueous species predominating under hyperalkaline conditions. This is consistent with the solubility equilibrium (10):

$$0.5\ M_2U_2O_7{\cdot}xH_2O(cr) + yH_2O(l) \Leftrightarrow UO_2(OH)_4^{2-} + H^+ + M^+ \qquad (10)$$

with $x + 2y = 5$, and M = Li, Na, K, etc.

In this pH_m-region, a decrease of approximately 1.5 orders of magnitude in the solubility was observed when increasing the concentration of KCl from 0.1 to 4.0 M. Such a behaviour reflects the impact of K^+ concentration in the equilibrium reaction (10), but also accounts for ion interaction processes between the negatively charged species $UO_2(OH)_4^{2-}$ and K^+.

At pH_m below ≈ 11, the solubility of U(VI) remains pH_m-independent for all investigated KCl concentrations (Figure 9). This is in excellent agreement with analogous solubility experiments performed in NaCl systems. The observed trend is consistent with the equilibrium reaction (11):

$$0.5\ M_2U_2O_7{\cdot}xH_2O(cr) + yH_2O(l) \Leftrightarrow UO_2(OH)_3^- + M^+ \qquad (11)$$

with $x + 2y = 3$, and M = Li, Na, K, etc.

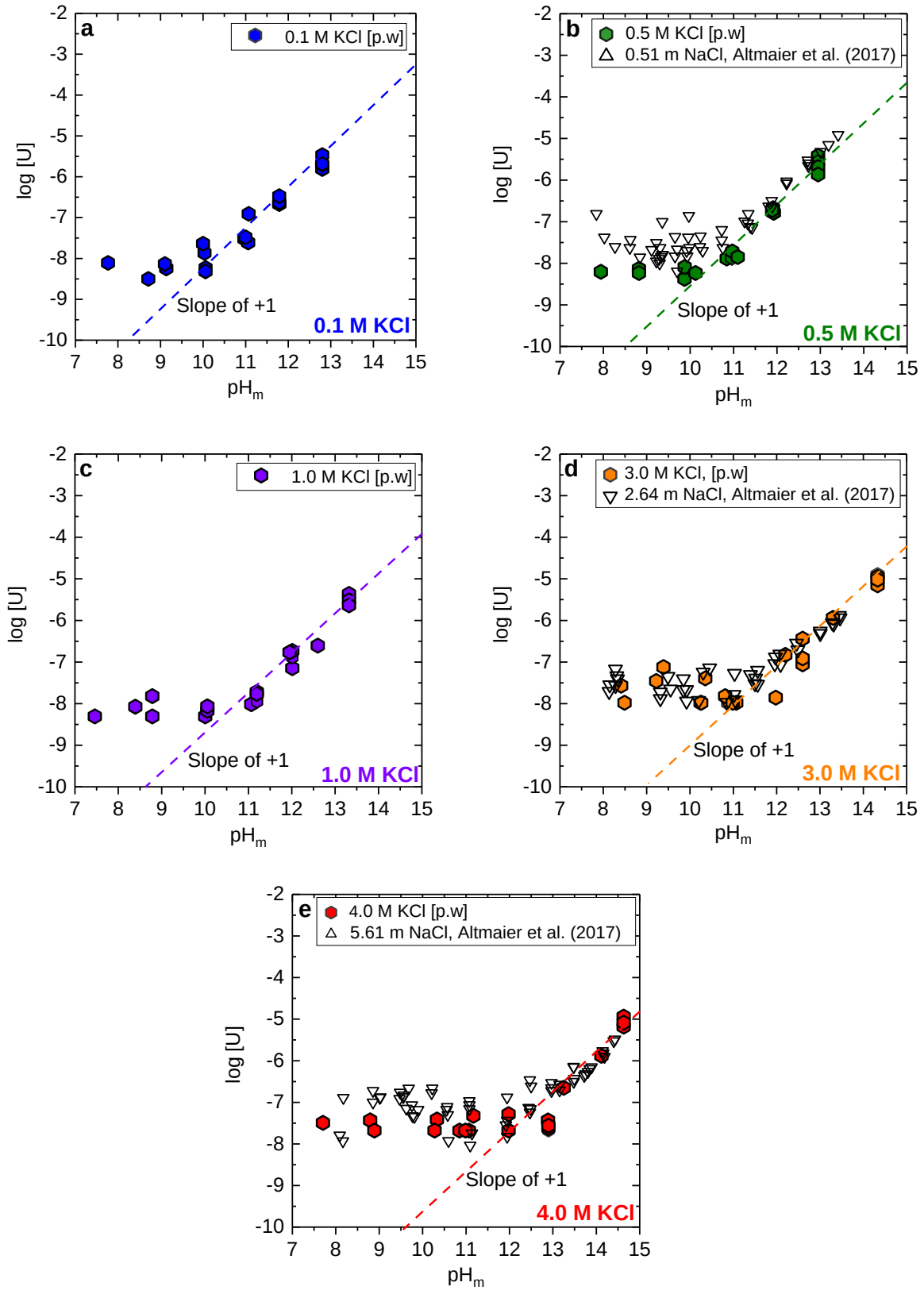

Figure 9. *Experimental solubility data of U(VI) obtained in this work in a. 0.1 M, b. 0.5 M, c. 1.0 M d. 3.0 M and e. 4.0 M KCl systems (colored symbols). Empty triangles show the solubility of U(VI) in dilute to concentrated NaCl solutions as reported in Section 4.2.1 and in [2017ALT/YAL]. Dashed lines indicate a slope of +1.*

4.2.2.2 Solid phase characterization

Table 5 summarizes the main outcome of the solid phase characterization using XRD, SEM-EDS, quantitative chemical analysis and DT-TGA. Figure 10 shows the diffraction patterns of the initial solid phase ("Starting material") and solid phases from selected solubility experiments at each ionic strength. Figure 10a compares the XRD patterns of the "Starting material" with reference spectra of several U(VI) solid phases, namely $UO_3 \cdot 2H_2O$(cr), $Na_2U_2O_7 \cdot H_2O$(cr), $K_2U_6O_{19} \cdot 11H_2O$(cr), $K_2U_4O_{13}$(cr), $K_2U_2O_7$(cr) and K_2UO_4(cr). Due to the less crystalline character of the solid phase synthesized at room temperature in the present work, the sharper peak observed at small angles was used as fingerprint for the identification of the U(VI) "Starting material". Hence, the peak found at $2\Theta = 13.1$ is very different from the values reported for $UO_3 \cdot 2H_2O$(cr) ($2\Theta = 12.0$) or $Na_2U_2O_7 \cdot H_2O$(cr) ($2\Theta = 14.9$), and in moderate agreement with the value of $2\Theta = 13.4$ reported for $K_2U_2O_7$(cr) (JCPDS file Nr. 29–1058). EDS and quantitative chemical analysis data summarized in Table 5 confirm a ratio K:U ≈ 1 in the "Starting material", further supporting that $K_2U_2O_7 \cdot xH_2O$(cr) was the solid phase used in the solubility experiments.

Figures 10b and 10c show XRD diffractograms collected for U(VI) solid phases equilibrated in 0.1, 0.5, 1.0, 3.0 and 4.0 M KCl solutions at $7.7 \leq pH_m \leq 10.3$ and $12.9 \leq pH_m \leq 13.3$, respectively. The same XRD patterns as the "Starting material" are retained in all cases (except one, see below), indicating that no transformation of the solid phase occurred during the equilibration time in these systems regardless of the pH_m and KCl concentration. A clear shift in the position of the first peak was observed for the solid phase equilibrated in 0.1 M KCl at $pH_m = 7.7$ ($2\Theta \approx 12.8$, see Figure 10b), hinting towards a possible solid phase transformation occurring at this pH_m and salt concentration. The shift of 2Θ values to lower angles is possibly related to a decrease in the K:U ratio of the solid phase, as deduced from the trend observed for the reference compounds $K_2U_2O_7$(cr), $K_2U_4O_{13}$(cr) and $K_2U_6O_{19} \cdot 11H_2O$(cr) (see Table 5).

In combination with XRD evidences, the ratio K:U ≈ 1 determined by EDS and quantitative chemical analysis for most of the solubility samples supports that the solid phase $K_2U_2O_7 \cdot xH_2O$(cr) was responsible of the solubility-control (see Table 5). The high K:U ratio (1.3) observed for the sample at $pH_m = 10.2$ in 4.0 M KCl is most likely due to the insufficient washing steps for such high KCl concentration.

Results on TG-DTA analysis summarized in Table 5 indicate that the number of hydration waters in the investigated potassium uranate phase is (1.5 ± 0.3). Based on all experimental evidences collected, the solid phase investigated in this series of solubility experiments was identified as $K_2U_2O_7 \cdot 1.5H_2O$(cr).

Table 5. *Summary of the main results obtained in the solid phase characterization of the "Starting material" and selected solubility samples equilibrated in KCl systems using XRD, SEM–EDS, quantitative chemical analysis (K:U ratio) and TG–DTA (number of hydration waters, x). Position of the first diffraction peak reported in the literature for some layered U(VI) structures is provided for comparison.*

Background electrolyte	**pH_m[a]**	**XRD (2Θ)**	**K:U ratio SEM–EDS**	**K:U ratio Chemical analysis**	**TG–DTA (number of hyd. H_2O)**
2.5 M KCl "Starting material"	12.7	13.1	1.0	0.9	1.4
0.1 M KCl	7.7	12.8	n.m.	n.m.	n.m.
0.1 M KCl	9.9	13.1	1.0	0.9	1.3
0.1 M KCl	12.9	13.2	n.m.	0.9	1.7
0.5 M KCl	10.0	13.2	0.9	0.9	1.3
0.5 M KCl	12.9	13.2	n.m.	0.9	1.7
1.0 M KCl	9.8	13.1	1.0	0.9	1.3
1.0 M KCl	13.3	13.2	n.m.	1.0	1.7
3.0 M KCl	10.3	13.0	0.9	0.9	1.3
3.0 M KCl	13.3	13.2	n.m.	1.0	1.7
4.0 M KCl	10.2	13.0	1.0	1.3	1.3
4.0 M KCl	13.2	13.1	n.m.	1.0	1.7
average[b]			**(1.0 ± 0.1)**	**(0.9 ± 0.1)[c]**	**(1.5 ± 0.3)**
$UO_3·2H_2O$(cr) [2017ALT/YAL]		12.0			
$Na_2U_2O_7·H_2O$(cr) [2017ALT/YAL]		14.9			
K_2UO_4(cr) JCPDS file Nr. 72–2228		13.5			
$K_2U_2O_7$(cr) JCPDS file Nr. 29–1058		13.4			
$K_2U_4O_{13}$(cr) JCPDS file Nr. 29–1059		12.6			
$K_2U_6O_{19}·11H_2O$(cr) JCPDS file Nr. 33–1049		11.9			

a. ± 0.05; **b.** uncertainty calculated as 2σ; **c.** results obtained in 4.0 M KCl at pH_m = 10.2 disregarded for calculating average and uncertainty; **n.m.** = not measured.

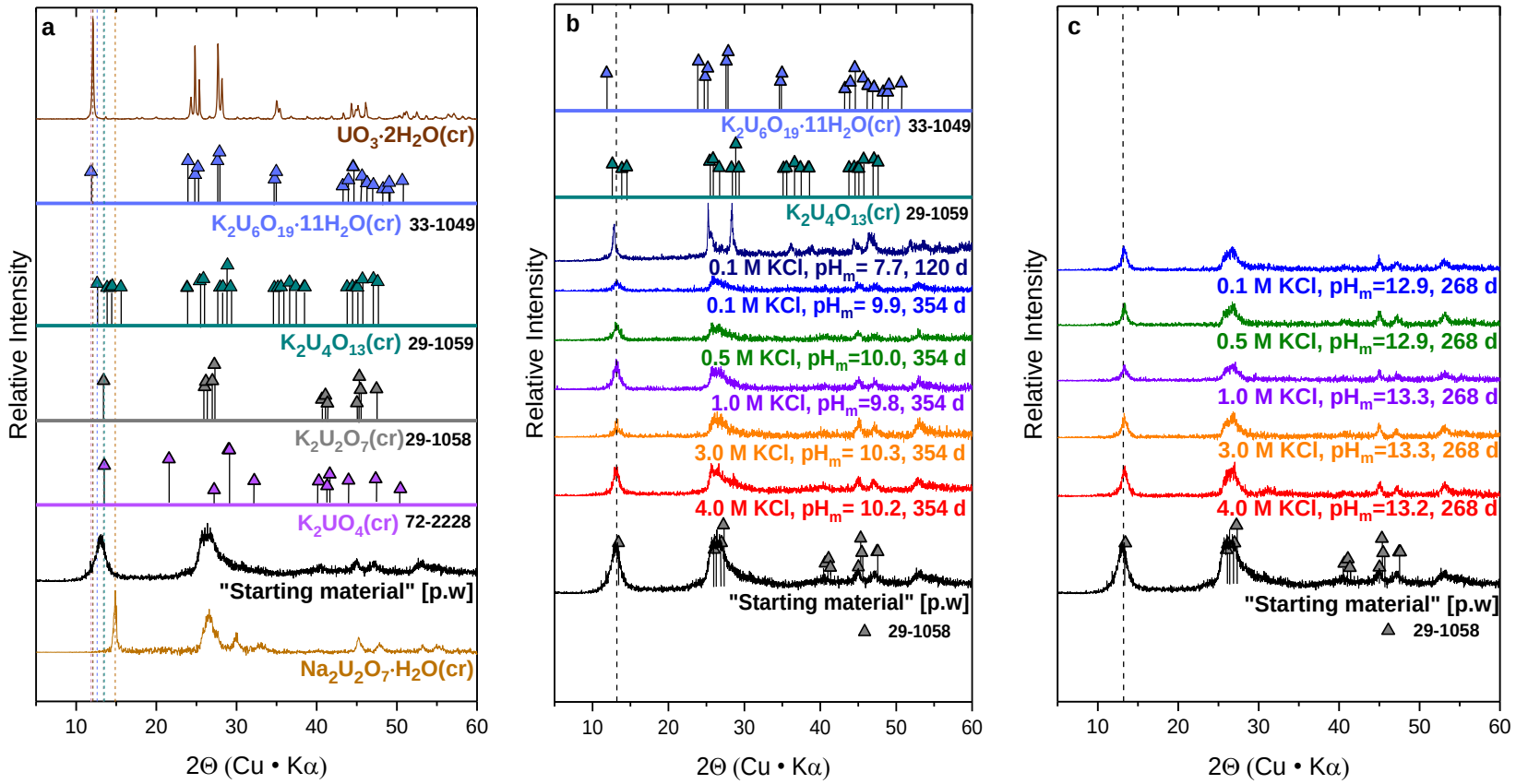

Figure 10. *XRD patterns of solid phases of selected solubility samples in dilute to concentrated KCl solutions: a. comparison between "Starting material" and XRD patterns reported by [2017ALT/YAL] for $Na_2U_2O_7{\cdot}H_2O$(cr) and $UO_3{\cdot}2H_2O$(cr), and reference data reported in the JCPDS database for $K_2U_6O_{19}{\cdot}11H_2O$(cr) (JCPDS file Nr. 33–1049), $K_2U_4O_{13}$(cr) (JCPDS file Nr. 29–1059), $K_2U_2O_7$(cr) (JCPDS file Nr. 29–1058) and K_2UO_4(cr) (JPDS file Nr. 72–2228); b. comparison between "Starting material" and solid phases at pH_m = 7.7–10.3. Diffractograms of $K_2U_2O_7$(cr) (JCPDS file Nr. 29–1058), $K_2U_4O_{13}$(cr) (JCPDS file Nr. 29–1059) and $K_2U_6O_{19}{\cdot}11H_2O$(cr) (JCPDS file Nr. 33–1049) provided for comparison; c. comparison between "Starting material" and solid phases recovered from solubility experiments at pH_m=12.9–13.3 after t = 268 days. Diffractogram of $K_2U_2O_7$(cr) (JCPDS file Nr. 29–1058) provided for comparison.*

4.2.2.3 Thermodynamic data derived using U(VI) solubility experiments in alkaline, dilute to concentrated KCl solutions

The equilibrium reaction (12) is responsible for the solubility control of U(VI) at $pH_m \geq 11$, as determined considering the slope analaysis (slope of +1) and solid phase characterization ($K_2U_2O_7 \cdot 1.5H_2O$(cr)):

$$0.5\ K_2U_2O_7 \cdot 1.5H_2O(cr) + 1.75H_2O(l) \Leftrightarrow UO_2(OH)_4^{2-} + H^+ + K^+ \quad (12)$$

The values of log $^*K'_{s,(1,4)}$ and log $^*K°_{s,(1,4)}$ can be accordingly defined as:

$$\log {}^*K'_{s,(1,4)} = \log [UO_2(OH)_4^{2-}] + \log[H^+] + \log[K^+] \quad (13)$$

$$\log {}^*K^o_{s,(1,4)} = \log {}^*K'_{s,(1,4)} + \log \gamma_{UO_2(OH)_4^{2-}} + \log \gamma_{H^+} + \log \gamma_{K^+} - 1.75 \log a_w \quad (14)$$

Solubility data obtained in 0.1, 0.5, 1.0, 3.0 and 4.0 M KCl solutions with $pH_m \geq 11$ were evaluated separately in order to determine the corresponding conditional constants, log $^*K'_{s,(1,4)}$. The resulting values of log $^*K'_{s,(1,4)}$ were considered in a SIT-plot to derive log $^*K°_{s,(1,4)}$ (intercept) and $-\Delta\varepsilon$ (slope). The SIT interaction coefficient $\varepsilon(UO_2(OH)_4^{2-}, K^+)$ was calculated from $-\Delta\varepsilon$ and using the values of $\varepsilon(H^+, Cl^-)$ and $\varepsilon(K^+, Cl^-)$ reported in the NEA-TDB [2003GUI/FAN]. The SIT-plot $\log {}^*K'_{s,(1,4)} - 6D - 1.75 \log a_w$ *vs.* [KCl] is shown in Figure 11 together with the SIT-plot for the analogous solubility equilibrium in NaCl systems with $Na_2U_2O_7 \cdot H_2O$(cr) (with $\log {}^*K'_{s,(1,4)} - 6D - 2\log a_w$ *vs* [NaCl]), as reported in Section 4.2.1 and in [2017ALT/YAL].

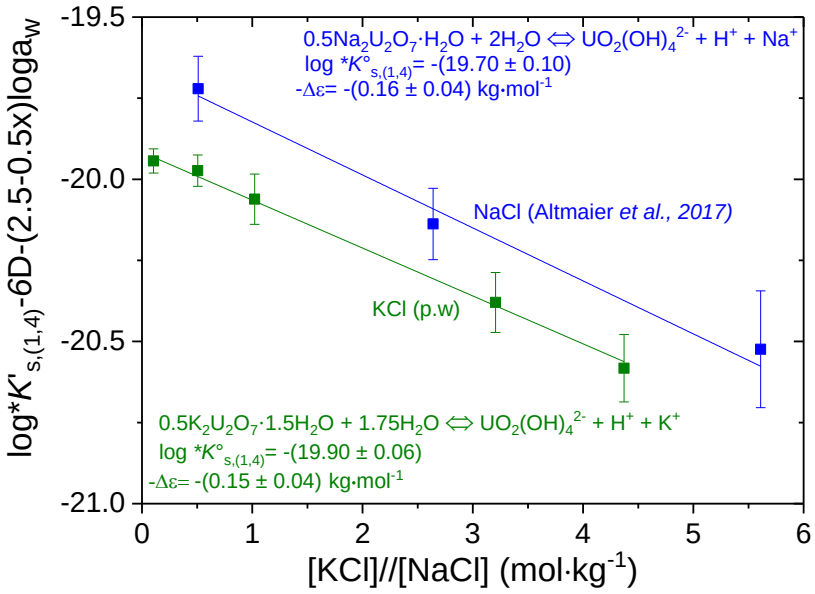

Figure 11. *SIT-plot for the solubility reactions 0.5 $M_2U_2O_7 \cdot xH_2O$(cr) + (2.5–0.5x) H_2O(l) ⇔ $UO_2(OH)_4^{2-} + H^+ + M^+$ (with M = K and Na) using experimental log $^*K'_{s,(1,4)}$ values determined in dilute to concentrated KCl (this section) and NaCl solutions (Section 4.2.1 and [2017ALT/YAL]).*

The intercept and slope of the linear SIT regression result in log ${}^{*}K°_{s,(1,4)}$ = –(19.90 ± 0.06) and –Δε= –(0.15 ± 0.04) kg·mol^{-1} with –Δε = – [ε($UO_2(OH)_4^{2-}$, K^+) + ε(H^+, Cl^-) + ε(K^+, Cl^-)]), respectively. The SIT interaction coefficient for $UO_2(OH)_4^{2-}$ with K^+ is accordingly calculated as ε($UO_2(OH)_4^{2-}$, K^+) = (0.03 ± 0.04) kg·mol^{-1}. Based on the solubility data in alkaline NaCl systems, Section 4.2.1 reports ε($UO_2(OH)_4^{2-}$, Na^+) = (0.01 ± 0.04) kg·mol^{-1}, which is in excellent agreement with the value determined in the present work for KCl systems and highights the similar behaviour of U(VI) in both salt systems.

The solubility product log *$K°_{s,0}${0.5 $K_2U_2O_7$·1.5H_2O(cr)} according with reaction (15) was calculated considering log ${}^{*}K°_{s,(1,4)}$ = –(19.90 ± 0.06) determined in the present work and log ${}^{*}\beta°_{(1,4)}$ = –(31.9 ± 0.2) reported in Section 4.2.1:

$$0.5\ K_2U_2O_7{\cdot}1.5H_2O(cr) + 3H^+ \Leftrightarrow UO_2^{2+} + K^+ + 2.25H_2O(l) \qquad (15)$$

The combination of log ${}^{*}K°_{s,(1,4)}$ and log ${}^{*}\beta°_{(1,4)}$ results in log ${}^{*}K°_{s,0}${0.5 $K_2U_2O_7$·1.5H_2O(cr)} = log ${}^{*}K°_{s,(1,4)}$ – log${}^{*}\beta°_{(1,4)}$ = (12.0 ± 0.2). Note that this value is in good agreement although slightly lower than log ${}^{*}K°_{s,0}${0.5 $Na_2U_2O_7$·H_2O(cr)} = (12.2 ± 0.2) reported in Section 4.2.1 for NaCl systems.

Solubility data at $pH_m \leq 11$ were not used to derived any thermodynamic quantity. Instead, log ${}^{*}K°_{s,0}${0.5 $K_2U_2O_7$·1.5H_2O(cr)} determined from solubility data at $pH_m \geq 11$ and hydrolysis constants reported in Section 4.2.1 were considered to reproduce the solubility of U(VI) in this pH_m-region. Ion interaction coefficients for $UO_2(OH)_3^-$ (13) and $(UO_2)_3(OH)_7^-$ (37) species (expected to prevail within $8 \leq pH_m \leq 11$) with K^+ were taken as ($UO_2(OH)_3^-$, K^+) = ε($UO_2(OH)_3^-$, Na^+) = –(0.24 ± 0.09) kg·mol^{-1} and ε($(UO_2)_3(OH)_7^-$), K^+) = ε($(UO_2)_3(OH)_7^-$), Na^+) = –(0.24 ± 0.09) kg·mol^{-1}, considering the close similarities between ε($UO_2(OH)_4^{2-}$, Na^+) and ε($UO_2(OH)_4^{2-}$, K^+).

4.2.3. Solubility and hydrolysis of U(VI) in $MgCl_2$ systems

4.2.3.1 Solubility measurements and solid phase characterization

Figure 12 shows the experimental solubility data of U(VI) determined in 0.01, 0.25, 2.67 and 5.15 m $MgCl_2$ systems compared to the solubility of $UO_3 \cdot 2H_2O$(cr) at I = 0. Analogous to NaCl systems, a significant increase in solubility (up to 3 orders of magnitude) is observed with increasing $MgCl_2$ concentration. This observation reflects very strong ion interaction processes taking place between cationic hydrolysis species and Cl^-. U(VI) solubility data in $MgCl_2$ solutions are limited to $pH_m \approx 9$ due to the precipitation of $Mg(OH)_2$(s) (or $Mg_2(OH)_3Cl \cdot 4H_2O$(cr)), except the system with 0.01 m $MgCl_2$. No decrease in solubility is observed in any of the investigated $MgCl_2$ systems within the timeframe of this study (200 days), which suggests that (in contrast to NaCl and KCl systems) no solid phase transformation towards a Mg-uranate takes place. This indirect observation is confirmed by XRD measurements before and after solubility experiments (data not shown), which indicate the predominance of the same solid phase ($UO_3 \cdot 2H_2O$(cr)) in both cases.

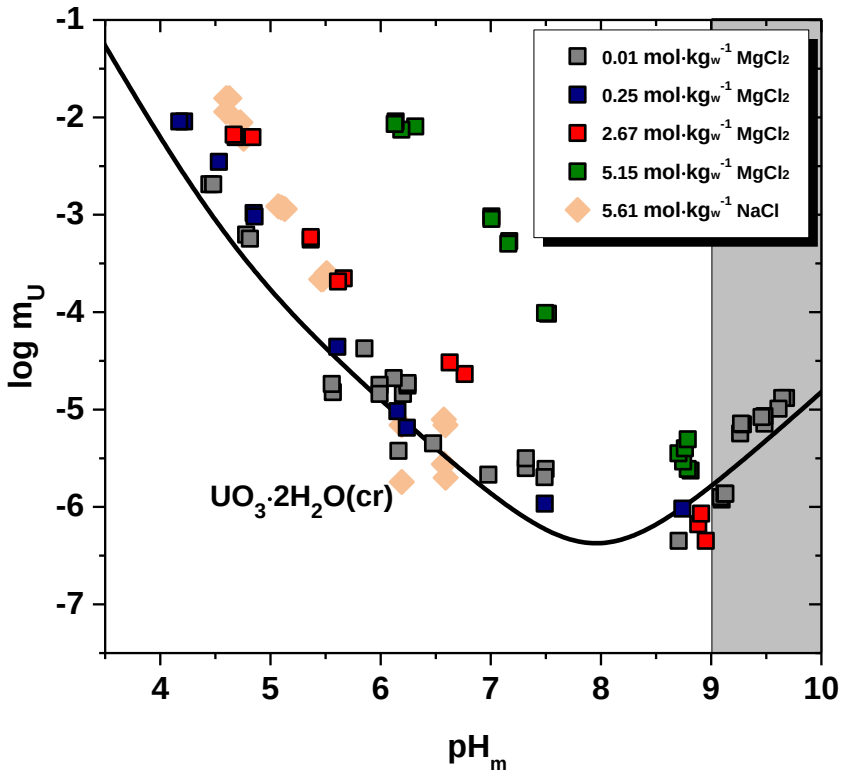

Figure 12. *Experimental solubility data of U(VI) in 0.01, 0.25, 2.67 and 5.15 m $MgCl_2$ solutions. Solid line corresponds to the solubility of $UO_3 \cdot 2H_2O$(cr) calculated at I = 0 with thermodynamic data derived in this study.*

4.2.3.2 Thermodynamic and Pitzer activity models

4.2.3.2.1 Pitzer activity model for U(VI) hydrolysis at acidic to near-neutral pH

The hydrolysis scheme for the solubility of U(VI) is adapted from Section 4.2.1. Due to the lack of experimental formation constants of the species $UO_2(OH)^+$ and $(UO_2)_4(OH)_7^+$ in chloride media, the Pitzer parameters for these species are defined based on the following assumptions and analogies: the binary parameter C_{MX}^{Φ} and mixing parameters θ_{Xa} (or θ_{Mc}) and Ψ_{Xac} (or Ψ_{Mac}) are set to zero; $\beta^{(0)}_{(UO2(OH)^+,\ Cl^-)}$ and $\beta^{(0)}_{((UO2)4(OH)7^+,\ Cl^-)}$ are calculated based on the correlation between SIT ion interaction coefficients for 1-1 electrolytes ($\beta^{(0)}_{MX} = 0.035 + \varepsilon(M,X)\cdot\ln(10)/2$), using the SIT coefficients $\varepsilon(UO_2(OH)^+,\ Cl^-)$ = (0.10 ± 0.10) kg·mol^{-1} and $\varepsilon(UO_2)_4(OH)_7^+,\ Cl^-)$ = (0.17 ± 0.18) kg·mol^{-1}. $\beta^{(1)}_{(UO2(OH)^+,\ Cl^-)}$ and $\beta^{(1)}_{((UO2)4(OH)7^+,\ Cl^-)}$ are set to tabulated values for 1:1 ions:

$\beta^{(0)}_{(UO2(OH)^+,\ Cl^-)}$ = 0.15 kg·mol^{-1} $\beta^{(1)}_{(UO2(OH)^+,\ Cl^-)}$ = 0.3 kg·mol^{-1}

$\beta^{(0)}_{((UO2)4(OH)7^+,\ Cl^-)}$ = 0.23 kg·mol^{-1} $\beta^{(1)}_{((UO2)4(OH)7^+,\ Cl^-)}$ = 0.3 kg·mol^{-1}.

The polyatomic hydrolysis species $(UO_2)_2(OH)_2^{2+}$, $(UO_2)_3(OH)_4^{2+}$ and $(UO_2)_3(OH)_5^+$ become predominant depending on the ionic strength, background electrolyte and pH region. Thus, experimental data in the literature and from the present study can be used for a more accurate determination of Pitzer parameters of these species. In the present study, the development of the Pitzer parameters for (22), (34) and (35) species are based on the following experimental data:

a) Experimental total U concentration provided in this section and in Section 4.2.1 for 0.01, 0.25, 2.67 and 5.15 m $MgCl_2$ and 0.03, 0.51, 2.64 and 5.61 m NaCl, respectively. It represents the contribution of all the hydrolysis species according to equation (16).

$$[U]_{tot} = [UO_2^{2+}] + \Sigma\, x[(UO_2)_x(OH)_y^{2x-y}] = {}^*K'_{s,0}\,[H^+]^2 + \Sigma\, x({}^*K'_{s,0}[H^+]^2)^x\, {}^*\beta'_{(x,y)}[H^+]^{-y} \qquad (16)$$

b) Experimentally determined formation constants of (22), (34) and (35) species reported in the literature in 0.1, 0.25, 0.5, 0.75, 1.0, 2.0, 3.0 and 4.5 M (0.1, 0.25, 0.51, 0.76, 1.02, 2.09, 3.2, 4.98 m) NaCl [1962RUS/JOH, 1963DUN/SIL, 2002DES/GIA].

c) The titration experiments performed in the present study providing experimental OH:U ratios at given pH_m.

Taking into account all the experimental data given above, the development of the Pitzer parameters for (22), (34) and (35) species was performed by fitting to experimental data, *i.e.*, by minimizing the difference between the calculated model and the experimental data a), b) and c). The overall fit was performed by weighing 50% to solubility experiments in both NaCl and $MgCl_2$, 38% to potentiometric

studies reported in literature and 12% to titration experiments performed in the present study.

Figure 13 shows the model calculation performed with the Pitzer parameters obtained by fitting to experimental data together with the experimental solubility data. The obtained model shows an excellent agreement with the solubility data in both NaCl and $MgCl_2$ systems.

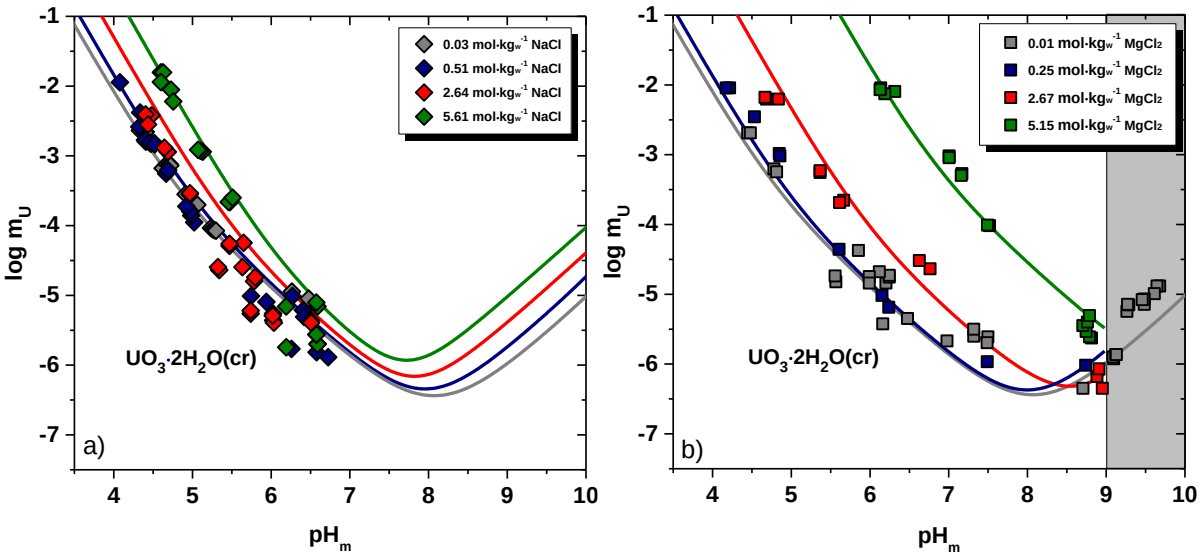

Figure 13. *Experimental solubility data of U(VI) in a) 0.03, 0.51, 2.64 and 5.61 m NaCl and b) 0.01, 0.25, 2.67 and 5.15 m $MgCl_2$ solutions. Solid lines are the calculated solubility with thermodynamic and Pitzer activity models derived in the present study.*

The determination of Pitzer parameters by fitting to three different available experimental datasets confirm the very good agreement with calculations and experiments. The selected Pitzer parameters for $(UO_2)_2(OH)_2^{2+}$, $(UO_2)_3(OH)_4^{2+}$ and $(UO_2)_3(OH)_5^{+}$ species in the present study are:

$\beta^{(0)}_{((UO_2)_2(OH)_2^{2+},Cl^-)}$ = 0.4714 kg·mol^{-1} $\beta^{(1)}_{((UO_2)_2(OH)_2^{2+},Cl^-)}$ = 2.02 kg·mol^{-1}

$\Psi_{((UO_2)_2(OH)_2^{2+},Na^+,Cl^-)}$ = –0.0272

$\beta^{(0)}_{((UO_2)_3(OH)_4^{2+},Cl^-)}$ = 0.1294 kg·mol^{-1} $\beta^{(1)}_{((UO_2)_3(OH)_4^{2+},Cl^-)}$ = 0.8519 kg·mol^{-1}

$\Psi_{((UO_2)_3(OH)_4^{2+},Na^+,Cl^-)}$ = 0.0549

$\beta^{(0)}_{((UO_2)_3(OH)_5^{+},Cl^-)}$ = 0.252 kg·mol^{-1} $\beta^{(1)}_{((UO_2)_3(OH)_5^{+},Cl^-)}$ = 0.096 kg·mol^{-1}

$\Psi_{((UO_2)_3(OH)_5^{+},Mg^{2+},Cl^-)}$ = –0.052

4.2.3.2.2 Pitzer activity model for U(VI) hydrolysis species at alkaline pH

The solubility of U(VI) in alkaline to hyper-alkaline pH conditions is dominated by two species $UO_2(OH)_3^-$ and $UO_2(OH)_4^{2-}$ in equilibrium with $Na_2U_2O_7{\cdot}H_2O$(cr) and $K_2U_2O_7{\cdot}1.5H_2O$(cr) in NaCl and KCl media, respectively. The equilibrium reactions are:

$$0.5\ Na_2U_2O_7{\cdot}H_2O(cr) + H_2O(l) \Leftrightarrow UO_2(OH)_3^- + Na^+ \quad (17)$$

$$0.5\ Na_2U_2O_7{\cdot}H_2O(cr) + 2\ H_2O(l) \Leftrightarrow UO_2(OH)_4^{2-} + Na^+ + H^+ \quad (18)$$

$$0.5\ K_2U_2O_7{\cdot}1.5\ H_2O(cr) + 1.5\ H_2O(l) \Leftrightarrow UO_2(OH)_3^- + K^+ \quad (19)$$

$$0.5\ K_2U_2O_7{\cdot}1.5\ H_2O(cr) + 1.75\ H_2O(l) \Leftrightarrow UO_2(OH)_4^{2-} + K^+ + H^+ \quad (20)$$

with

$$\log {}^*K'_{s,(1,3)} = \log\ [UO_2(OH)_3^-] + \log [Na^+] \quad (21)$$

$$\log {}^*K^\circ_{s,(1,3)} = \log {}^*K'_{s,(1,3)} + \log \gamma_{UO_2(OH)_3^-} + \log \gamma_{Na^+} - \log a_w \quad (22)$$

$$\log {}^*K'_{s,(1,3)} = \log\ [UO_2(OH)_3^-] + \log [K^+] \quad (23)$$

$$\log {}^*K^\circ_{s,(1,3)} = \log {}^*K'_{s,(1,3)} + \log \gamma_{UO_2(OH)_3^-} + \log \gamma_{K^+} - 1.5 \log a_w \quad (24)$$

and

$$\log {}^*K'_{s,(1,4)} = \log\ [UO_2(OH)_4^{2-}] + \log [Na^+] + \log [H^+] \quad (25)$$

$$\log {}^*K^\circ_{s,(1,4)} = \log {}^*K'_{s,(1,4)} + \log \gamma_{UO_2(OH)_4^{2-}} + \log \gamma_{Na^+} + \log \gamma_{H^+} - 2 \log a_w \quad (26)$$

$$\log {}^*K'_{s,(1,4)} = \log\ [UO_2(OH)_4^{2-}] + \log [K^+] + \log [H^+] \quad (27)$$

$$\log {}^*K^\circ_{s,(1,4)} = \log {}^*K'_{s,(1,4)} + \log \gamma_{UO_2(OH)_4^{2-}} + \log \gamma_{K^+} + \log \gamma_{H^+} - 1.75 \log a_w \quad (28)$$

Conditional solubility constants determined in alkaline to hyper-alkaline NaCl and KCl systems are fitted according to reactions (17) – (20) following the Pitzer formulism. The binary parameter $\beta^{(2)}$, $C^{(\Phi)}$ and the mixing parameters θ and Ψ are set to zero for both aqueous species. $\log {}^*K^\circ_{s,UO_2(OH)_3^-}$ and $\log {}^*K^\circ_{s,UO_2(OH)_4^{2-}}$ are taken from Section 4.2.1 and 4.2.2. $\beta^{(0)}$ and $\beta^{(1)}$ are fitted by minimizing the difference between calculated and experimental $\log {}^*K'_{s,UO_2(OH)_4^{2-}}$ in 0.51, 2.64 and 5.61 m NaCl and in 0.1, 0.51, 1.02, 3.2 and 4.37 m KCl systems. $\log {}^*K'_{s,UO_2(OH)_3^-}$ are fitted only in 0.51, 2.64 and 5.61 m NaCl system. The Pitzer parameters for the KCl system are adapted by analogy with NaCl as was

done for the SIT coefficient $\varepsilon(UO_2(OH)_3^-, K^+) = \varepsilon(UO_2(OH)_3^-, Na^+)$ in Section 4.2.2. The resulting Pitzer parameters are:

$\beta^{(0)}_{(UO2(OH)3-,\,Na+)} = -0.26$ kg·mol^{-1} $\quad$ $\beta^{(1)}_{(UO2(OH)3-,\,Na+)} = 0.34$ kg·mol^{-1}

$\beta^{(0)}_{(UO2(OH)42-,\,Na+)} = 0.06$ kg·mol^{-1} $\quad$ $\beta^{(1)}_{(UO2(OH)42-,\,Na+)} = 1.98$ kg·mol^{-1}

$\beta^{(0)}_{(UO2(OH)3-,\,K+)} = -0.26$ kg·mol^{-1} $\quad$ $\beta^{(1)}_{(UO2(OH)3-,\,K+)} = 0.34$ kg·mol^{-1}

$\beta^{(0)}_{(UO2(OH)42-,\,K+)} = 0.07$ kg·mol^{-1} $\quad$ $\beta^{(1)}_{(UO2(OH)42-,\,K+)} = 1.23$ kg·mol^{-1}

Figure 14 shows that the Pitzer activity model derived in this work results in a very good agreement with experimental log ${}^*K'_{s,UO_2(OH)_3^-}$ and log ${}^*K'_{s,UO_2(OH)_4^{2-}}$ obtained from solubility experiment in both NaCl and KCl systems.

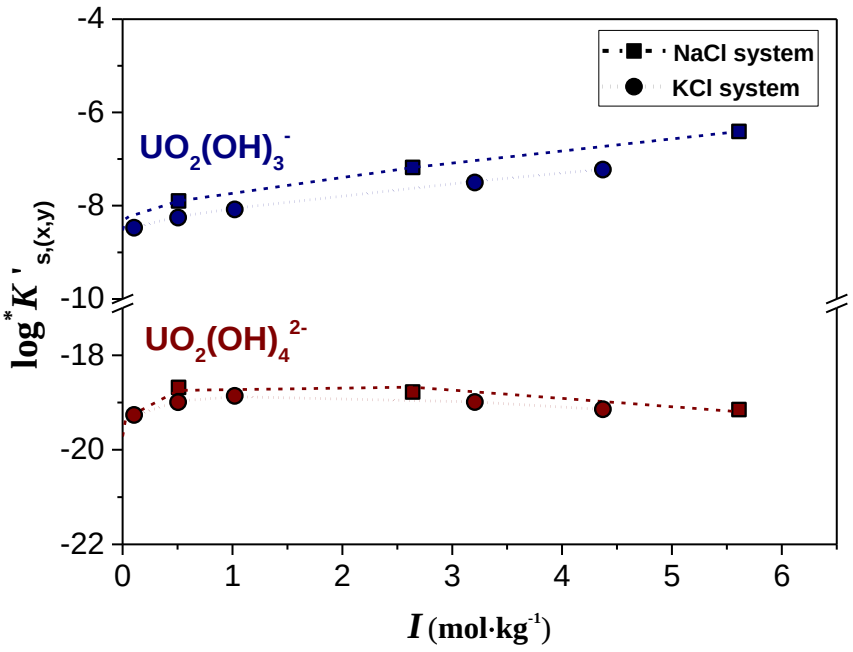

Figure 14. *Conditional formation constants log ${}^*K'_{s,(x,y)}$ for anionic (13) and (14) hydroxide complexes as a function of NaCl and KCl molalities: experimental values (symbols) and calculated functions based on the Pitzer activity model derived in this work (dashed line: NaCl, dotted line: KCl).*

4.2.3.2.3 Summary of Pitzer parameters for the U^{VI}–Na^+–K^+–Mg^{2+}–H^+–OH^-–Cl^-–H_2O(l) system

Table 6 shows newly generated Pitzer parameters for hydrolysis species of U(VI) in NaCl, KCl and $MgCl_2$ systems. The selection is based on the overall fit to the experimental solubility and titration data gathered in the present study as well as in the literature.

Table 6. *Pitzer parameters for UO_2^{2+} and U(VI) hydrolysis species selected in the present work based on the experimental data and simplified Pitzer model.*

U(VI) species			**Pitzer binary parameters**				
I	***J***		$\beta^{(0)}$	$\beta^{(1)}$	$\beta^{(2)}$	C^{φ}	**References**
UO_2^{2+}	Cl^-		0.4274	1.644	0	–0.0368	[1991PIT]
UO_2OH^+	Cl^-		0.15	0.3	0	0	(p.w.)
$(UO_2)_2(OH)_2^{2+}$	Cl^-		0.4714	2.02	0	0	(p.w.)
$(UO_2)_3(OH)_4^{2+}$	Cl^-		0.1294	0.8519	0	0	(p.w.)
$(UO_2)_3(OH)_5^+$	Cl^-		0.252	0.096	0	0	(p.w.)
$(UO_2)_4(OH)_7^+$	Cl^-		0.23	0.3	0	0	(p.w.)
$UO_2(OH)_3^-$	Na^+		–0.26	0.34	0	0	(p.w.)
	K^+		–0.26	0.34	0	0	(p.w.)[a]
	Mg^{2+}		0.20	1.6	0	0	(p.w.)
$UO_2(OH)_4^{2-}$	Na^+		0.06	1.98	0	0	(p.w.)
	K^+		0.07	1.23	0	0	(p.w.)
$(UO_2)_3(OH)_7^-$	Na^+		–0.26	0.34	0	0	(p.w.)[b]
	K^+		–0.26	0.34	0	0	(p.w.)[a]
	Mg^{2+}		0.20	1.6	0	0	(p.w.)
$UO_2(OH)_2$(aq)	Na^+, K^+, Mg^{2+},Cl^-		0	0	0	0	(p.w.)
I	***j***	***i′***	**Pitzer ternary parameters**				
UO_2^{2+}	Cl^-	Na^+	$\Theta_{ii'}$ = 0.03	$\Psi_{iji'}$ = –0.01			[2009ALT/NEC]
	Cl^-	Mg^{2+}	$\Theta_{ii'}$ = 0.08	$\Psi_{iji'}$ = –0.072			[2009ALT/NEC]
$(UO_2)_2(OH)_2^{2+}$	Cl^-	Na^+		$\Psi_{iji'}$ = –0.0272			(p.w.)
$(UO_2)_3(OH)_4^{2+}$	Cl^-	Na^+		$\Psi_{iji'}$ = 0.0549			(p.w.)
$(UO_2)_3(OH)_5^+$	Cl^-	Mg^{2+}		$\Psi_{iji'}$ = –0.052			(p.w.)

a. set equal to the Pitzer parameters of the same species with Na^+; b. Set equal to ($UO_2(OH)_3^-$, Na^+).

4.2.4. Solubility and complexation of the system Ca–U(VI)–CO_3

4.2.4.1 Solubility measurements in NaCl systems

The solubility of liebigite, $Ca_2UO_2(CO_3)_3 \cdot 10H_2O$(cr), was investigated in water, 0.5 and 5.0 M NaCl systems. Because of the possible precipitation of calcite and degassing of CO_2(g), the pH_m of solution was initially set to be 8.0 with HCl/NaOH. The results of log $[U]_{tot}$ (after 0.1 μm filtration) *vs.* pH_m are shown in Figure 15.

Relatively high concentrations of uranium in equilibrium with $Ca_2UO_2(CO_3)_3 \cdot 10H_2O$(cr) are measured in water and 0.5 M NaCl systems. For these two systems, the concentration of calcium in solution determined by ICP-OES was approximately twice the concentration of uranium, thus indicating a congruent dissolution of liebigite. These results are consistent with previous solubility data reported in the literature for the same solid phase in 0.1 M $NaClO_4$ solutions [2002AMA]. In contrast to dilute systems, a significantly lower solubility (with log $[U]_{tot} \approx -4$) is observed in 5.0 M NaCl solutions. The decrease in solubility is also accompanied by a slight change in the colour of the solid phase controlling the solubility. In spite of the drop in log $[U]_{tot}$, high concentrations on [Ca] are retained in solution for this sample. All these observations strongly support that the liebigite in concentrated NaCl systems transforms into a secondary phase with a lower content in Ca.

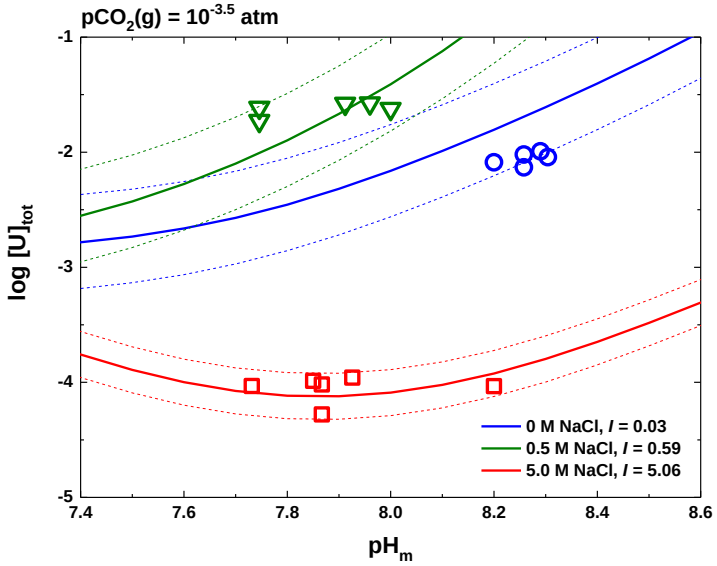

Figure 15. *Solubility of $Ca_2UO_2(CO_3)_3 \cdot 10H_2O$(cr) "starting material" in water ($I \approx 0.02$ M), 0.5 and 5.0 M NaCl systems. Solid lines represent the solubility of U(VI) calculated based on liebigite, $Ca_2UO_2(CO_3)_3 \cdot 10H_2O$(cr) for water and 0.5 M NaCl, and andersonite, $Na_2CaUO_2(CO_3)_3 \cdot 6H_2O$(cr) for 5.0 M NaCl, as solubility limiting phases in equilibrium with $pCO_2(g) = 10^{-3.5}$ atm.*

4.2.4.2 Solid phase characterization

Figure 16 shows the XRD patterns of liebigite equilibrated in water (sample A), 0.5 M NaCl (sample B) and 5.0 M NaCl (sample C). Sample A and B show very similar XRD patterns, in good agreement with those reported for $Ca_2UO_2(CO_3)_3 \cdot 9H_2O$(cr). On the other hand, a different diffractogram is obtained for sample C. The latter agrees well with the patterns previously reported for andersonite, $Na_2CaUO_2(CO_3)_3 \cdot xH_2O$(cr). These results are further supported by EDX and quantitative chemical analysis (see Table 7). The solid phase transformation is also clearly visualized in Figure 17, where SEM pictures of solids A, B and C are shown.

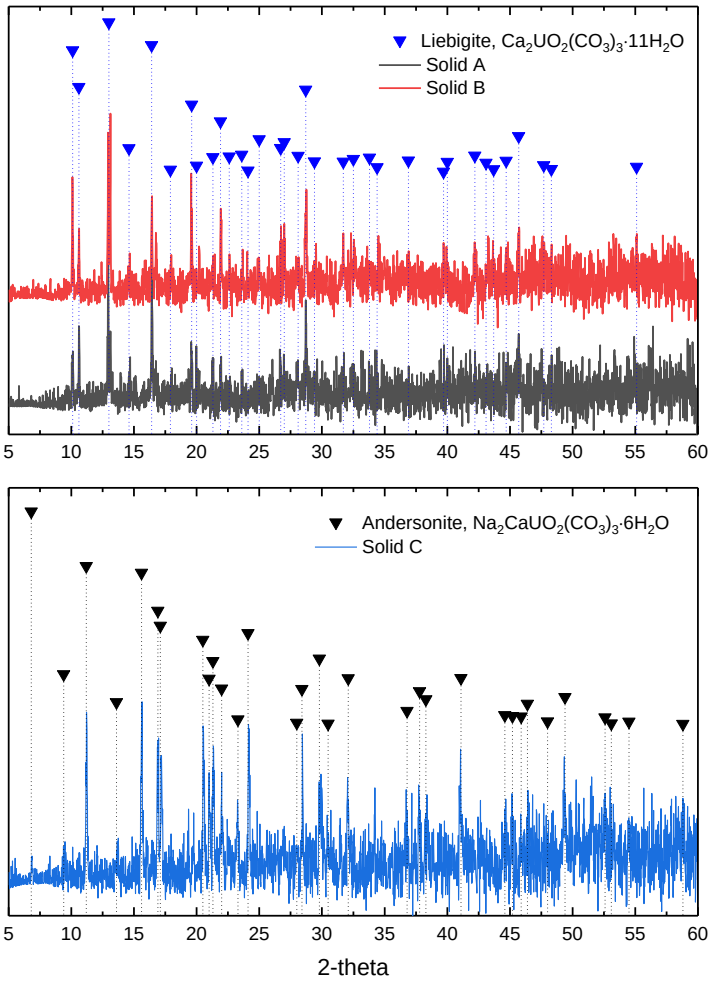

Figure 16. *XRD patterns of solid phases in samples A, B and C, equilibrated in water, 0.5 and 5.0 M NaCl, respectively. Inverse triangles correspond to reference patterns of liebigite and andersonite.*

Table 7. *Ca:U and Na:U ratio in the investigated solid phases, as quantified by EDX and quantitative chemical analysis.*

Sample	Ca:U		Na:U	
	EDX	**Chem. anal.**	**EDX**	**Chem. anal.**
A, water	2.3	2.1	-	-
B, 0.5 M NaCl	1.8	2.0	-	-
C, 5.0 M NaCl	1.0	1.1	2.0	1.9

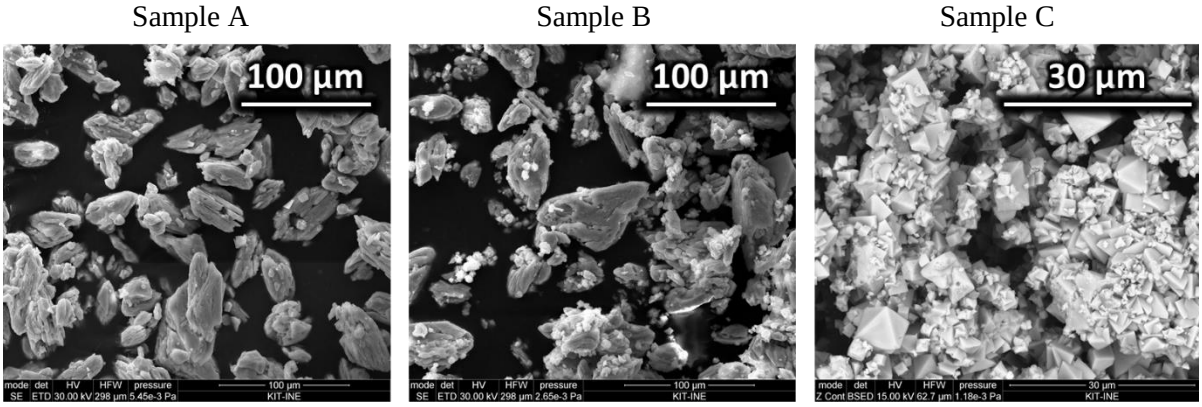

Figure 17. *SEM images of solid phases in samples A, B and C, equilibrated in water, 0.5 and 5.0 M NaCl, respectively.*

4.2.5 Solubility of U(VI) in nitrate containing solution

Nitrate is a ligand potentially relevant in the context of nuclear waste disposal, as nitrate may occur in rather large inventories in certain wasteform relevant for low and intermediate level waste. When leached from the emplaced waste after water intrusion, high nitrate concentrations can be generated in aqueous solutions, potentially impacting radionuclide redox chemistry and solubility. The work performed by KIT-INE within EDUKEM focusses on a first assessment of dissolved nitrate on U(VI) solubility in saline systems. Aspects related to the impact of nitrate on uranium redox chemistry (i.e. re-oxidation of U(IV) by dissolved nitrate under reducing conditions) is not addressed in EDUKEM.

The solubility studies by KIT-INE presented in this report for dilute to concentrated NaCl and $MgCl_2$ solutions (see Chapter 3.2.1 and Chapter 3.2.3) allow a comparison between these solubility studies under absence of nitrate with comparable studies in nitrate containing solutions of similar ionic strenght. Data on U(VI) solubility for the $CaCl_2$ system are taken from unpublished studies of KIT-INE which were produced by M. Altmaier of KIT-INE earlier outside the scope of EDUKEM. The same solubility

limiting solid phases identified as solubility limiting U(VI) solid phases in the nitrate free systems were used in new solublity studies under the presence of nitrate. A solubility increase relative to the nitrate free systems can be taken as evidence on additional U(VI)-nitrate complexes in solution, and hence increased total uranium concentration in solution. The nitrate concentrations in the reported experiments are set to very high values, to allow for an unambiguous identification of any potential nitrate impact on U(VI) solubility. In the $MgCl_2$ system, the nitrate concentrations were strongly varied over a very large concentration range for a more systemetic assessment. The uranium concentration were measured by ICP-MS after ultrafiltration, the pH_m values were derived by using combination pH combination electrodes and considering the required correction of the measures experimental pH_{exp} values in saline systems to theremodynamically measingful pH_m values, using empirical correction factors.

The systems studied by KIT-INE within EDUKEM on U(VI) nitrate interactions are:

(a) Concentrated NaCl solution at I = 5 M. The solubility of Na-uranate $Na_2U_2O_7 \cdot H_2O$(cr) is investigated in (3 M NaCl + 2 M $NaNO_3$) solution at pH_m = 10.8 and pH_m = 13.1, relative to a study in pure 5 M NaCl solution.

(b) Concentrated $CaCl_2$ solution. The solubility of Ca-uranate $Ca_2U_2O_7 \cdot 3H_2O$(cr) is investigated in (1 M $CaCl_2$ + 1.5 M $Ca(NO_3)_2$) solution at pH_m = 12.0, the maximum pH_m in this system, relative to studies in 1 M and 4 M $CaCl_2$ solutions.

(c) Concentrated $MgCl_2$ solution. The solubility of Metashoepite $UO_3 \cdot 2H_2O$(cr) is investigated in $MgCl_2$-$Mg(NO_3)_2$ mixtures under strong variation of nitrate concentration (0 M $\leq [NO_3^-] \leq$ 7 M) relative to studies in 2.5 M (2.67 m) and 4.5 M (5.15 m) $MgCl_2$ solutions. The pH_m in this series is at pH_m = 8.6 ± 0.2, the maximum pH_m in these systems. The variation of pH_m is reflecting changes in the matrix electrolyte system composition and not measurement uncertainties.

As shown in Figure 18, no solubility increase due to nitrate complexation of U(VI) species can be evidenced in the solubility studies. This can be rationalized by the fact that the early and strong hydrolysis in the U(VI) system will outcompete complexation with the relatively weak nitrate ligand. The studies perfomed by KIT-INE clearly show that nitrate complexation does not contribute to a solubility increase under the investigated conditions, even under extremely high nitrate concentrations and at high ionic strength. In view of the reported new solubility data, there is no need to derive a full thermodynamic model for the investigated nitrate containing systems.

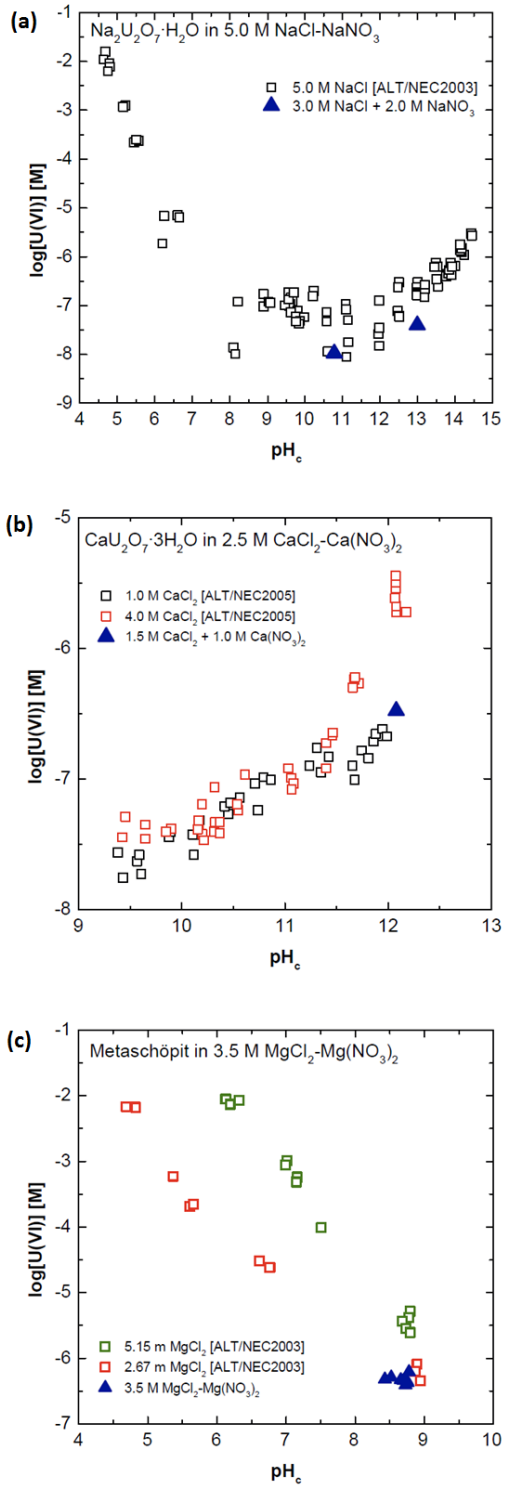

Figure 18. *Impact of dissolved nitrate (data in blue symbols) on U(VI) solubility. (a) Solubility of Na-uranate $Na_2U_2O_7{\cdot}H_2O(cr)$ in 5 M NaCl and in nitrate containing (3 M NaCl + 2 M $NaNO_3$) solution. (b) Solubility of Ca-uranate $Ca_2U_2O_7{\cdot}3H_2O(cr)$ in 1 M and 4 M $CaCl_2$ and in nitrate containing (1 M $CaCl_2$ + 1.5 M $Mg(NO_3)_2$) solution. (c) Solubility of Metashoepite $UO_3{\cdot}2H_2O(cr)$ in 2.5 and 3. 5 M $MgCl_2$ and nitrate containing 3.5 M $MgCl_2/(NO_3)_2$ mixtures. All three inviestigated systems show no solubility increase by nitrate relative to the comparable nitrate-free systems.*

4.3. Solubility and hydrolysis of U(IV). Thermodynamic description

4.3.1. Solubility and hydrolysis of U(IV) in NaCl, $MgCl_2$ and $CaCl_2$ solutions

4.3.1.1 Solubility data of U(IV) in reducing, dilute to concentrated NaCl solutions

Figure 19 shows the concentration of U(IV) in equilibrium with UO_2(s, hyd) as determined in 0.1, 0.5, 2.0 and 5.0 M NaCl solutions. Under acidic conditions ($pH_m \leq 5$), a steep decrease in the solubility is observed with increasing pH_m. Furthermore, a slight increase of the solubility takes place with increasing ionic strength. Figure 19 shows also experimental solubility data with UO_2(am, hyd) as reported in [1997RAI/FEL], as well as the solubility curve of UO_2(am, hyd) calculated using the thermodynamic model reported in [2001NEC/KIM]. The trend in the solubility data determined in this work is in good agreement with solubility data reported in [1997RAI/FEL] and model calculations using thermodynamic data in [2001NEC/KIM], although uranium concentrations measured in the present work are approximately 2 orders of magnitude lower. Such discrepancies could be attributed to the particle size of the solid phase used in different studies. The method used by Rai and co-workers and in the present work for the synthesis of UO_2(s, hyd) is very similar. However, most of the data reported by the former authors were collected after equilibration times of 50 – 100 days. Only for a limited number of samples / systems, an additional, long-term sampling step was performed after 300 – 400 days. Indeed, a clear trend to decrease [U] with time can be observed in most of their NaCl systems. In this study, the freshly prepared UO_2(s, hyd) was aged 3 months before starting the undersaturation solubility experiments. After preparation of the individual samples, these were equilibrated for up to 605 days in the corresponding matrix solutions. Such differences in the equilibration time may have resulted in differences in the particle size and, accordingly, in the solubility. A thorough discussion on the UO_2(s, hyd) solid phase used in the present study and in [1997RAI/FEL] is provided in Section 4.3.1.4.

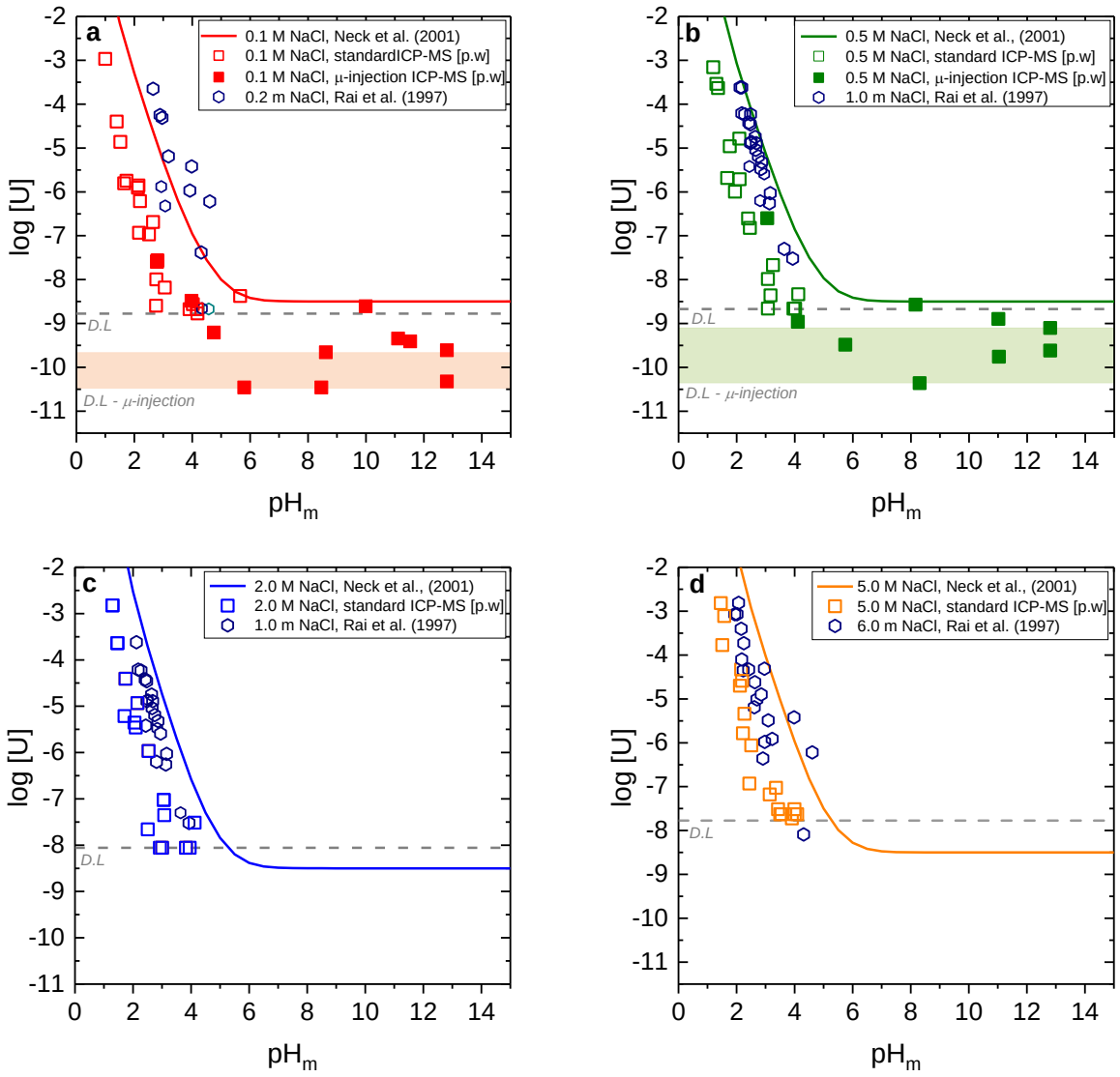

Figure 19. *Experimental solubility data obtained in this work in a. 0.1 M, b. 0.5 M, c. 2.0 M and d. 5.0 M NaCl systems, in comparison with previously reported data by [1997RAI/FEL]. Solid lines corresponding to the solubility of UO_2(am, hyd) solid phase calculated for each ionic strength by using the data reported by [2001NEC/KIM]. Detection limits for μ-injection ICP-MS measurements in 0.1 and 0.5 M NaCl systems are shown as shadowed areas in light red and light green and correspond to detection limits from different measurements (calculated as 3σ of the blank).*

The detection of [U] at $pH_m \geq 4$ / 5 (depending upon ionic strength) is challenging due to the very low solubility and the strong dilution steps (100 to 5000 times) needed in the most concentrated NaCl systems. For this reason, μ-injection ICP-MS was used to achieve lower detection limits in 0.1 and 0.5 M NaCl solutions. This technique could not be applied to 2.0 and 5.0 M NaCl.

Figure 19 shows also the experimental solubility data in dilute to concentrated NaCl solutions at $pH_m \geq 5$ after 10 kD ultrafiltration. The largely scattered solubility data observed in this pH_m-region is most likely caused by the formation / presence of U(IV) intrinsic colloids, the very low U(IV) solubility and / or the sorption of neutral $U(OH)_4(aq)$ species in the filter. All uranium concentrations measured after 10 kD ultrafiltration in 2.0 and 5.0 M NaCl systems were below the detection limit of the standard ICP-MS. In 0.1 and 0.5 M NaCl systems, the experimentally measured $[U]_{aq}$ falls clearly below the solubility of UO_2(am, hyd) calculated using the thermodynamic and activity models available in the literature. This finding is consistent with the observations obtained under acidic conditions, thus further supporting a solubility-control by a more crystalline solid phase. A pH_m-independent behaviour of the solubility was observed at $5 \leq pH_m \leq 13$ (Figures 19a and 19b). Assuming a solubility-control by UO_2(s, hyd), this behaviour implies that the neutral species $U(OH)_4(aq)$ prevails in the aqueous phase in this pH region as described by equation (29).

$$UO_2(s, hyd) \Leftrightarrow U(OH)_4(aq) + xH_2O(l) \quad (29)$$

Although the predominance of the anionic hydrolysis species $U(OH)_5^-$ and $U(OH)_6^{2-}$ was reported by some authors [2005FUJ/YAM], the undersaturation solubility data obtained in this study allows disregarding the formation of such species within the investigated pH_m-range. This observation is in excellent agreement with the main conclusions derived in Section 4.1 from oversaturation experiments.

4.3.1.2 Solubility data of U(IV) in reducing, dilute to concentrated $MgCl_2$ solutions

Solubility data of U(IV) determined in 0.25, 2.0 and 4.5 M $MgCl_2$ are shown in Figure 20, together with experimental solubility data reported by [1997RAI/FEL] in analogous $MgCl_2$ solutions and with solubility curves calculated using thermodynamic and SIT activity models reported by [2001NEC/KIM]. Note that ionic strength in 4.5 M $MgCl_2$ systems (I = 13.5 M) is well beyond the generally accepted range of SIT, and thus calculations performed for this system must be considered as orientative.

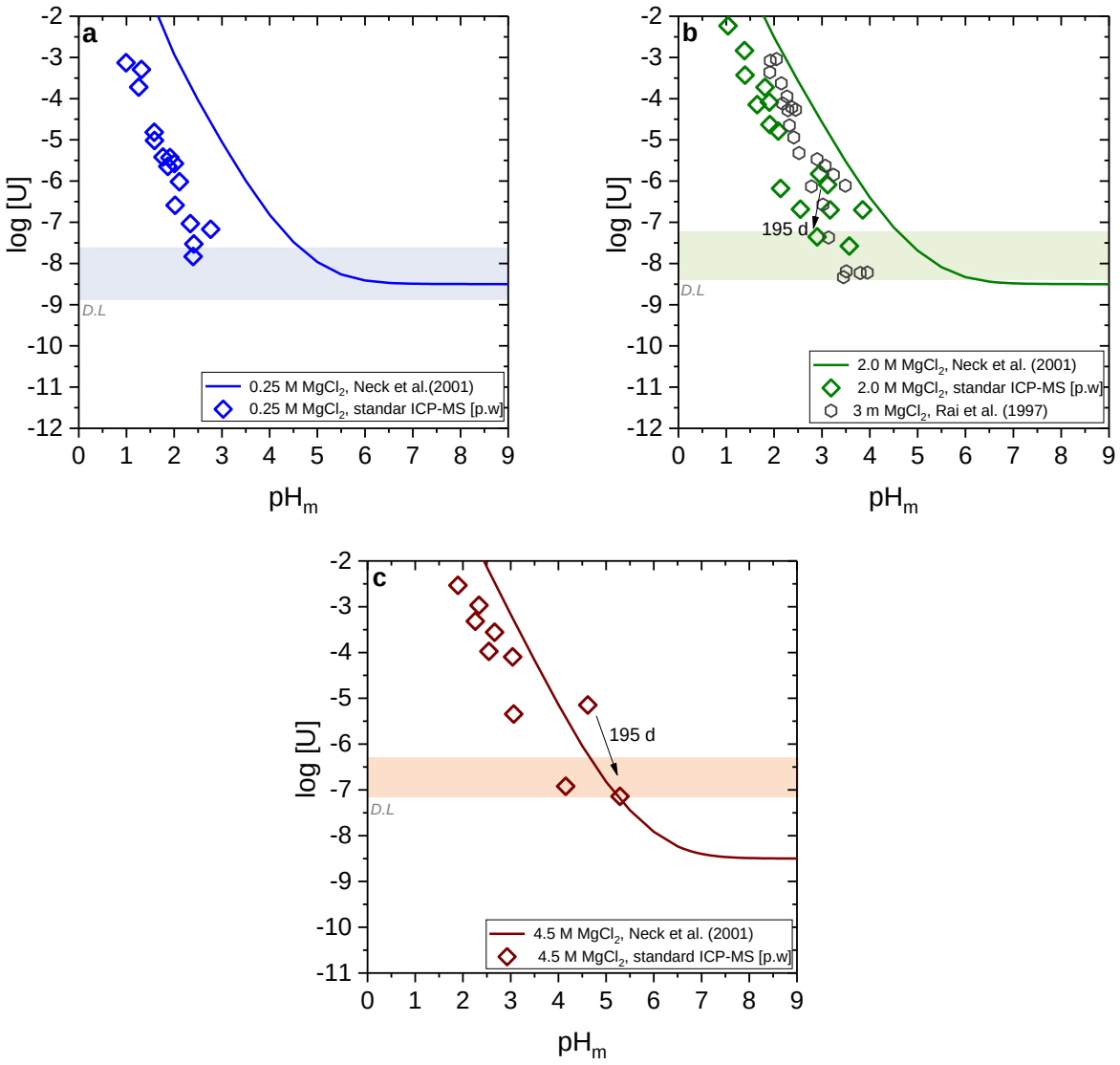

Figure 20. *Experimental solubility data obtained in this work for U(IV) in a. 0.25 M, b. 2.0 M and c. 4.5 M $MgCl_2$ systems, in comparison with solubility data reported by [1997RAI/FEL] for analogous $MgCl_2$ systems. Solid lines corresponding to the solubility curve of UO_2(am, hyd) calculated for each ionic strength using thermodynamic data reported by [2001NEC/KIM]. Detection limits are shown as shadowed areas in light blue, green and red for 0.25 M, 2.0 and 4.5 M $MgCl_2$ systems respectively, involving different detection limits from different measurements (calculated as 3σ of the blank).*

Under acidic conditions ($pH_m \leq 4$) and analogously to NaCl systems, a steep decrease in the solubility of U(IV) is observed with increasing pH_m in all $MgCl_2$ systems. The increase in $MgCl_2$ concentration results in a significant increase in the solubility (*ca.* 3 orders of magnitude from 0.25 to 4.5 M $MgCl_2$). Such a relevant increase in the solubility expectedly results from strong ion interaction processes. In contrast to

NaCl systems, the solubility of U(IV) in $MgCl_2$ systems show slow equilibration kinetics, specially in 2.0 and 4.5 M systems. For these two systems, thermodynamic equilibrium is very likely not attain even after *t* = 351 days. Solubility data in 0.25 M $MgCl_2$ (Figure 20a) are virtually the same as in 0.5 M NaCl (Figure 19b), with the same chloride concentration but slightly lower ionic strength. This observation supports that the same solid phase is responsible for the control of U(IV) solubility in both salt systems, at least in dilute solutions. At $pH_m \geq 3$–4 (depending upon $MgCl_2$ concentration), the concentration of uranium in equilibrium with UO_2(s, hyd) drops below the detection limit of ICP–MS, and thus no information could be gained for this salt system and pH_m-range. However, based on the results obtained in NaCl systems and data reported for the solubility of Th(IV) in $MgCl_2$ systems [2004ALT/NEC], a solubility control by the pH_m-independent solubility reaction $UO_2(s, hyd) \Leftrightarrow U(OH)_4(aq) + xH_2O(l)$ is expected.

The solubility of UO_2(am, hyd) calculated using thermodynamic and activity models reported by [2001NEC/KIM] clearly overestimates (approximately 2 orders of magnitude) the experimental solubility data determined in the present work. The differences between the current data and solubility data reported by Rai *et al*. in both NaCl and $MgCl_2$ systems indicates the higher crystallinity degree (smaller particle size) of the solid phase used in the present study.

4.3.1.3 Solubility data of U(IV) in reducing, dilute to concentrated $CaCl_2$ solutions

The solubility of U(IV) was also investigated in 0.25, 2.0 and 4.5 M $CaCl_2$ solutions under alkaline conditions $9.5 \leq pH_m \leq 12$. Based on previous solubility studies with Th(IV), Pu(IV) and Np(IV) in alkaline $CaCl_2$ solutions [2008ALT/NEC, 2010FEL/NEC], a solubility increase above $pH_m \approx 11$ for $[CaCl_2] \geq 2.0$ M is expected as a result of the formation of ternary Ca-An(IV)-OH complexes. The solubility and hydrolysis constants $\log {}^{*}K^{o}_{s,(4,1,8)} = -(57.2 \pm 1.4)$ and $\log {}^{*}\beta^{o}_{(4,1,8)} = -(57.2 \pm 1.4)$ were estimated for $Ca_4[U(OH)_8]^{4+}$ in [2010FEL/NEC] using linear free energy relationships (LFER).

Figure 21 shows experimental solubility data determined in this work together with the solubility curves calculated for each ionic strength using the thermodynamic and SIT activity models reported by [2001NEC/KIM], including also the formation of the complex $Ca_4[U(OH)_8]^{4+}$ as estimated by Fellhauer *et al.* [2010FEL/NEC]. Uranium concentrations below the detection limit are observed in all investigated $CaCl_2$ systems under alkaline conditions. Based on the solubility curves calculated for UO_2(am, hyd) and including the formation of the ternary complex $Ca_4[U(OH)_8]^{4+}$, however, U(IV) solubility should be well above the current detection limit for $[CaCl_2] \geq 2.0$ M and $pH_m \geq 11.5$. On the other hand, this result is

consistent with the sistematically lower U(IV) solubility observed in the present study for NaCl and $MgCl_2$ systems. Accordingly, these findings can neither confirm nor disregard the formation of ternary complexes Ca-U(IV)-OH. An extended discussion on this dataset is provided in Section 4.3.1.

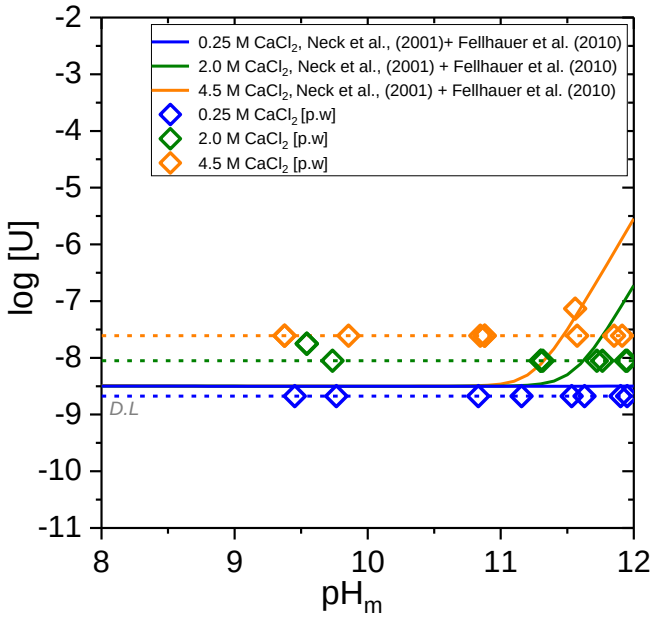

Figure 21. *Experimental solubility data obtained in this work for U(IV) in $CaCl_2$ systems. Solid lines corresponding to the solubility curve of UO_2(am, hyd) calculated for each ionic strength using thermodynamic data reported by [2001NEC/KIM] and [2010FEL/NEC]. Dashed lines correspond to the detection limits of ICP-MS determined (as 3σ of the blank) for each $CaCl_2$ concentration.*

4.3.1.4 Solid phase characterization

4.3.1.4.1 XRD, SEM-EDS, quantitative chemical analysis and TG-DTA

The starting material and solid phases of selected solubility samples were investigated by XRD, SEM-EDS, quantitative chemical analysis and TG-DTA. The main outcome of this characterization is summarized in Table 8, together with the experimental conditions of the investigated samples. Additional characterization of selected samples using EXAFS is described in a separate Section below.

Table 8. *Experimental conditions of investigated samples and XRD, SEM-EDS, quantitative chemical analysis and TG-DTA results.*

Background electrolyte	**pH_m**	**XRD (2Θ)**	**Na:U ratio SEM–EDS**	**Na:U ratio Quantitative chem. analysis**	**TG–DTA (number of H_2O)**
"Starting material"	12.1	28.4	0.30	0.17	1.0
0.1 M NaCl	2.8	28.6	0.08	0.04	n.m.
0.1 M NaCl	11.4	28.4	0.0	0.02	n.m.
0.5 M NaCl	3.3	28.4	n.m.	0.0	n.m.
0.5 M NaCl	11.1	28.4	n.m.	0.0	n.m.
2.0 M NaCl	3.1	28.5	n.m.	0.0	n.m.
2.0 M NaCl	11.3	28.6	n.m.	0.06	n.m.
5.0 M NaCl	3.1	28.6	0.0	0.07	n.m.
5.0 M NaCl	11.3	28.6	0.06	0.02	n.m.
uncertainty	±0.05		±0.1	±0.03	±0.5

Figures 22a – 22c show the XRD diffractograms of the "starting material" and solid phases of selected solubility samples. In all cases, well-defined but broad XRD patterns are observed. This indicates that the solid phases investigated in this study are not amorphous, but rather hold a (nano-)crystalline character. XRD patterns of the "starting material" (Figure 22a) are in excellent agreement with those reported for UO_2(cr). The first and most intense peak in the XRD of the "starting material" is found at $2\Theta = 28.4$, which agrees very well with $2\Theta = 28.2$ (JCPDS file Nr. 73–2293) and 28.3 (JCPDS file Nr. 41-1422) reported for UO_2(cr). No reflections are observed in the region $10° \leq 2\Theta \leq 20°$, where the first and most intense peak of relevant (layered) U(VI) solid phases is observed, *i.e.* $UO_3 \cdot 2H_2O$(cr) ($2\Theta = 12.0$) or $Na_2U_2O_7 \cdot H_2O$(cr) ($2\Theta = 14.9$) (see Section 4.3.2). These results confirm the absence of any crystalline U(VI) phase in the "starting material". Furthermore, Rietveld analysis of the XRD data indicates the average crystal size of (3 ± 1) nm.

XRD of the solid phases equilibrated in 0.1, 0.5, 2.0 and 5.0 M NaCl solutions under acidic and alkaline conditions are shown in Figure 22b and 22c, respectively. Solid phases in both acidic and alkaline systems retain the same XRD patterns of the "starting material", indicating that no phase transformation occurred in the course of the solubility experiment. On the other hand, some additional sharp features are observed in 0.1, 0.5 and 2.0 M NaCl solutions at $pH_m \approx 3$ and in 0.5, 2.0 and 5.0 M NaCl systems at $pH_m \approx 11$. These sharp patterns match those of SnO(cr) (JCPDS file Nr. 72–1012) very well in both investigated pH conditions.

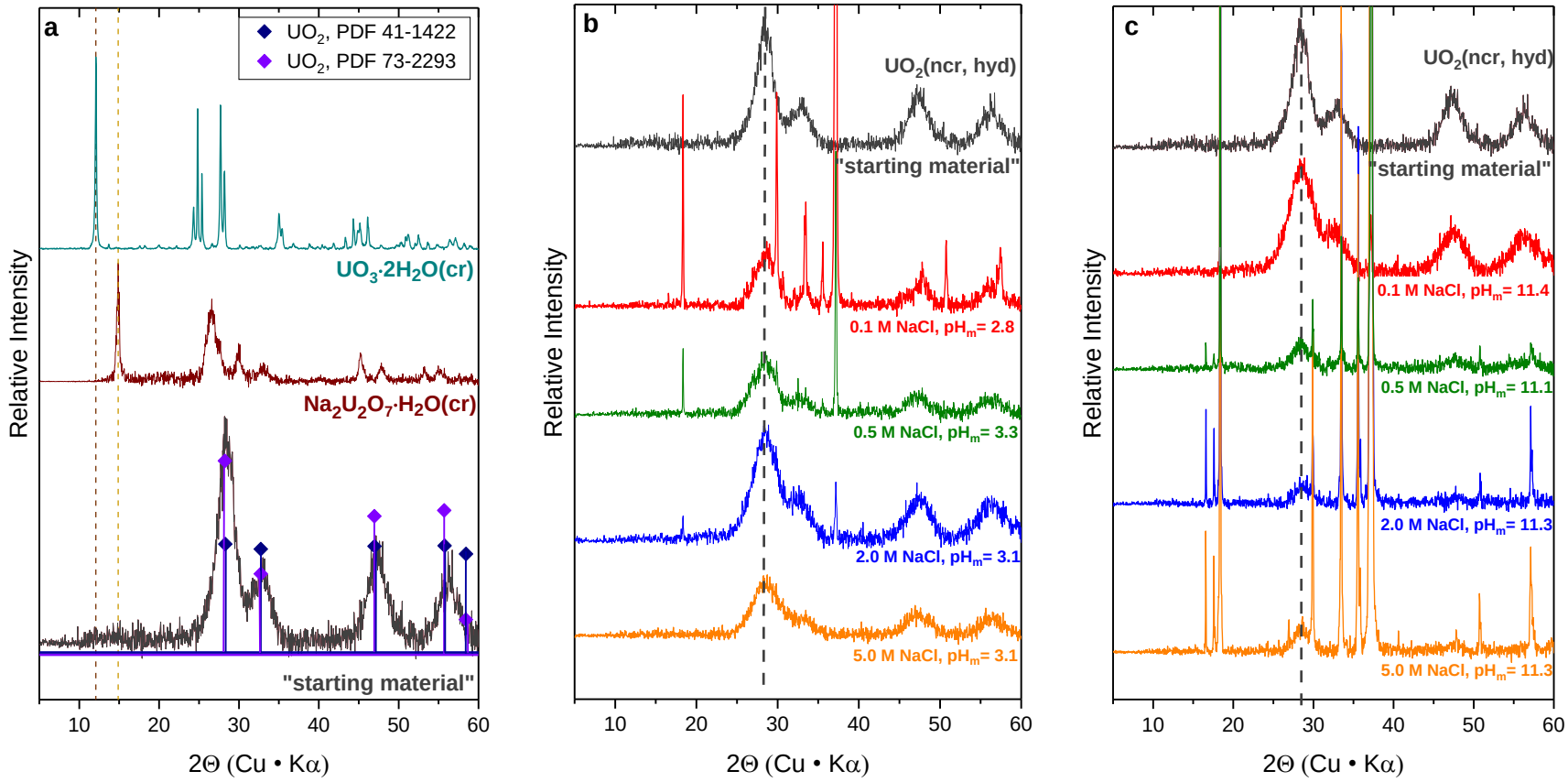

Figure 22. *XRD diffractograms of a. "starting material" and reference data for $UO_3{\cdot}2H_2O$(cr) and $Na_2U_2O_7{\cdot}H_2O$(cr) solid phases (see section 4.3.2 and [2017ALT/YAL]); and of solid phases collected from selected solubility samples in NaCl systems b. in acidic pH_m range and c. in alkaline pH_m range. Green and blue diamonds indicate the main patterns and relative intensities of UO_2(cr) reference material (PDF 41-1422 and 73-2293).*

EDS results summarized in Table 8 for the "Starting material" indicate the presence of a small fraction of Na in the solid, in good agreement with results obtained by quantitative chemical analysis (ICP–OES). This observation likely arises from the insufficient washing of $Na_2S_2O_4$ (or its degradation products) present in the "starting material" suspension, although may also result from the sorption of Na on the surface of the solid phase and/or incorporation to the solid phases, as reported previously for Th(IV) hydrous oxide [1991FEL/RAI]. EDS analyses of solid phases recovered from NaCl systems with Sn(II) as reducing chemical indicate that these crystalline compounds mostly contain Sn, in agreement with the XRD patterns obtained for these samples. Note that, in contrast to the "starting material" prepared and stored in $Na_2S_2O_4$, no (or very small fraction of) Na is determined by EDS and quantitative chemical analysis in the solubility samples equilibrated in the presence of Sn(II). This observation supports that the Na-content identified in the "starting material" is likely resulting from the deposition of $Na_2S_2O_4$ (or its degradation product) in the surface of the uranium solid, rather than from Na sorption or incorporation in the UO_2 structure.

Aliquots of the U(IV) "starting material" were collected after different equilibration times (30, 365, 418 and 798 days) and characterized by TG-DTA in order to quantify the number of hydration waters present. Samples were washed 3-5 times with ethanol and dried under Ar atmosphere before the measurement. The weight loss in the four investigated samples indicated the presence of 0.9, 1.4, 0.8 and 1.0 water molecules, respectively. No clear trend in the number of hydration waters was observed with increasing equilibration time, and the unweighted average of all measurements (1.0 ± 0.5, with uncertainty calculated as 3 times the standard deviation) is taken as the water content in the investigated UO_2(ncr, hyd) material.

Based on the combination of all solid characterization techniques, the solid phase used in this solubility study is identified as $UO_2 \cdot H_2O$(ncr). To the best of the authors' knowledge, this is the most accurate characterization of "UO_2(s)" used in solubility experiments at ambient temperature conditions.

4.3.1.4.2 EXAFS

Figure 23 shows the k^2-weighted uranium L_{III} EXAFS data and corresponding Fourier transforms of the two investigated samples: (i) the "starting material" $UO_2 \cdot H_2O$(ncr) in the presence of 20 mM $Na_2S_2O_4$ (t = 293 days), and (ii) the solid phase $UO_2 \cdot H_2O$(ncr) equilibrated in 0.1 M NaCl at pH_m= 8.5 in the presence of 5 mM $SnCl_2$ (t = 455 days). Table 9 summarizes the structural parameters derived from the EXAFS fit: coordination numbers (N), distances (R), Debye-Waller factors (σ^2) and energy shift parameter (ΔE^0). The goodness of the fit is given in terms of the percentage misfit between data and theory (R-factor). Fits are

performed in R-space simultaneously in k^1-, k^2- and k^3-weighted data. The k- and R-ranges used for the fit are given in Table 9. The overall intensity factor (S_0^2) was set to 0.65 in the fit.

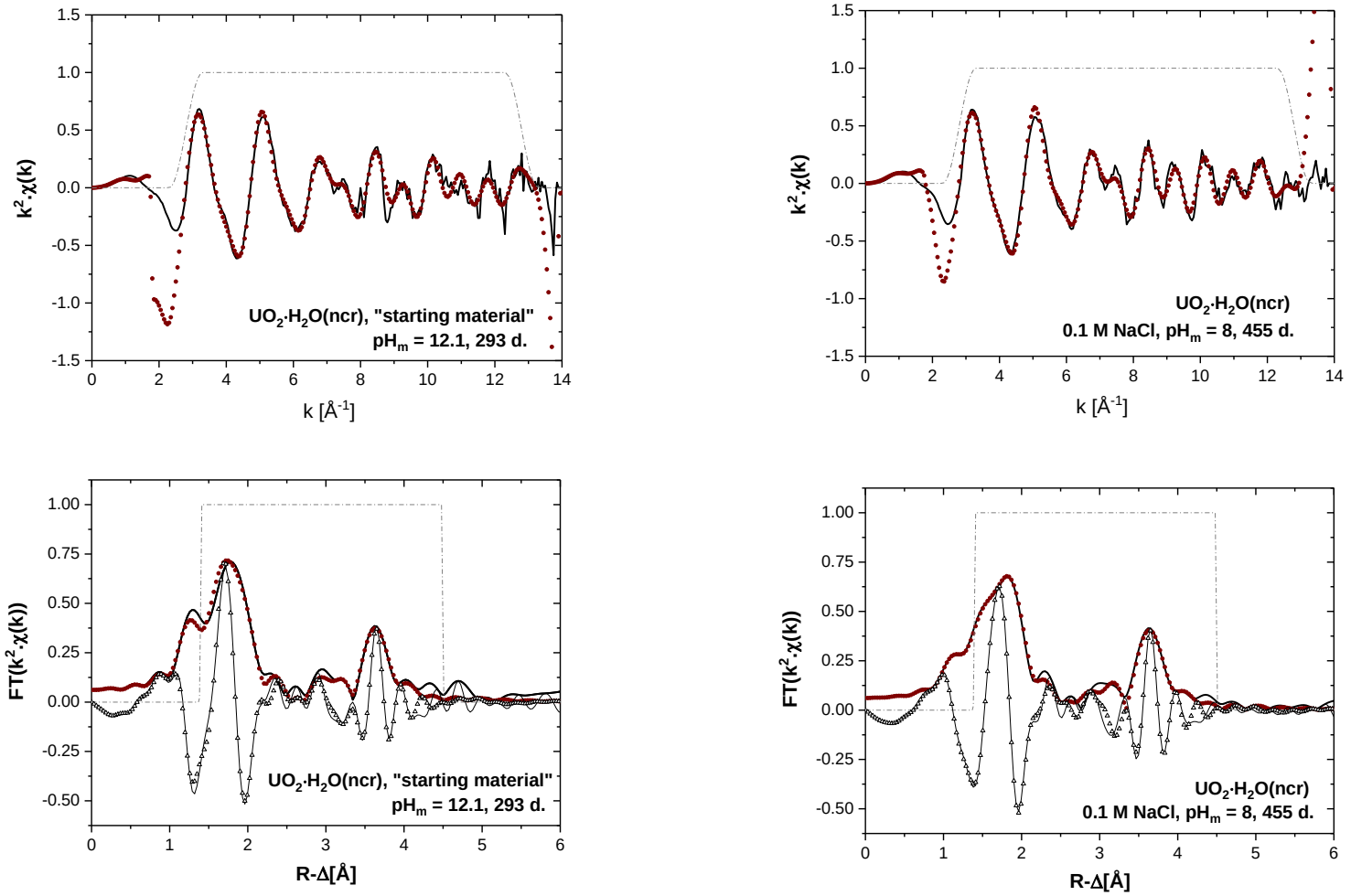

Figure 23. *U L_{III}–edge EXAFS results for $UO_2 \cdot H_2O$(ncr) "starting material" at pH_m = 12.1 (left) and $UO_2 \cdot H_2O$(ncr) in 0.1 M NaCl at pH_m = 8.5 (right). k^2-weighted EXAFS spectra (upper panel) and Fourier Transform (lower panel); experimental data are depicted as solid lines, whereas fits are shown as red circles and black triangles (modulus and imaginary parts, respectively). Dashed lines correspond to the FT hanging windows used in the EXAFS fit.*

Table 9. *Structural parameters obtained from the EXAFS evaluation of $UO_2{\cdot}H_2O$(ncr) "starting material" at pH_m = 12.1 and $UO_2{\cdot}H_2O$(ncr) in 0.1 M NaCl at pH_m = 8.5.*

Sample	Eq. time (days)	Path	CN	R(Å)	σ^2 (Å^2)	ΔE_0	R-factor
$UO_2{\cdot}H_2O$(ncr) "starting mat.", pH_m= 12.1	293	U-O_1	6.5	2.33	0.007	-1.38	0.02
R-space (1.4-4.5 Å)		U-U	12*	3.86	0.010		
k-Range (2.8-12.8 Å^{-1})		U-O_2	24*	4.44	0.008		
$UO_2{\cdot}H_2O$(ncr), 0.1 M NaCl, pH_m= 8.5	455	U-O_1	8.0	2.33	0.010	-2.66	0.03
R-space (1.4-4.5 Å)		U-U	12*	3.86	0.009		
k-Range (2.8-12.8 Å^{-1})		U-O_2	24*	4.45	0.008		

Fit errors: CN: ± 20%, R: 0.01 Å, σ^2: 0.001 Å^2..
*parameter fixed during the fit (coordination number from the UO_2 crystal structure)

EXAFS spectra and Fourier Transforms of the two investigated samples show great similarities (see Figure 4.10), denoting that the structure of the starting material $UO_2{\cdot}H_2O$(ncr) is mostly retained throughout the solubility experiments (up to t = 455 days). Fourier Transforms in Figure 4.10 show two well-defined shells at R–Δ ≈ 1.8 and 3.7 Å corresponding to the backscattering of O and U atoms, respectively. The prominent U-U backscattering at R–Δ ≈ 3.7 Å observed in both samples supports the presence of a well-ordered, (nano-)crystalline solid phase. The good quality (signal-to-noise ratio) of the EXAFS data collected allowed the fit within $2.8 \leq k$ (Å^{-1}) ≤ 12.8 and $1.5 \leq R$ (Å) ≤ 4.5. The fit was performed using as starting structure UO_2(cr) as reported in [1982COO], and included the shells U-O_1 and U-U, but also a distant U-O_2 shell. In order to limit the number of free parameters in the fit and avoid a too strong correlation between fit parameter, the coordination numbers of U-U and U-O_2 shells were fixed to 12 and 24 as reported for the original UO_2(cr) structure.

Virtually the same distances U-O_1 ($R_{U\text{-}O1}$), U-U ($R_{U\text{-}U}$) and U-O_2 ($R_{U\text{-}O2}$) were determined for the two solid phases investigated (Table 9), strongly supporting that both solid phases hold the same structure. Furthermore, the distances determined in this work for $R_{U\text{-}O1}$= 2.33 Å and $R_{U\text{-}U}$ = 3.86 Å are in good agreement with data reported in the literature for $UO_{2.00}$(cr), *i.e.* [1982COO] ($R_{U\text{-}O1}$ = 2.37 Å and $R_{U\text{-}U}$ = 3.87 Å) and [2004CON/MAN] ($R_{U\text{-}O1}$= 2.36 Å and $R_{U\text{-}U}$ = 3.87 Å). Conradson and co-workers [149] investigated also the impact of x in UO_{2+x}(cr) (with x = 0.05, 0.08, 0.12, 0.17 and 0.20) in the original structural parameters of $UO_{2.00}$(cr), and thus the comparison with experimental data determined in this work arises as specially relevant. Hence, these authors observed a clear increase in $R_{U\text{-}O1}$ when going from $UO_{2.00}$(cr) ($R_{U\text{-}O1}$= 2.36 Å) to $UO_{2.20}$(cr) ($R_{U\text{-}O1}$= 2.42 Å). As indicated above, an invariant value of $R_{U\text{-}O1}$ was determined in the present work for the two investigated samples ($R_{U\text{-}O1}$= 2.36 Å), thus supporting the presence of a stoichiometric UO_2 solid phase with $x \rightarrow 0$ in both cases.

[2004CON/MAN] observed also a significant impact of an increasing *x* in the U-U backscattering. Hence, the authors reported a decrease in the coordination number of U, from 10.6 in $UO_{2.00}$(cr) to 2.5 in $UO_{2.20}$(cr), in both cases holding the same distance R_{U-U} = 3.88 Å. Coordination numbers U-U were set constant in the present work (12), but the fit resulted in virtually the same R_{U-U} and Debye-Waller factors for both investigated samples. This observation supports again the presence of an structure close to ideal $UO_{2.00}$(cr) in the two solid phases characterized in the present work. It is also interesting to note the differences observed in CN_{O1} for the $UO_2 \cdot H_2O$(ncr) samples investigated in this study. Hence, the solid phase equilibrated for a longer time (t = 455 days) shows CN_{O1} = 7.95, a value very close to the ideal CN_{O1} = 8 in $UO_{2.00}$(cr). On the other hand, a slightly lower value, CN_{O1}= 6.53, is determined for the solid phase aged 293 days. This observation possibly hints towards an increased order in the structure of $UO_2 \cdot H_2O$(ncr) with increasing equilibration time.

EXAFS results obtained in the present work complement and further extend the characterization of the solid phase achieved by XRD, SEM-EDS, quantitative chemical analysis and TG-DTA. Structural parameters derived from EXAFS data evaluation strongly support the presence of stoichiometric $UO_{2.00} \cdot H_2O$(ncr). Uranium is thus predominantly found as +IV, as expected on the basis of the very reducing conditions imposed by Sn(II) ($pe + pH_m \approx 2$) and in agreement with the low solubility observed within the complete pH_m-range investigated.

4.3.1.4 Chemical, thermodynamic and SIT activity models for the system U^{IV}–Na^+–Mg^{2+}–Ca^{2+}–H^+–OH^-–Cl^-–H_2O(l)

The chemical model of the system controlling the solubility of U(IV) in the absence of complexing ligands other than water is, *a priori*, well-defined and includes the solid phase $UO_2 \cdot H_2O$(ncr) and the aqueous species UOH^{3+}, $U(OH)_2^{2+}$, $U(OH)_3^+$ and $U(OH)_4$(aq). Accordingly, data evaluation in this work is restricted to these hydrolysis species and the solid phase $UO_2 \cdot H_2O$(ncr). Due to the large number of parameters controlling the solubility in the investigated systems (log ${}^*K^o_{s,0}$, log ${}^*\beta^o_{(1,1)}$, log ${}^*\beta^o_{(1,2)}$, log ${}^*\beta^o_{(1,3)}$, log ${}^*\beta^o_{(1,4)}$ and corresponding SIT coefficients for UOH^{3+}, $U(OH)_2^{2+}$ and $U(OH)_3^+$), the following modelling approach is considered in the context of this PhD thesis.

The approach used is based on the fit of only three parameters, namely log ${}^*K^o_{s,0}$, log ${}^*\beta^o_{(1,2)}$ and log ${}^*\beta^o_{(1,3)}$. The values of log ${}^*\beta^o_{(1,1)}$, log ${}^*\beta^o_{(1,4)}$ are kept constant as selected in the [2003GUI/FAN], whereas SIT coefficients of all charged species are either taken from [2003GUI/FAN] or from the charge analogy reported in [2001NEC/KIM].

Five different datasets are considered for the fit of the three parameters indicated above: 0.1, 0.5, 2.0, 5.0 M NaCl and 0.25 M $MgCl_2$. Data collected so far in 2.0 and 4.5 M $MgCl_2$ solutions are disregarded

in the fit due to the absence of thermodynamic equilibrium within the considered timeframe ($t \leq 351$ days, see text above). Because of the considerably larger number of experimental data points at $pH_m \leq 5$, a weighting factor of 4 has been given to the limited data collected in the near-neutral to hyperalkaline pH_m-range using micro-injection ICP–MS (data only available for 0.1 and 0.5 M NaCl solutions).

The five datasets are simultaneously fitted by minimizing the function $\sum((\log [U]_{exp} - \log [U]_{calc})^2)^{1/2}$. The value of $[U]_{calc}$ is the sum of $[UOH^{3+}]$, $[U(OH)_2^{2+}]$, $[U(OH)_3^{+}]$ and $[U(OH)_4(aq)]$, and can be calculated based on equations (30) – (33) and using equation (34):

$$UO_2 \cdot H_2O(ncr) + 4H^+ \Leftrightarrow U^{4+} + 3H_2O(l) \quad (30)$$

$$^*K^0_{s,0} = a_{U^{4+}} a_w^3 / a_{H^+}^4 \quad (31)$$

and

$$U^{4+} + nH_2O(l) \Leftrightarrow U(OH)_n^{(4-n)} + nH^+ \quad (32)$$

$$^*\beta^0_{(1,n)} = a_{U(OH)_n^{4-n}} a_{H^+}^n / a_{U^{4+}} a_w^n \quad (33)$$

with

$$[U]_{calc} = {}^*K^0_{s,0} \gamma_{H^+} m_{H^+}^4 a_w^{-3} (1 + \sum {}^*\beta^0_{(1,n)} \gamma_{H^+} m_{H^+}^{-n} a_w^n) \quad (34)$$

where $a_i = \gamma_i \cdot m_i$, γ_i is the activity coefficient calculated by SIT, and m_i is the concentration in molal units. The outcome of this modelling exercise is summarized in Table 10, whereas Table 11 shows the SIT interaction coefficients used in the fit. As observed in the discussion of the experimental data, the value of $\log {}^*K^o_{s,0}\{UO_2 \cdot H_2O(ncr)\}$ determined in this work is clearly lower than $\log {}^*K^o_{s,0}\{UO_2(am, hyd)\}$ reported in [2001NEC/KIM] and selected in the [2003GUI/FAN]. This result reflects the differences in the observed solubility, and highlights the larger particle size of the solid phase used in the present solubility study. Note that the currently used solid phase was equilibrated at T = 22 °C but for significantly longer time periods than in previous solubility studies. Accordingly, the value of $\log {}^*K^o_{s,0}\{UO_2 \cdot H_2O(ncr)\}$ is possibly more representative of the U(IV) solubility expected under repository conditions, if such a oxy-hydroxide is formed as secondary phase. A different behaviour is likely to be expected for UO_2(cr) present in spent fuel.

The fit of the experimental solubility data derived in this work results in a very similar $\log {}^*\beta^o_{(1,3)}$ to the equilibrium constant estimated by [2001NEC/KIM]. On the contrary, the fit results in a very low value of $\log {}^*\beta^o_{(1,2)}$ indicating a negligible contribution of this species to the overall solubility. The incorporation of this species to the solubility calculation using the hydrolysis constant estimated by [2001NEC/KIM] results in a significantly worse fit (quality parameter $\sum((\log [U]_{exp} - \log [U]_{calc})^2)^{1/2}$) equal to 72, compared with 41 for the set of constants summarized in Table 10). The model together with the experimental data are shown in Figures 24 and 25 for 0.1-5.0 M NaCl and 0.25 M $MgCl_2$ systems, respectively.

Table 10. *Equilibrium constants for U(IV) solubility and hydrolysis as determined in the present work and reported in [2003GUI/FAN], [2001NEC/KIM] and [2010FEL/NEC].*

	log **K°*			
	[p.w.]	**NEA–TDB**	**Neck and Kim**	**Fellhauer *et al.***
Solubility				
$UO_2 \cdot H_2O(ncr) + 4H^+ \Leftrightarrow U^{4+} + 4H_2O(l)$	–(0.32 ± 0.60)	(1.5 ± 1.0)[a]	(1.5 ± 1.0)[a]	
Hydrolysis				
$U^{4+} + H_2O(l) \Leftrightarrow UOH^{3+} + H^+$	–(0.54 ± 0.06)[b]	–(0.54 ± 0.06)	–(0.40 ± 0.20)	
$U^{4+} + 2H_2O(l) \Leftrightarrow U(OH)_2^{2+} + 2H^+$	–(8.6 ± 0.5)	–	–(1.10 ± 1.00)	
$U^{4+} + 3H_2O(l) \Leftrightarrow U(OH)_3^{+} + 3H^+$	–(4.2 ± 0.5)	–	–(4.70 ± 1.00)	
$U^{4+} + 4H_2O(l) \Leftrightarrow U(OH)_4(aq) + 4H^+$	–(10.0 ± 1.4)[b]	–(10.0 ± 1.4)	–(10.0 ± 1.4)	
Ternary Ca(II)–U(IV)–OH complexes				
$4Ca^{2+} + U^{4+} + 8H_2O(l) \Leftrightarrow Ca_4[U(OH)_8]^{4+} + 8H^+$	≤ –58.4[c]			–(58.7 ± 1.0)[d]

a. value reported for UO_2(am, hyd); b. set constant in the fit. Value taken as reported in NEA–TDB; c. extrapolated to $I = 0$ considering $\varepsilon(Ca_4[U(OH)_8]^{4+}, Cl^-) = \varepsilon(Ca_4[Th(OH)_8]^{4+}, Cl^-)$ as reported in [2008ALT/NEC] and [2010FEL/NEC]; d. estimated from LFER.

Table 11. *SIT interaction coefficients (in kg·mol^{-1}) used in the present work for the modelling of U(IV) experimental solubility data in 0.1, 0.5, 2.0 and 5.0 M NaCl solutions.*

I	***j***	***ε(i,j)***	***Reference***
U(IV) species			
U^{4+}	Cl^-	(0.36 ± 0.10)	[2001NEC/KIM]
$U(OH)^{3+}$	Cl^-	(0.20 ± 0.10)	[2001NEC/KIM]
$U(OH)_2^{2+}$	Cl^-	(0.10 ± 0.10)	[2001NEC/KIM]
$U(OH)_3^{+}$	Cl^-	(0.05 ±0.10)	[2001NEC/KIM]
$U(OH)_4(aq)$	Na^+, Cl^-	0	A
	Mg^{2+}, Cl^-	0	A
	Ca^{2+}, Cl^-	0	A
$Ca_4[U(OH)_8]^{4+}$	Cl^-	–(0.01 ± 0.10)[b]	[2008ALT/NEC, 2010FEL/NEC]

a. by definition in SIT; b. in analogy to $\varepsilon(Ca_4[Th(OH)_8]^{4+}, Cl^-)$ as reported in [2008ALT/NEC] and [2010FEL/NEC].

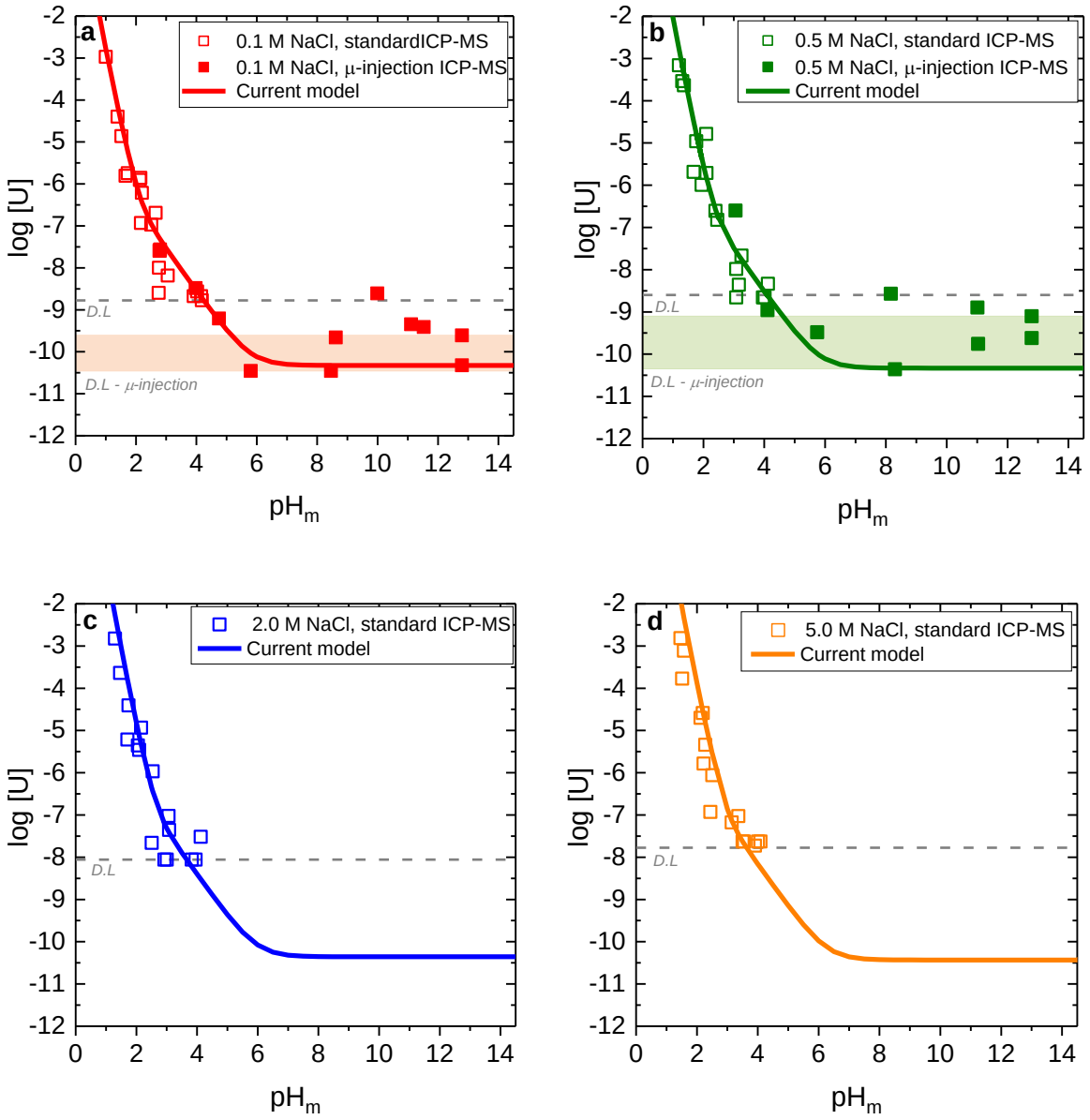

Figure 24. *Comparison of experimental U(IV) solubility data determined in 0.1 M, 0.5 M, 2.0 M and 5.0 M NaCl solutions with solubility calculations using the thermodynamic model derived in the present work (see Tables 10 and 11) and activity model reported by [2001NEC/KIM]. Detection limits for μ-injection ICP-MS measurements are shown as shadowed areas in light red and light green in 0.1 and 0.5 M NaCl systems involving detection limits from different measurements (calculated as 3σ of the blank). Gray dashed lines show the detection limit of standard ICP-MS measurements.*

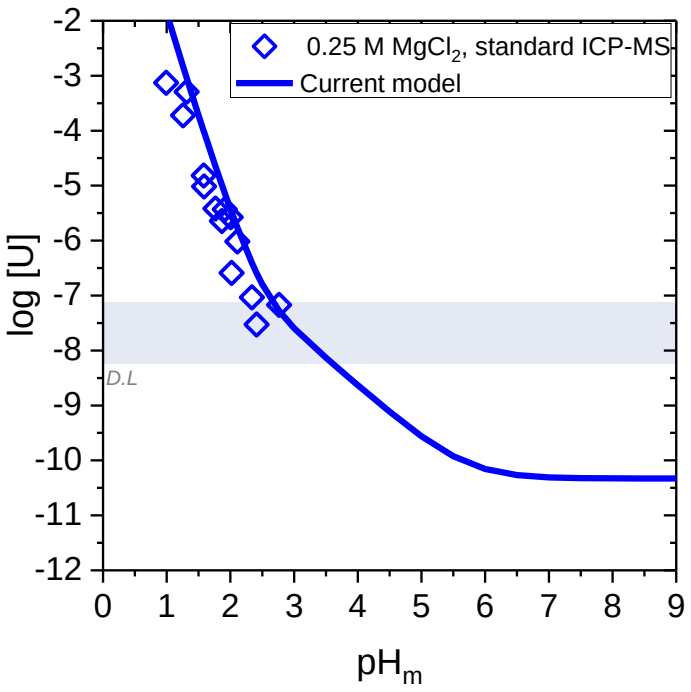

Figure 25. *Comparison of experimental U(IV) solubility data determined in 0.25 M $MgCl_2$ solutions with solubility calculations using the thermodynamic model derived in the present work (see Table 10) and activity model reported by [2001NEC/KIM]. Detection limit is shown as a light red area, involving several different detection limits from different standard ICP-MS measurements (calculated as 3σ of the blank).*

4.3.2. Solubility and complexation of Th(IV) and U(IV) in NaCl–$NaHCO_3$–Na_2CO_3 solutions

The solubility of tetravalent AnO_2(am, hyd) oxyhydroxides in alkaline carbonate containing NaCl solutions (C_{tot} = [$NaHCO_3$] + [Na_2CO_3] = 0.02 to 0.1 M, [NaCl] = 0.1 - 4.0 M) up to high ionic strengths were systematically investigated for Th(IV) by Altmaier *et al*. [2006ALT/NEC]. Experimental data after phase separation by 10kD ultrafiltration or ultracentrifugation at 90000 rpm ($5 \cdot 10^5$ g) and the thermodynamic SIT model are displayed in Figure 26 for the series with C_{tot} = 0.02 M and [NaCl] = 0.1-4.0 M. Compared to carbonate-free systems where the Th(IV) solubility is at or below the analytical detection limit (log [Th(IV)] < −8.0), Th(IV) concentrations are enhanced by up to five orders of magnitude in presence of carbonate. Th(IV) solubility systematically increases with the total carbonate concentration and the concentration of NaCl. For example, at constant C_{tot} = 0.02 M, the Th(IV) solubility systematically increases by up to 3 orders of magnitude between [NaCl] = 0.1 M and 4.0 M, *c.f.* Figure 26. Based on the comprehensive chemical and thermodynamic models derived, the enhanced Th(IV) concentration in dilute to concentrated $NaHCO_3$–Na_2CO_3–NaCl solutions can be described by the equilibrium reaction

$$ThO_2(am,hyd) + 3\ H^+ + 4\ CO_3^{2-} \Leftrightarrow Th(OH)(CO_3)_4^{5-} + H_2O(l) \quad (35)$$

At low ionic strength ($I \approx 0.1$ M), the following reaction also play a role at near-neutral conditions

$$ThO_2(am,hyd) + 2\ H^+ + 2\ CO_3^{2-} \Leftrightarrow Th(OH)_2(CO_3)_2^{2-} \quad (36)$$

Analogous solubility experiments were performed within this project for U(IV) at C_{tot} = 0.04 and 0.1 M and [NaCl] = 0.5 to 4.0 M, *c.f.* Figure 27. As for Th(IV), U(IV) solubility is enhanced in presence of carbonate compared to the carbonate-free solutions, but the dependence of U(IV) solubility on both [CO_3^{2-}] and [NaCl] is less pronounced. Systematic evaluation of the experimental data revealed that the enhanced solubility for U(IV), Np(IV) and Pu(IV) and pH_m > 7 can be adequately described by the following reaction

$$UO_2(am,hyd) + 2\ H^+ + 3\ CO_3^{2-} \Leftrightarrow U(OH)_2(CO_3)_3^{4-} \quad (37)$$

i.e. by an equilibrium between UO_2(am, hyd) solid phase and a mixed U(IV)–OH–CO_3 complex as predominant species. Note that the $U(OH)_2(CO_3)_3^{4-}$ species identified in the present work shows a slightly different stoichiometry as found for the dominant Th(IV) species $Th(OH)(CO_3)_4^{5-}$. On the contrary, the main aqueous species identified for U(IV) was also reported to properly explain the solubility of Np(IV) and Pu(IV) in carbonate solutions [2017SCH/YAL]. These results hint at a higher degree of chemical analogy between U(IV), Np(IV) and Pu(IV) than found for Th(IV).

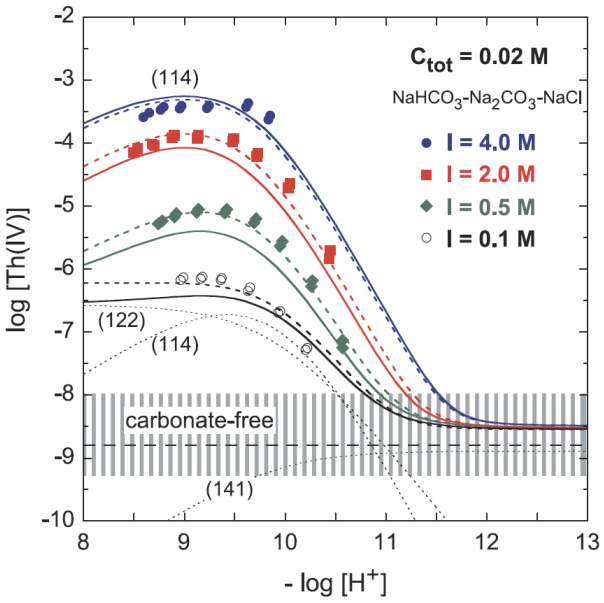

Figure 26. *Experimental solubility of ThO_2(am, hyd) at total carbon concentration (C_{tot}) = 0.02 M and I = 0.1, 0.5, 2.0 and 4.0 M ($NaHCO_3$-Na_2CO_3-NaCl) in comparison to SIT model (solid lines and dotted speciation lines for I = 0.1 M). Dashed lines represent best fits to the experimental data. From [2006ALT/NEC]. At a constant total carbonate concentration of 0.02 M, a very strong impact of ionic strength on Th(IV) solubility spanning over more than 2.5 orders of magnitude has been observed for pH_m = 8.5 – 10.*

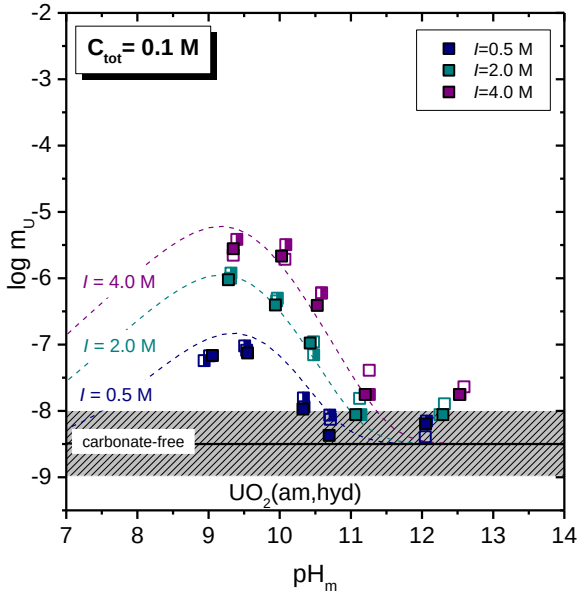

Figure 27. *Experimental solubility of UO_2(am, hyd) at total carbon concentration C_{tot} = 0.1 M and I = 0.5–4.0 M ($NaHCO_3$-Na_2CO_3-NaCl) in comparison to U(IV) solubility in carbonate-free solutions (solid line). The tendency towards U(IV) hydroxo-carbonate complex formation and the impact of ionic strength on total U(IV) solubility is much less pronounced than for Th(IV) (Figure 26).*

5. References

[1962RUS/JOH] Rush, R.M., J.S. Johnson, and K.A. Kraus, Hydrolysis of Uranium(VI) - Ultracentrifugation and Acidity Measurements in Chloride Solutions. Inorganic Chemistry, 1962. 1(2): p. 378.

[1963DUN/SIL] Dunsmore, H.S. and L.G. Sillen, Studies on Hydrolysis of Metal Ions .47. Uranyl Ion in 3 M NaCl Medium. Acta Chemica Scandinavica, 1963. 17(10): p. 2657-&.

[1980CIA] Ciavatta, L., The Specific Interaction Theory in Evaluating Ionic Equilibria. Annali Di Chimica, 1980. 70(11-1): p. 551-567.

[1982COO] Cooper, M.J., The Analysis of Powder Diffraction Data, Acta Crystallographica Section A, 38, 264-269, (1982).

[1983RYA/RAI] Ryan, J.L., Rai, D., The solubility of uranium(IV) hydrous oxide in sodium-hydroxide solutions under reducing conditions, Polyhedron, 2, 947-952, (1983).

[1991FEL/RAI] Felmy, A.R., Rai, D., Mason, M.J., The Solubility of Hydrous Thorium(IV) Oxide in Chloride Media: Development of an Aqueous Ion-Interaction Model, Radiochimica Acta, 55, 177-185, (1991)

[1991PIT] Pitzer, K.S., ed. Activity coefficients in electrolyte solutions. Chap. 3. 1991: Boca Raton, FL.

[1992GRE/FUG] Grenthe, I., Fuger, J., Konings, R.J.M., J., L.R., Müller, A.B., Nguyen-Trung, C., Wanner, H., Chemical Thermodynamics of Uranium, Vol 1 of Chemical Thermodynamics, Elseiver Science Publishers, Amsterdam, (1992).

[1997GRE/PUI] Grenthe, I., Puigdoménech, I., Modelling in Aquatic Chemistry, OECD Nuclear Energy Agency Paris, (1997).

[1997RAI/FEL] Rai, D., Felmy, A.R., Sterner, S.M., Moore, D.A., Mason, M.J., Novak, C.F., The solubility of Th(IV) and U(IV) hydrous oxides in concentrated NaCl and $MgCl_2$ solutions, Radiochimica Acta, 79, 239-247, (1997).

[2001NEC/KIM] Neck, V., Kim, J.I., Solubility and hydrolysis of tetravalent actinides, Radiochimica Acta, 89, 1-16, (2001).

[2002AMA] Amayri, S., "Synthese, Charakterisierung und Löslichkeit von Erdalkaliuranylcarbonaten $M_2[UO_2(CO_3)_3]\cdot xH_2O$; M: Mg, Ca, Sr, Ba", PhD thesis, Technischen Universität Dresden (2002).

[2002DES/GIA] De Stefano, C., Gianguzza, A., Leggio, T., Sammartano, S., Dependence on ionic strength of the hydrolysis constants for dioxouranium(VI) in NaCl(aq) and $NaNO_3$(aq), at pH 6 and t=25 ^{o}C. Journal of Chemical and Engineering Data, 2002. 47(3): p. 533-538.

[2003ALT/MET] Altmaier, M., Metz, V., Neck, V., Muller, R., Fanghänel, T., Solid-liquid equilibria of $Mg(OH)_2$(cr) and $Mg_2(OH)_3Cl.4H_2O$(cr) in the system Mg-Na-H-OH-O-Cl-H_2O at 25°C, Geochimica Et Cosmochimica Acta, 67, 3595-3601, (2003).

[2003GUI/FAN] Guillaumont, R., Fanghänel, T., Fuger, J., Grenthe, I., Neck, V., Palmer, D.A., Rand, M.H., Update on the Chemical Thermodynamics of Uranium, Neptunium, Plutonium, Americium and Technetium, Vol.5 of Chemical Thermodynamics, in, Elseiver Science Publishers, Amsterdam, (2003).

[2004ALT/NEC] Altmaier, M., Neck, V., Fanghanel, T., Solubility and colloid formation of Th(IV) in concentrated NaCl and $MgCl_2$ solution, Radiochimica Acta, 92, 537-543, (2004).

[2004CON/MAN] Conradson, S.D., Manara, D., Wastin, F., Clark, D.L., Lander, G.H., Morales, L.A., Rebizant, J., Rondinella, V.V., Local structure and charge distribution in the UO_2-U_4O_9 system, Inorganic Chemistry, 43, 6922-6935, (2004).

[2005FUJ/YAM] Fujiwara, K., Yamana, H., Fujii, T., Kawamoto, K., Sasaki, T., Moriyama, H., Solubility of uranium(IV) hydrous oxide in high pH solution under reducing condition, Radiochimica Acta, 93, 347-350, (2005).

[2005RAB/NEW] Ravel, B., Newville, M., ATHENA, ARTEMIS, HEPHAESTUS: data analysis for X-ray absorption spectroscopy using IFEFFIT, Journal of Synchrotron Radiation, 12, 537-541, (2005).

[2006ALT/NEC] Altmaier, M., Neck, V., Denecke, M. A., Yin, R., Fanghänel, Th., Solubility of $ThO_2 \cdot xH_2O$(am) and the formation of ternary Th(IV) hydroxide-carbonate complexes in $NaHCO_3$-Na_2CO_3 solutions containing 0–4M NaCl, Radiochim. Acta 94, 495–500 (2006).

[2008ALT/NEC] Altmaier, M., Neck, V., Fanghanel, T., Solubility of Zr(IV), Th(IV) and Pu(IV) hydrous oxides in $CaCl_2$ solutions and the formation of ternary Ca-M(IV)-OH complexes, Radiochimica Acta, 96, 541-550, (2008).

[2009ALT/NEC] Altmaier, M., V. Neck, and J. Lützenkirchen. SIT and Pitzer model for the UO_2^{2+} ion in NaCl, $MgCl_2$ and $CaCl_2$ solutions applied to trace activity coefficients determined by solvent extraction by TBP, Migration conference. 2009.

[2010FEL/NEC] Fellhauer, D., Neck, V., Altmaier, M., Lutzenkirchen, J., Fanghanel, T., Solubility of tetravalent actinides in alkaline $CaCl_2$ solutions and formation of $Ca_4[An(OH)_8]^{4+}$ complexes: A study of Np(IV) and Pu(IV) under reducing conditions and the systematic trend in the An(IV) series, Radiochimica Acta, 98, 541–548, (2010).

[2012ROT/BUT] Rothe, J., Butorin, S., Dardenne, K., Denecke, M.A., Kienzler, B., Loble, M., Metz, V., Seibert, A., Steppert, M., Vitova, T., Walther, C., Geckeis, H., The INE-Beamline for actinide science at ANKA, Rev. Sci. Instrum., 83, (2012).

[2013FEL] Fellhauer, D., Untersuchungen zur Redoxchemie und Löslichkeit von Neptunium und Plutonium, PhD thesis, University of Heidelberg, Germany, (2013).

[2013GAO/FEL] Gaona, X., Fellhauer, D., Altmaier, M., Thermodynamic description of Np(VI) solubility, hydrolysis, and redox behavior in dilute to concentrated alkaline NaCl solutions, Pure Applied Chemistry, 85, 2027–2049, (2013).

[2013KOB/SCH] Kobayashi, T., Scheinost, A.C., Fellhauer, D., Gaona, X., Altmaier, M., Redox behavior of Tc(VII)/Tc(IV) under various reducing conditions in 0.1 M NaCl solutions, Radiochimica Acta, 101, 323-332, (2013).

[2017ALT/YAL] Altmaier, M., Yalcintas, E., Gaona, X., Neck, V., Müller, R., Schlieker, M., Fanghänel, T., Solubility of U(VI) in chloride solutions. I. The stable oxides/hydroxides in NaCl systems solubility products, hydrolysis constants and SIT coefficients, Journal of Chemical Thermodynamics, 114, 2-13, (2017).

[2017BAU/YAL] Baumann, A., Yalcintas, E., Gaona, X., Altmaier, M., Geckeis, H., Solubility and hydrolysis of Tc(IV) in dilute to concentrated KCl solutions: an extended thermodynamic model for Tc^{4+}–H^{+}–K^{+}-Na^{+}–Mg^{2+}–Ca^{2+}-OH^{-}–Cl^{-}–H_2O(l) mixed systems, New J. Chem., 41, 9077–9086, (2017).

[2017SCH/YAL] Schepperle, J., Yalcintas, E., Fellhauer, D., Cevirim, N., Gaona, X., Altmaier, M., Geckeis, H., Hydroxo-carbonate complex formation and solubility of tetravalent actinides at alkaline pH conditions, proceedings of the Migration conference, Barcelona, September 2017.

[2017ZIM/DAR] Zimina, A., Dardenne, K., Denecke, M.A., Doronkin, D.E., Huttel, E., Lichtenberg, H., Mangold, S., Pruessmann, T., Rothe, J., Spangenberg, T., Steininger, R., Vitova, T., Geckeis, H., Grunwaldt, J.D., CAT-ACT-A new highly versatile x-ray spectroscopy beamline for catalysis and radionuclide science at the KIT synchrotron light facility ANKA, Review of Scientific Instruments, 88, (2017).

6. List of Figures

Figure 9. *Experimental solubility data of U(VI) obtained in this work in a. 0.1 M, b. 0.5 M, c. 1.0 M d. 3.0 M and e. 4.0 M KCl systems (colored symbols). Empty triangles show the solubility of U(VI) in dilute to concentrated NaCl solutions as reported in Section 4.2.1 and in [2017ALT/YAL]. Dashed lines indicate a slope of +1.*

Figure 10. *XRD patterns of solid phases of selected solubility samples in dilute to concentrated KCl solutions: a. comparison between "Starting material" and XRD patterns reported by [2017ALT/YAL] for $Na_2U_2O_7{\cdot}H_2O(cr)$ and $UO_3{\cdot}2H_2O(cr)$, and reference data reported in the JCPDS database for $K_2U_6O_{19}{\cdot}11H_2O(cr)$ (JCPDS file Nr. 33–1049), $K_2U_4O_{13}(cr)$ (JCPDS file Nr. 29–1059), $K_2U_2O_7(cr)$ (JCPDS file Nr. 29–1058) and $K_2UO_4(cr)$ (JPDS file Nr. 72–2228); b. comparison between "Starting material" and solid phases at pH_m = 7.7–10.3. Diffractograms of $K_2U_2O_7(cr)$ (JCPDS file Nr. 29–1058), $K_2U_4O_{13}(cr)$ (JCPDS file Nr. 29–1059) and $K_2U_6O_{19}{\cdot}11H_2O(cr)$ (JCPDS file Nr. 33–1049) provided for comparison; c. comparison between "Starting material" and solid phases recovered from solubility experiments at pH_m=12.9–13.3 after t = 268 days. Diffractogram of $K_2U_2O_7(cr)$ (JCPDS file Nr. 29–1058) provided for comparison.*

Figure 11. *SIT-plot for the solubility reactions 0.5 $M_2U_2O_7{\cdot}xH_2O(cr)$ + (2.5–0.5x) $H_2O(l)$ ⇔ $UO_2(OH)_4^{2-}$ + H^+ + M^+ (with M = K and Na) using experimental log $^*K'_{s,(1,4)}$ values determined in dilute to concentrated KCl (this section) and NaCl solutions (Section 4.2.1 and [2017ALT/YAL]).*

Figure 12. *Experimental solubility data of U(VI) in 0.01, 0.25, 2.67 and 5.15 m $MgCl_2$ solutions. Solid line corresponds to the solubility of $UO_3{\cdot}2H_2O(cr)$ calculated at I = 0 with thermodynamic data derived in this study.*

Figure 13. *Experimental solubility data of U(VI) in a) 0.03, 0.51, 2.64 and 5.61 m NaCl and b) 0.01, 0.25, 2.67 and 5.15 m $MgCl_2$ solutions. Solid lines are the calculated solubility with thermodynamic and Pitzer activity models derived in the present study.*

Figure 14. *Conditional formation constants log $^*K'_{s,(x,y)}$ for anionic (13) and (14) hydroxide complexes as a function of NaCl and KCl molalities: experimental values (symbols) and calculated functions based on the Pitzer activity model derived in this work (dashed line: NaCl, dotted line: KCl).*

Figure 15. *Solubility of $Ca_2UO_2(CO_3)_3{\cdot}10H_2O(cr)$ "starting material" in water (I ≈ 0.02 M), 0.5 and 5.0 M NaCl systems. Solid lines represent the solubility of U(VI) calculated based on liebigite, $Ca_2UO_2(CO_3)_3{\cdot}10H_2O(cr)$ for water and 0.5 M NaCl, and andersonite, $Na_2CaUO_2(CO_3)_3{\cdot}6H_2O(cr)$ for 5.0 M NaCl, as solubility limiting phases in equilibrium with $pCO_2(g) = 10^{-3.5}$ atm.*

Figure 16. *XRD patterns of solid phases in samples A, B and C, equilibrated in water, 0.5 and 5.0 M NaCl, respectively. Inverse triangles correspond to reference patterns of liebigite and andersonite.*

Figure 17. *SEM images of solid phases in samples A, B and C, equilibrated in water, 0.5 and 5.0 M NaCl, respectively.*

Figure 18. *Impact of dissolved nitrate (data in blue symbols) on U(VI) solubility. (a) Solubility of Na-uranate $Na_2U_2O_7{\cdot}H_2O(cr)$ in 5 M NaCl and in nitrate containing (3 M NaCl + 2 M $NaNO_3$) solution. (b) Solubility of Ca-uranate $Ca_2U_2O_7{\cdot}3H_2O(cr)$ in 1 M and 4 M $CaCl_2$ and in nitrate containing (1 M $CaCl_2$ + 1.5 M $Mg(NO_3)_2$) solution. (c) Solubility of Metashoepite $UO_3{\cdot}2H_2O(cr)$ in 2.5 and 3. 5 M $MgCl_2$ and nitrate containing 3.5 M $MgCl_2/(NO_3)_2$ mixtures. All three inviestigated systems show no solubility increase by nitrate relative to the comparable nitrate-free systems.*

Figure 19. *Experimental solubility data obtained in this work in a. 0.1 M, b. 0.5 M, c. 2.0 M and d. 5.0 M NaCl systems, in comparison with previously reported data by [1997RAI/FEL]. Solid lines corresponding to the solubility of UO_2(am, hyd) solid phase calculated for each ionic strength by using the data reported by [2001NEC/KIM]. Detection limits for μ-injection ICP-MS measurements in 0.1 and 0.5 M NaCl systems are shown as shadowed areas in light red and light green and correspond to detection limits from different measurements (calculated as 3σ of the blank).*

Figure 20. *Experimental solubility data obtained in this work for U(IV) in a. 0.25 M, b. 2.0 M and c. 4.5 M $MgCl_2$ systems, in comparison with solubility data reported by [1997RAI/FEL] for analogous $MgCl_2$ systems. Solid lines corresponding to the solubility curve of UO_2(am, hyd) calculated for each ionic strength using thermodynamic data reported by [2001NEC/KIM]. Detection limits are shown as shadowed areas in light blue, green and red for 0.25 M, 2.0 and 4.5 M $MgCl_2$ systems respectively, involving different detection limits from different measurements (calculated as 3σ of the blank).*

Figure 21. *Experimental solubility data obtained in this work for U(IV) in $CaCl_2$ systems. Solid lines corresponding to the solubility curve of UO_2(am, hyd) calculated for each ionic strength using thermodynamic data reported by [2001NEC/KIM] and [2010FEL/NEC]. Dashed lines correspond to the detection limits of ICP-MS determined (as 3σ of the blank) for each $CaCl_2$ concentration.*

Figure 22. *XRD diffractograms of a. "starting material" and reference data for $UO_3{\cdot}2H_2O$(cr) and $Na_2U_2O_7{\cdot}H_2O$(cr) solid phases (see section 4.3.2 and [2017ALT/YAL]); and of solid phases collected from selected solubility samples in NaCl systems b. in acidic pH_m range and c. in alkaline pH_m range. Green and blue diamonds indicate the main patterns and relative intensities of UO_2(cr) reference material (PDF 41-1422 and 73-2293).*

Figure 23. *U L_{III}–edge EXAFS results for $UO_2{\cdot}H_2O$(ncr) "starting material" at pH_m = 12.1 (left) and $UO_2{\cdot}H_2O$(ncr) in 0.1 M NaCl at pH_m = 8.5 (right). k^2-weighted EXAFS spectra (upper panel) and Fourier Transform (lower panel); experimental data are depicted as solid lines, whereas fits are shown as red circles and black triangles (modulus and imaginary parts, respectively). Dashed lines correspond to the FT hanging windows used in the EXAFS fit.*

Figure 24. *Comparison of experimental U(IV) solubility data determined in 0.1 M, 0.5 M, 2.0 M and 5.0 M NaCl solutions with solubility calculations using the thermodynamic model derived in the present work (see Tables 10 and 11) and activity model reported by [2001NEC/KIM]. Detection limits for μ-injection ICP-MS measurements are shown as shadowed areas in light red and light green in 0.1 and 0.5 M NaCl systems involving detection limits from different measurements (calculated as 3σ of the blank). Gray dashed lines show the detection limit of standard ICP-MS measurements.*

Figure 25. *Comparison of experimental U(IV) solubility data determined in 0.25 M $MgCl_2$ solutions with solubility calculations using the thermodynamic model derived in the present work (see Table 10) and activity model reported by [2001NEC/KIM]. Detection limit is shown as a light red area, involving several different detection limits from different standard ICP-MS measurements (calculated as 3σ of the blank).*

Figure 26. *Experimental solubility of ThO_2(am, hyd) at total carbon concentration (C_{tot}) = 0.02 M and I = 0.1, 0.5, 2.0 and 4.0 M ($NaHCO_3$-Na_2CO_3-NaCl) in comparison to SIT model (solid lines and dotted speciation lines for I = 0.1 M). Dashed lines represent best fits to the experimental data. From [2006ALT/NEC]. At a constant total carbonate concentration of 0.02 M, a very strong impact of ionic*

strength on Th(IV) solubility spanning over more than 2.5 orders of magnitude has been observed for pH_m = 8.5 – 10.

Figure 27. *Experimental solubility of UO_2(am, hyd) at total carbon concentration C_{tot} = 0.1 M and I = 0.5–4.0 M ($NaHCO_3$-Na_2CO_3-NaCl) in comparison to U(IV) solubility in carbonate-free solutions (solid line). The tendency towards U(IV) hydroxo-carbonate complex formation and the impact of ionic strength on total U(IV) solubility is much less pronounced than for Th(IV) (Figure 26).*

7. List of Tables

C. Veröffentlichungen und Auszeichnungen

Veröffentlichungen in wissenschaftlichen (peer-reviewed) Zeitschriften

(1) Altmaier, M., Yalcintas, E., Gaona, X., Neck, V., Müller, R., Schlieker, M., Fanghänel, T., Solubility of U(VI) in chloride solutions. I. The stable oxides/hydroxides in NaCl systems solubility products, hydrolysis constants and SIT coefficients, Journal of Chemical Thermodynamics, 114, 2-13, (2017).

(2) Çevirim-Papaioannou, N., Yalçıntaş, E., Gaona, X., Altmaier, M., Geckeis, H. (2018). Solubility of U(VI) in chloride solutions. II. The stable oxides/hydroxides in alkaline KCl solutions: Thermodynamic description and relevance in cementitious systems. Applied Geochemistry, 98, 237-246

(3) Çevirim-Papaioannou, N., Yalçıntaş, E., Gaona, X., Dardenne, K., Altmaier, M., Geckeis, H. (2018). Redox chemistry of uranium in reducing, dilute to concentrated NaCl solutions. Applied Geochemistry, 98, 286-300

(4) Yalçıntaş, E., Çevirim-Papaioannou, N., Gaona, X., Fellhauer, D., Neck, V., Altmaier, M. (2019). Solubility of U(VI) in chloride solutions. III. The stable oxides/hydroxides in MgCl2 systems: Pitzer activity model for the system UO22+–Na+–K+–Mg2+–H+–OH−–Cl−–H2O(l). Journal of Chemical Thermodynamics, 131, pp. 375-386.

(5) Lee, J.-Y., Amayri, S., Montoya, V., Fellhauer, D., Gaona, X., Altmaier, M. (2019). Solubility and stability of liebigite, Ca2UO2(CO3)3·10H2O(cr), in dilute to concentrated NaCl and NaClO4 solutions at T = 22–80 °C. Applied Geochemistry, 111, art. no. 104374.

Sonstige Veröffentlichungen und Publikationen

(1) Cevirim, N., Doktorarbeit zu “Redox chemistry, solubility and hydrolysis of uranium in dilute to concentrated salt systems”, Karlsruhe Institut für Technologie, 2018.

Vorträge bei wissenschaftlichen Konferenzen und Workshops

(1) Gaona, X. (eingeladener Vortrag), "Redox chemistry of Pu, Np and U under alkaline to hyperalkaline pH conditions", Konferenz “Plutonium Futures - The Science”, 18-22 September 2016, Baden-Baden (Deutschland).

(2) Dardenne, K., et al. “X-ray absorption fine structure (XAFS) determination of radionuclide speciation in aqueous systems”, Actinide XAS Konferenz, 11-13 April 2017, Oxford (UK)

(3) Yalcintas, E., et al. „Redox behavior of U(VI)/U(IV) and solubility of U(IV) in repository relevant dilute to concentrated solutions in the absence and presence of complexing ligands“, Konferenz “ACS meeting”, April 1-6 2017, San Francisco, CA (USA).

(4) Yalcintas, E., et al. „Redox chemistry and solubility of uranium in dilute to concentrated NaCl systems: impact of carbonate and EDTA“, Konferenz “ABC-Salt Workshop”, 26-29 March 2017, Ruidoso, NM (USA).

(5) Altmaier, M., et al. (eingeladener Vortrag) “Studies on An(IV)-hydroxo-carbonate complex formation along the An(IV) = Th, U, Np, Pu series”, Konferenz “ACS meeting”, August 19-23 2018, Boston, MA (USA)

(6) Cevirim, N., et al. “Solution chemistry of uranium in cementitious systems”, NUWCEM conference, Cement-based Materials for Nuclear Wastes, 24 – 26 October 2018, Avignon (France)

Poster bei wissenschaftlichen Konferenzen und Workshops

(1) Cevirim, N., et al. „Redox chemistry and solubility of Uranium in alkaline to hyperalkaline NaCl/KCl systems“, Konferenz “Mechanisms and Modelling of Waste/Cement Interactions”, May 22-25, 2016, Murten (Schweiz).

(2) Yalcintas, E., et al. „Solubility of UO2(am,hyd) in alkaline carbonate solutions“, Konferenz „ISSP 17th International Symposium on Solubility Phenomena and Related Equilibrium Processes“, Juli 24-29, 2016, Geneva (Schweiz).

(3) Gaona, X., et al. “Impact of carbonate on the solubility of An(IV) under alkaline to hyperalkaline pH conditions”, Konferenz “ACS meeting”, 20-24 August 2017, Washington DC (USA)

(4) Cevirim, N., et al. „Redox chemistry, solubility and hydrolysis of uranium in reducing, dilute to concentrated NaCl, MgCl2 and CaCl2 systems“, Konferenz “Migration”, September 10-15, 2017, Barcelona (Spanien).

(5) Schepperle, J., et al. “Hydroxo-carbonate complex formation and solubility of tetravalent actinides at alkaline pH conditions”, Konferenz “Migration”, September 10-15, 2017, Barcelona (Spanien).

Preise und Auszeichnungen

(1) *Posterpreis*: Posterpräsentation Cevirim, N., et al. „Redox chemistry and solubility of Uranium in alkaline to hyperalkaline NaCl/KCl systems“, Konferenz “Mechanisms and Modelling of Waste/Cement Interactions”, May 22-25, 2016, Murten (Schweiz).

(2) *Posterpreis*: Posterpräsentation Yalcintas, E., et al. „Solubility of UO_2(am,hyd) in alkaline carbonate solutions“, Konferenz „ISSP 17th International Symposium on Solubility Phenomena and Related Equilibrium Processes“, Juli 24-29, 2016, Geneva (Schweiz).

(3) *Posterpreis*: Posterpräsentation Cevirim, N., et al. „Redox chemistry, solubility and hydrolysis of uranium in reducing, dilute to concentrated NaCl, $MgCl_2$ and $CaCl_2$ systems“, Konferenz “Migration”, September 10-15, 2017, Barcelona (Spanien).

KIT Scientific Working Papers
ISSN 2194-1629

www.kit.edu